

Anna Nicola Messinger

Deposition Patterns of PAHs, PCBs, and Selected Elements in Snow on Glaciers

Covering a Latitudinal Gradient from Southern
Norway (60.54°N) to Svalbard (78.87°N)

Master's thesis in Environmental Toxicology and Chemistry

Supervisor: Øyvind Mikkelsen

Co-supervisor: Gijsbert Breedvald

July 2022



Anna Nicola Messinger

Deposition Patterns of PAHs, PCBs, and Selected Elements in Snow on Glaciers

Covering a Latitudinal Gradient from Southern Norway (60.54°N) to Svalbard (78.87°N)

Master's thesis in Environmental Toxicology and Chemistry
Supervisor: Øyvind Mikkelsen
Co-supervisor: Gijsbert Breedvald
July 2022

Norwegian University of Science and Technology
Faculty of Natural Sciences
Department of Chemistry

Abstract

Svalbard is a remote Arctic Archipelago, often considered to have a pristine environment. However, volatile and persistent compounds have been suggested to be transported from lower latitudes to the Arctic via long-range atmospheric transport (LRAT), whereby the distance a compound can travel is correlated to its temperature-dependent volatility, resulting in global (latitudinal) fractionation. Additionally, seasonal temperature changes may lead to the reemission of compounds into the atmosphere, referred to as the grasshopper effect. This study aimed to investigate the deposition patterns of contaminants in snow on remote glaciers along a latitudinal gradient ranging from southern Norway (60.54°N) to Svalbard (78.87°N). In Svalbard, also seasonal changes were investigated. Altogether, surface snow samples from 16 glaciers were collected: 12 glaciers in spring, 3 in summer, and 1 in both seasons. The snow was analyzed for 62 elements using ICP-MS and for the 16 U.S. EPA priority PAHs and 7 PCBs using GC-MS. To identify potential source regions, air pathways to the glaciers were studied using the HYSPLIT model by NOAA, and for emission source identification PCAs were plotted. The study showed that major and trace element concentrations increased by 5.3 and 2.9 times, respectively, with increasing proximity to the ocean, whereby Na, Cl, Br, and Mg were the most significant contributors due to their abundance in seawater. A different trend was seen for the total heavy metal concentration, which decreased by 89% from low to high latitude. Specific markers were Cu and Zn, which correlated with the location of non-ferrous metal production plants in southern Norway. A similar latitudinal trend was found for the two PAH congeners PHE and FLT, which decreased by 59% and 80% respectively. None of the low-volatile 5- and 6-ring PAHs, and none of the PCB congeners could be detected in the samples. Comparing concentrations in spring and summer snow of Svalbard, no difference in the total PAH concentration was seen. However, major and trace elements decreased by nearly 80%, most likely due to salt lowering the freezing point of water leading to run-off. Phosphorous concentration, on the other hand, increased by 4.6 times, potentially due to uptake in snow algae. Thus, the global fractionation process theory could explain the trends seen in 2 out of 16 PAHs, Ba, the total heavy metal concentration, and for 4 out of 6 individually investigated heavy metals (Cu, Zn, Cd, Cr). For other elements, such as Na, Cl, Br, and Mg, natural local sources and aerosol transport and deposition appears to be the dominating process. Seasonal changes in snow concentrations were most likely due to run-off and not reemission, therefore no proof of the grasshopper effect in Svalbard could be found.

Acknowledgment

First and foremost, I would like to thank my main supervisor Øyvind Mikkelsen for helping me plan and execute this study. Without your help and guidance, this master's thesis would not have been possible. I greatly appreciate the unique opportunity to conduct a study in the Arctic with you and all your help during this process.

Further, I would like to thank UNIS, and in particular my co-supervisor Gijsbert Breedvald at UNIS. I am thankful for the help and guidance UNIS provided for sampling two of the glaciers on Svalbard and for letting me write the thesis in such an inspiring environment.

I would further like to acknowledge the glacier department of the Norwegian Water Resources and Energy Directorate (NVE) and the Norwegian Polar Institute (NPI) for taking the time to take my samples during their own fieldwork on the glaciers. In particular, I would like to thank Liss Marie Andreassen for being my contact person at NVE and arranging the sampling of the 10 glaciers in mainland Norway for my thesis with the glacier department of NVE. I also want to thank you for letting me join you and your team on Hellstugubreen for the sampling. It was a fantastic experience.

Susanna Villa Gonzalez further deserves a big thank you for helping me with the GC-MS analysis. I appreciate you taking your time teaching and helping me with the GC-MS, especially when it did not want to cooperate. Thank you for always staying positive and offering me reinsurance and guidance when needed.

I would also like to acknowledge the NOAA Air Resources Laboratory (ARL) for the provision of the HYSPLIT transport and dispersion model and the READY website (<https://www.ready.noaa.gov>) used in this thesis.

Lastly, I want to thank my family and friends for always being loving and supportive.

Table of Content

Abstract	iii
Acknowledgment	iv
Table of Content.....	v
List of Figures	viii
List of Tables.....	x
Abbreviations	xi
1. Introduction.....	1
2. Theory	3
2.1 Long-Range Atmospheric Transport (LRAT).....	3
2.2 Atmospheric Trajectory Models.....	4
2.3 Matrixes for measuring LRAT	5
2.4 Element Groups and Sources.....	5
2.4.1 Relevant Previous Studies on Element Concentrations	7
2.4.2 Analytical Techniques for Element Analysis.....	12
2.5 Polycyclic Aromatic Hydrocarbons (PAHs)	14
2.5.1 Relevant Previous Studies on PAHs	18
2.6 Polychlorinated Biphenyls (PCBs).....	19
2.6.1 Relevant Previous Studies on PCBs.....	22
2.7 Sample Pretreatment and GC-MS Analysis for PAHs and PCBs	24
2.8 Principal Component Analysis (PCA).....	27
3 Method	28
3.1 Sampling Sites	28
3.2 Back Trajectory Analysis	30
3.3 Sampling Technique	30
3.4 Analytical Method	31
3.4.1 Element Analysis.....	31

3.4.2	PAH and PCB Analysis.....	32
3.5	Data Analysis.....	34
4	Results and Discussion	36
4.1	Quality of the Dataset.....	36
4.1.1	Quality of the Element Analysis	36
4.1.2	Quality of the PAH and PCB Analysis	36
4.1.3	Quality of the Seasonal Dataset	39
4.2	Airmass Back Trajectories.....	39
4.3	Element Composition and Distribution	42
4.3.1	Major Elements Composition and Distribution	44
4.3.2	Trace Elements Composition and Distribution	47
4.3.3	Heavy Metals Composition and Distribution.....	50
4.3.4	Source Identification of Elements using PCA.....	57
4.3.5	Seasonal Changes in Element Concentration in Snow on Svalbard	61
4.4	Polycyclic Aromatic Hydrocarbon (PAH) Composition and Distribution.....	67
4.4.1	Source Identification of PAHs using PCA.....	71
4.4.2	Seasonal Changes in PAH Concentration in Snow on Svalbard.....	76
4.5	Polychlorinated biphenyls (PCB) Concentrations	80
4.6	Future Studies	80
5	Conclusion	82
	References	83
	Appendices	92
A.	Sampling Sites	92
B.	Materials and Chemicals	108
C.	Sample Weight	109
D.	Trajectory Models.....	110
E.	Results elements.....	115

F.	Results PAHs	132
G.	Results PCBs	134

List of Figures

Figure 1 Position of the 16 glaciers sampled.	28
Figure 2 Absolute recovery (AR) and relative recovery (RR) of the 16PAHs and 7PCBs. ...	37
Figure 3 NOAA HYSPLIT atmospheric back trajectory models.....	41
Figure 4 Map of the total element concentration ($\mu\text{g L}^{-1}$) on the 16 measured glaciers.	42
Figure 5 Major elements ($\mu\text{g L}^{-1}$) concentration and composition (%)......	45
Figure 6 Map of the major element concentration ($\mu\text{g L}^{-1}$) in the snow on the glaciers.....	46
Figure 7 Map of the Na and Cl concentration ($\mu\text{g L}^{-1}$) in the snow on the glaciers.....	47
Figure 8 Trace element concentration ($\mu\text{g L}^{-1}$) and composition (%)......	48
Figure 9 Map of the trace element concentration ($\mu\text{g L}^{-1}$) in the snow on the glaciers.	49
Figure 10 Map of the Br and Ba concentration ($\mu\text{g L}^{-1}$) in the snow on the glaciers.....	50
Figure 11 Heavy metal concentration ($\mu\text{g L}^{-1}$) and composition (%).	52
Figure 12 Map of the heavy metal concentration ($\mu\text{g L}^{-1}$) in the snow on the glaciers.	52
Figure 13 Map of the Cu and Zn concentrations ($\mu\text{g L}^{-1}$) in the snow on the glaciers.	53
Figure 14 Heavy metal concentration ($\mu\text{g L}^{-1}$) and composition (%). Cu and Zn excluded. ...	55
Figure 15 Map of the concentrations of the Mn, Cr, Pb and Cd ($\mu\text{g L}^{-1}$) in the snow on the glaciers.	56
Figure 16 PCA of the element composition found on the glaciers.	59
Figure 17 PCA plot of the element concentrations showing 3 groups of glaciers for each factor: Latitude, Altitude, Distance to fjord.	61
Figure 18 Trace elements, major elements, and heavy metal concentration ($\mu\text{g L}^{-1}$) in the snow on the glaciers sampled on Svalbard.....	63
Figure 19 PCA plot of the glaciers from Svalbard sampled in spring and summer.....	66
Figure 20 PAH concentrations (ng L^{-1}) and composition (%).	68
Figure 21 Map of the total PAH concentration (ng L^{-1}) in the snow on the glacier.....	69
Figure 22 Map of the NAP, ACY, PHE, FLU, FLT, and PYR concentration (ng L^{-1}) in the snow on the glaciers.	71
Figure 23 PCA plot of the PAH concentration of the glaciers.....	73
Figure 24 PCA plot of the PAH concentration showing 3 groups of glaciers for each factor: Latitude, Altitude, and Distance to the fjord.	76
Figure 25 PAH concentration (ng L^{-1}) and composition (%) in the glaciers taken in spring and summer on Svalbard.....	78

Figure 26 PCA plot of PAH concentrations on glacier sampled in spring and summer in snow on Svalbard..... 79

List of Tables

Table 1 Relevant previous studies on elements.....	9
Table 2 PAH characteristics important for LRAT.....	16
Table 3 Relevant previous studies on PAHs.	19
Table 4 PCB characteristics important for LRAT.	21
Table 5 Relevant previous studies on PCBs.....	23
Table 6 The sampled glaciers sample date, coordinates (dd), altitude (masl) and distance to the closest fjord (km).....	29
Table 7 Input parameters used for the NOAA HYSPLIT trajectory model.....	30
Table 8 ICP-MS settings used for the analysis of the 62 elements.	32
Table 9 Calibration standards used for the analysis of PAHs and PCBs.	33
Table 10 Criteria used for groupig the glaciers depending on the latitude, altitude, and distance to fjord.....	35
Table 11 LOD and LOQ (ng mL ⁻¹) in the extract.....	38
Table 12 Element groups: Major elements, Trace elements, Lanthanides and Heavy metals.	43

Abbreviations

ACE	Acenaphthene
ACY	Acenaphthylene
ANT	Anthracene
AR	Absolute recovery
BaA	Benzo[a]anthracene
BaP	Benzo[a]pyrene
BbF	Benzo[b]fluoranthene
BgP	Benzo[ghi]perylene
BkF	Benzo[k]fluoranthene
CHR	Chrysene
DCM	Dichloromethane
DBA	Dibenzo[a,h]anthracene
FLT	Fluoranthene
FLU	Fluorene
GC-MS	Gas Chromatography–Mass Spectrometry
ICP-MS	Inductively Coupled Plasma Mass Spectrometry
IND	Indeno[1,2,3-cd]pyrene
LOD	Limit of Detection
LOQ	Limit of Quantification
LRAT	Long-range atmospheric transport
NAP	Naphthalene
NPI	Norwegian Polar Institute
NVE	Norwegian Water Resources and Energy Directorate
PAH	Polycyclic Aromatic Hydrocarbons
PCA	Principal Component analysis
PCB	Polychlorinated Biphenyls
PHE	Phenanthrene
POP	Persistent Organic Pollutant
PYR	Pyrene
RR	Relative recovery
SPE	Solid Phase Extraction

1. Introduction

The Arctic Archipelago Svalbard, located in the arctic ocean halfway between Norway and the North Pole, is often considered to be a remote and pristine environment. However, an assessment by AMAP (2004) concluded that the arctic is contaminated by emission sources outside the Arctic region. In their assessment, four main types of long-range transportation pathways of pollutants to the arctic were suggested: ocean currents, transpolar ice packs, large arctic rivers, and through the atmosphere (AMAP, 2004). Depending on the pollutant's chemical characteristics and how it was emitted to the environment, the importance of each of these pathways changes (AMAP, 2004). The most important route of volatile to semi-volatile pollutants to the arctic is through long-range atmospheric transport (LRAT) (Wania and Mackay, 1996a, 1993). A process called global fractionation was first suggested by Wania and Mackay (1993), meaning that compounds reach their condensation point at different ambient temperature levels, depending on their vapor pressure. Therefore, more volatile compounds can reach polar regions, while less volatile compounds will deposit closer to their emission point. This theory has since been studied in atmospheric samples and become proven for a couple of different pollutants such as perchlorate, some Polycyclic aromatic hydrocarbons (PAHs), and some of the heavier polychlorinated biphenyl (PCB) congeners (Garrido et al., 2014; Jaward et al., 2004; Jiang et al., 2021; Shen et al., 2005). However, atmospheric concentrations can change rapidly and compounds in the atmosphere are usually not available for uptake in the ecosystem. Therefore, measuring the deposition of the pollutants indicates the exposure of the ecosystem in a better way than measuring the atmospheric concentration (Wania and Mackay, 1993). Sensitivity simulations suggest that snow scavenging is effective at depositing gas-phase PAHs (Friedman and Selin, 2012).

PCBs, PAHs, and heavy metals have been identified as pollutants of emerging concern due to their potential risk to the arctic ecosystems (AMAP, 2017; AMAP, 2002). Several studies have been conducted measuring the concentration of these elements in different matrixes in the Arctic (Abramova et al., 2016; Garmash et al., 2013; Platt et al., 2022; Szczybelski et al., 2016), however, only one study, by Agrell et al. (2002), reports latitudinal gradients of these compounds in precipitation. In an assessment report by Gallet et al. (2019), a need for further investigation of contaminant deposition and accumulation in the snowpack on Svalbard and the fate of the contaminants upon snowmelt was identified.

To address these knowledge gaps, the present study aims to investigate the deposition patterns of selected elements, PAHs, and PCBs in snow on a latitudinal gradient, identify potential pollution sources, and detect differences in the concentrations of these compounds in the snow from spring to summer on Svalbard. Specifically, three research questions were identified: (1) Is there a spatial distribution of elements, PAHs, and PCBs deposited in the snow on remote glaciers from southern Norway to Svalbard (60-79°N)? (2) What are the potential sources of the compounds? (3) How does the concentration and composition of these compounds change from spring to summer on Svalbard?

2. Theory

2.1 Long-Range Atmospheric Transport (LRAT)

In 1974, researchers first started to suggest that persistent organic compounds (POPs) might be able to migrate as gases or aerosols through the atmosphere to low-temperature regions where they would condensate (see reference Rappe C. in Wania and Mackay, 1996). In 1993, the process “global fractionation” was suggested meaning that compounds deposit at different latitudes due to differences in their volatility (Wania and Mackay, 1993). As volatility is dependent on temperature, the natural temperature decrease towards the polar regions leads to a latitudinal fractionation of the compounds. Wania and Mackay (1993) suggest that compounds within a certain low range of vapor pressure might be transported that way to polar regions. This process has been studied by, among others, Garrido et al. (2014), who found negative latitudinal gradients for 4 out of 15 PAHs in the atmosphere on a gradient from 48 to 79°N.

Additionally, another process called the grasshopper effect has been suggested. The grasshopper effect can be explained as the seasonal or diurnal cycle of a compound being deposited and reemitted into the atmosphere (Wania and Mackay, 1993). In between the hops the compound could then travel further towards the polar regions (Wania and Mackay, 1993). Hoff et al. (1992) studied vapor-phase PCB and organo-halogen pesticides in air samples obtained in southern Ontario from July 1988 until September 1989. Their study showed that all these compounds increased by 14-20 times the minimum value in the summer. This provides proof of the summer reemission of the compounds and the winter deposition and thereby the grasshopper effect.

Agrell et al. (2002) studied the concepts of global fractionation and the grasshopper effect of PCB congeners in the Baltic Sea region in precipitation. The study showed that PCB deposition varied seasonally with a factor of 2-3. Further, they found that the concentration of the PCBs in precipitation decreased with increasing temperature proving the theory of the grasshopper effect. The study could, however, not statistically show a latitudinal trend of the PCB concentrations for any congeners except PCB-180. The congener is the least volatile PCB congener tested and it showed a decreasing trend with latitude, which agrees with the global fractionation theory by Wania and Mackay (1993).

Various chemical properties need to be taken into consideration when estimating the fate of a compound. Of special interest are the different equilibrium partitioning coefficients such as the aqueous solubility (S_w), vapor pressure (P), octanol-water coefficient (K_{ow}), Henry's law constant (K_H), octanol air coefficient (K_{OA}), and solubility in octanol (S_o) (Li et al., 2003). These properties are temperature dependent and are usually given at a temperature from 20-25°C. It is important to consider the properties' temperature dependence if the fate at another temperature is determined (Li et al., 2003). The fate of the compounds is further influenced by several other factors, such as their emission point, ambient meteorological regimes, vertical exchange, interactions with clouds, chemical and physical transformations in the air, coastal zones, and the chemicals' interactions with aerosols and dust particles, which could influence the pattern of deposition (Knap and Kaiser, 1988; Wania and Mackay, 1996b).

If the compound released into the atmosphere has a short residence time the ambient meteorological conditions during the release are most important for the fate of the compound. If the substance instead has a longer residence time the large-scale meteorological regime determines the fate (Knap and Kaiser, 1988). Pollutants and substances with very short residence times will mostly affect local air quality. Residence times of days to weeks will lead to local and regional air quality changes, weeks to months will affect the continental and hemispherical air quality, and residence times of years lead to global dispersion of the pollutant (Ferreira, 2008).

The pollutants are often removed from the atmosphere through wet or dry deposition. For wet deposition to occur precipitation is needed, leading to scavenger events of pollutants from the atmosphere to the surface. Scavenging of the pollutants by precipitation can occur both in the clouds, called rainout, or below the clouds, called washout (Leelőssy et al., 2014). Dry deposition, on the other hand, is a continuous exchange of gases between the surface and the atmosphere. Further, dry deposition of particles, and pollutants associated with particles, are highly dependent on the size of the particle. While smaller particles are deposited similar to gases, larger particles are deposited due to gravitational settling (Leelőssy et al., 2014).

2.2 Atmospheric Trajectory Models

Atmospheric trajectory models simulate air mass movement in the atmosphere by using meteorological data and mathematical equations (Stein et al., 2015). There are two main model calculation approaches: the Lagrangian and the Eulerian. The Lagrangian method uses a moving computational grid to track the motion of individual masses, which makes it easy to

implement air mass history-dependent constitutive models (Zhang et al., 2017). In the Eulerian method, the computational grid is fixed in space and the flow through the grid is calculated instead of following the flow (Rakhsha et al., 2021). Additionally, also hybrid methods of the Eulerian and the Lagrangian have been developed (Stein et al., 2015).

Trajectory models can both simulate air mass movement forward and backward in time, making them useful both for analyzing where a pollutant could be transported to starting from a pollution source point, or from where a pollutant might have derived from to the research area (Stein et al., 2015). It is common to use these models to determine potential sources of pollutants in research papers (Chance et al., 2015; Conca et al., 2019; Stein et al., 2015; Wang et al., 2010). Trajectory models rely on measurements of vertical profiles of pressure, temperature, and wind. The regularity of these measurements both in time and space is therefore highly important to receive accurate model predictions (Stein et al., 2015).

2.3 Matrixes for measuring LRAT

The most intuitive matrix for measuring atmospherically transported pollutants is air, therefore also many studies focus on air concentrations when studying LRAT (Chen et al., 2021; Garrido et al., 2014; Jaward et al., 2004; Platt et al., 2022). However, as pointed out by Wania and Mackay (1993), concentration in air can change rapidly and the pollutants are usually not environmentally available until they deposit. Therefore, moss, snow, and rain have been used in addition to air to study atmospheric deposition and transportation (Berg et al., 2008; Hermanson et al., 2020a; Steinnes, 1995).

Snow has been suggested to be a suitable matrix to measure atmospheric composition, as compounds can be absorbed in the snow during the formation of snowflakes in the atmosphere or by dry deposition onto the snow surface (Hibberd, 1984). Snow has a very high specific surface area which can absorb a wide variety of different gases and aerosols from the atmosphere (Gallet et al., 2019). These could be derived from natural sources, local sources, or from long-range atmospheric transport. Compounds that have been either absorbed or deposited onto the snow will be stored and accumulated in the snow until the snow melts (Hibberd, 1984). This makes snow a good matrix to measure atmospheric composition and deposition.

2.4 Element Groups and Sources

All elements can be naturally found in the environment. Typical natural pathways of elements to the atmosphere are volcanic eruptions, soil erosions, and sea spray (AMAP, 2005).

However, anthropogenic activities such as industrial processes, agricultural practices, transportation, and waste disposal have shown to lead to significantly higher emissions and redistributions of metals than natural processes (AMAP, 2005). Elements can be divided into several subgroups such as major elements, trace elements, lanthanoids (also referred to as Rare Earth Elements (REE)), and heavy metals.

Major elements are classified as elements that are present in the earth's crust at amounts greater than 1 % by weight, e.g. Si, Al, Fe, Ca, Mg, Na, P, Ti, Cl, S, and K (Lagowski et al., 2018). Elements such as Na, Mg, S, Cl, K, and Ca are present naturally in high concentrations in seawater (Duxbury et al., 2020). Aluminum and Fe are usually associated with a crustal signature and mineral aerosols, however, soot particles from coal combustion can also be characterized by a strong crustal signature and contain high Fe and Al concentrations (Colin et al., 1997).

Trace elements in geology are defined as elements that occur in minerals at less than 0.1 wt.% in the Earth's crust e.g. Br, Ba, Sr, Zr, Rb, Co, Nb, Li, Sc, Ga, Th, Hf, and U (Kennedy, 1998). Per the definition of trace elements, lanthanides and heavy metals are also trace elements. Some of the trace elements are like major elements present in seawater, such as Br, B, Sr, Ba, Rb, Cs, and Li, and could be transported in the atmosphere as sea spray aerosols (Duxbury et al., 2020). There are also anthropogenic sources of trace elements to the atmosphere. For instance, Ba can be emitted through mining, refining, and production of Ba and Ba chemicals, fossil fuel combustion, entrainment of soil and rock dust, and coal ash (Gad, 2014).

Lanthanides (also referred to as Rare Earth Elements (REEs)) consist of 15 elements: La, Ce, Pr, Nd, Pm, Sm, Eu, Gd, Tb, Dy, Ho, Er, Tm, Yb, and Lu. Although referred to as rare earth elements, these elements are abundant and exist in many mineral deposits around the world. Together they fall into the 50th percentile of element abundance (Pecharsky and Gschneidner, 2019). Natural lanthanides sources include crustal sources such as weathering, and oceanic sources such as sea spray. Anthropogenic sources of lanthanoids are a variety of high-temperature anthropogenic processes (Zhang and Liu, 2004). Further, studies have suggested lanthanides to be potential indicators of environmental pollution (Olmez and Gordon, 1985).

There are several definitions of heavy metals, but the most commonly used is a metal with a density of at least 5 g cm⁻³, e.g. As, Cd, Cr, Cu, and Hg (Koller and Saleh, 2018). Fossil fuel combustion, non-ferrous metal production, and waste incineration have been identified as the

major contributors to anthropogenic atmospheric heavy metal concentrations (AMAP, 2005). According to Pacyna et al. (2007) fuel combustion for heat and electricity, non-ferrous metal, iron and steel production, waste disposal, gasoline combustion, cement production, and other sources contributed in total to 763 metric tons As, 590 metric tons Cd, 2711 metric tons Cr, 4797 metric tons Ni and 13156 metric tons Pb to the atmosphere in Europe year 2000. Coal combustion contributes, according to AMAP (2002), to 69% of Cr, 66% of Hg, 85% of Mn, 47% of Sb, 89% of Se, 89% of Sn, and almost 100% of TI emissions to the atmosphere. The major contributor of atmospheric Pb emissions (74% in 1995) is the combustion of leaded, low-leaded, and 'unleaded' gasoline. Oil combustion contributes 90% of Ni emissions and almost 100% of V emissions. Non-ferrous metal production is the main contributor of atmospheric As (69%), Cd (73%), Cu (70%), In (100%), and Zn (72%). Further, the contribution of waste incineration is challenging to estimate due to that a couple of countries do not report their emissions (AMAP, 2005).

According to AMAP (2002), about two-thirds of the heavy metal concentrations in the Arctic region derives from outside sources such as the Kola Peninsula, the Norilsk region, the Pechora Basin, and the Urals in winter. The behavior, fate, and removal of heavy metals during long-range atmospheric transport are influenced by their physical and chemical form when they are emitted into the atmosphere (AMAP, 2005). Most heavy metals are emitted as aerosols, which means that the transportation distance is highly influenced by the size of the particle (AMAP, 2005). Heavy metals as part of aerosols can be transported up to a few thousand kilometers. Mostly mercury (Hg) and selenium (Se) are emitted in the gaseous phase. In the gaseous phase, heavy metals can become globally distributed (AMAP, 2005). Mainly heavy metals and beryllium are known to be hazardous for human health, out of which lead is of greatest concern in urban atmospheres, followed by mercury (Manahan, 2010).

2.4.1 Relevant Previous Studies on Element Concentrations

Three studies were found that report concentrations of different elements in Arctic snow. De Caritat et al. (2005) studied concentration levels and regional distribution of major elements in arctic snow. Their study showed that major element concentration in the snow was consistent with diluted seawater composition. Additionally, a study on Hansbreen, Svalbard, showed predominant concentrations of Na, Mg, and K followed by Zn, Ca, Al, and Fe (Koziol et al., 2021). Using cluster analysis, the study divided the measured metals and metalloids on the glacier into three groups: 1. Ag, As, Bi, Cd, Hg, Mo, Sb, Se, and Zn, 2. Al, Fe, Cu, and

Mn, 3. Na, Ca, Mg, K, and Sr. Group 1 mainly represents long-range transported volatile elements, group 2 elements with crustal sources, and group 3 elements deriving from sea spray aerosols (Koziol et al., 2021). Similar to the study on Hansbreen, another study on Austré Brøggerbreen, Svalbard, found predominant concentrations of Na and Cl followed by Mg, Ca, K, Br, and I (Spolaor et al., 2021). The study on Austré Brøggerbreen researched the dynamics of ionic species in the snow. Over the spring season a general decrease in concentration was found for Na, K, Ca, and Mg (Spolaor et al., 2021). On Midtre Lovénbreen, Svalbard, a study on element concentrations in surface and subsurface ice showed that either local or transboundary anthropogenic sources affect the element concentrations on the glacier (Singh et al., 2015).

Studies found on element concentration in snow on mainland Norway focused on urban pollution and are therefore not relevant for this study. Instead, studies showing spatial distributions in moss and surface soils in Norway were found. Harmens et al. (2010) studied heavy metal deposition in moss in Europe. Their main finding was that spatial patterns of heavy metal concentrations are metal specific but that in general the lowest concentrations could be found in northern Scandinavia. In surface soil, the influence of natural and anthropogenic atmospheric sources on the soil concentrations in Norway was investigated (Steinnes and Lierhagen, 2018). They found that Pb, As, Sb, and Cd concentrations are influenced by transboundary atmospheric transport and that Na, Mg, Se, and Br concentrations are mainly influenced by atmospheric deposition of marine origin (Steinnes and Lierhagen, 2018). The mentioned studies are summarized in Table 1.

Table 1 Relevant previous studies on elements. The matrix the elements were measured in, location, elements measured, the concentrations (as specified in the publications), when the study was conducted and reference to the studies are listed in the table.

Matrix	Location	Elements measures	Concentration	When	Reference
Snow	Svalbard, Norway, Canada, Finland, Greenland, Iceland, Russia, USA	Ca K Mg Na S	0.26 mg L ⁻¹ (0.02-7.82) 0.18 mg L ⁻¹ (<0.050-7.33) 0,449 mg L ⁻¹ (0.008-23.642) 2.86 mg L ⁻¹ (0.02-232.3) 0.32 mg L ⁻¹ (0.06-7.64)	1997	(De Caritat et al., 2005)
Seasonal snow	Austré Brøggerbreen, Svalbard	Na ⁺ Cl ⁻ Mg ²⁺ Ca ²⁺ K ⁺ Br ⁻ I ⁻	2-8 µg g ⁻¹ 1.1-3.5 µg g ⁻¹ 0.1-0.8 µg g ⁻¹ 81-580 ng g ⁻¹ 88-313 ng g ⁻¹ 0.7-2.0 ng g ⁻¹ 0.2-0.8 ng g ⁻¹	2015	(Spolaor et al., 2021)
Snow	Hansbreen, Svalbard	Ag Al As Bi Ca Cd Cu Fe Hg K	0.059 µg L ⁻¹ (0.000-1.883) 5.74 µg L ⁻¹ (3.97-14.3) 0.274 µg L ⁻¹ (0.027-1.91) 0.933 µg L ⁻¹ (0.358-9.26) 15.1 µg L ⁻¹ (11.4-53.8) 0.065 µg L ⁻¹ (0.037-0.186) 1.86 µg L ⁻¹ (1.16-5.64) 4.31 µg L ⁻¹ (3.08-8.31) 0.000 µg L ⁻¹ (0.000-0.167) 154 µg L ⁻¹ (69.9-270)	2018	(Koziol et al., 2021)

		Mg Mn Mo Na Sb Se Sr Zn	192 $\mu\text{g L}^{-1}$ (30.2-563) 1.10 $\mu\text{g L}^{-1}$ (0.629-3.23) 0.000 $\mu\text{g L}^{-1}$ (0.000-2.05) 1020 $\mu\text{g L}^{-1}$ (210-2490) 0.226 $\mu\text{g L}^{-1}$ (0.113-2.72) 0.889 $\mu\text{g L}^{-1}$ (0.139-2.74) 2.17 $\mu\text{g L}^{-1}$ (1.30-4.45) 9.25 $\mu\text{g L}^{-1}$ (0.228-132)		
Surface and sub-surface ice	Midtre Lovénbreen, Svalbard	As B Ba Ca Cd Co Cr Cs Cu Fe Li Mg Mn Ni Pb Rb Se Sr V Zn	0.0003 – 0.0410 ppm 0-3.4123 ppm 0.0240 – 0.5007 ppm 13.37 – 713.77 ppm 0.0007 – 0.0217 ppm 0.001 – 0.0283 ppm 0 – 0.2027 ppm 0 – 0.007 ppm 0.2297- 8.8860 ppm 0 – 5.1660 ppm 0 – 3.282 ppm 5.68 – 752.40 ppm 0.0787 – 1.0807 ppm 0 – 1.0390 ppm 0 – 0.0467 ppm 0.004 – 0.081 ppm 0 – 0.0820 ppm 0.054 – 6.7870 ppm 0 – 0.0923 ppm 0.38 – 49.59 ppm	2009	(Singh et al., 2015)

Moss	Europe (Concentrations listed are from Norway)	As Cd Cr Cu Fe Hg Ni Pb V Zn Al Sb	0.12 mg kg ⁻¹ (STD 0.28) 0.089 mg kg ⁻¹ (STD 0.15) 0.58 mg kg ⁻¹ (STD 3.37) 4.37 mg kg ⁻¹ (STD 33.2) 273 mg kg ⁻¹ (STD 693) 0.054 mg kg ⁻¹ (STD 0.024) 1.24 mg kg ⁻¹ (STD 50.6) 2.17 mg kg ⁻¹ (STD 3.13) 1.40 mg kg ⁻¹ (STD 1.69) 31.4 mg kg ⁻¹ (STD 38.2) 255 mg kg ⁻¹ (STD 834) 0.070 mg kg ⁻¹ (STD 0.10)	2005/2006	(Harmens et al., 2010)
Natural surface soils	Norway	Na Br Se Eu Ba Rb Fe Al Sc As Pb Cd	25.2 – 1624 mg kg ⁻¹ 1.1 – 236 mg kg ⁻¹ 0.07 – 3.30 mg kg ⁻¹ 0.2 – 12.7 mg kg ⁻¹ 8.1 – 440 mg kg ⁻¹ 0.9 –71.2 mg kg ⁻¹ 293 – 61016 mg kg ⁻¹ 319 – 33812 mg kg ⁻¹ 0.07 – 6.10 mg kg ⁻¹ 0.1 – 24.5 mg kg ⁻¹ 3.8 – 1260 mg kg ⁻¹ 0.05 – 5.71 mg kg ⁻¹	2005	(Steinnes and Lierhagen, 2018)

2.4.2 Analytical Techniques for Element Analysis

There are several different methods for analyzing element concentrations in samples, such as Flame Atomic Emission/Absorption, Graphite Furnace Atomic Absorption, and ICP-MS. However, Flame Atomic Emission/Absorption and Graphite Furnace Atomic Absorption are only suitable for single or limited amounts of elements, while ICP-MS is capable of analyzing multiple elements in one sample (Wilschefski and Baxter, 2019; Yeung et al., 2017).

Inductively coupled plasma mass spectrometry (ICP-MS) is an analytical technique used to measure the elemental composition of both organic and inorganic samples at trace levels (Wilschefski and Baxter, 2019). The technique was first developed 30 years ago and is now the most widely used method for the determination of metal concentrations in samples, due to its capability to measure multiple elements in the same sample (Wilschefski and Baxter, 2019). Although the technique has several advantages, such as multi-element analysis, large analytical range, low detection limit, simple sample preparation, and low sample volume, there are also disadvantages such as equipment cost, operating cost, a requirement of multiple high purity gases, high level of staff expertise, and that interferences need to be controlled (Wilschefski and Baxter, 2019).

ICP-MS systems usually consist of a nebulizer, spray chamber, plasma torch, interface cones, vacuum chamber, ion optics, a mass analyzer, and a detector (Thomas, 2013). The sample is usually injected as a liquid and converted to a fine aerosol spray with argon gas in the nebulizer. As only fine aerosol droplets should enter the plasma torch, the spray chamber removes about 98-99% of the aerosols and only the finest droplets can pass on (Thomas, 2013). The torch produces the plasma, which is an ionized gas that consists of positively charged ions and free electrons, by letting a tangential flow of gas (e. g. argon) interact with an intense magnetic field (Wilschefski and Baxter, 2019). The magnetic field is produced by a radiofrequency (RF) that is passing through a copper coil that surrounds a concentric tube through which the gas flows. This leads to ionization of the gas, which together with a source of electrons from a high-voltage spark forms a plasma (Thomas, 2013). The plasma torch is used to desolvate, vaporize, atomize, and ionize the sample (Wilschefski and Baxter, 2019). The next step is the interface, which consists of two coaxial cones, which separate the plasma from the mass spectrometer's vacuum chamber. The purpose of the interface is to transport the ions from the plasma, having an atmospheric pressure of about 760 torr, to the mass analyzer region with an atmospheric pressure of 10^{-6} torr (Thomas, 2013). Through a small orifice at the tip of the first cone, called the sample cone, the ions, photons, and neutral atoms

or molecules are extracted from the plasma into the interface region between the cones. From there on, only the ions are extracted from the interface through an even smaller orifice in the second cone, called the skimmer cone, into the main vacuum chamber. In the vacuum chamber, a set of electrostatic lenses are positioned to guide the stream of ions towards the mass analyzer, referred to as the ion optics. It further prevents photons and other neutral species from reaching the mass analyzer (Wilschefski and Baxter, 2019).

Several different mass analyzers can be used such as magnetic sector, time-of-flight (TOF), or quadrupole, all serving the same purpose of measuring the mass-to-charge (m/z) ratio of the analytes in the sample (Thomas, 2013). A quadrupole consists of four parallel hyperbolic or cylindrical metallic rods that are positioned in a square array. On opposite pairs of the rods a direct current (DC) field and a time-dependent alternating current (AC) of radiofrequency are placed, which creates a time-varying electrical field through which the ions pass. Only specific combinations of the alternating current potential and the direct current potential lead to a stable ion flight for an ion with a specific m/z ratio, through which the ions will be separated from each other (Thomas, 2013). A triple quadrupole, consisting of two quadrupoles separated by an octupole reaction system (ORS), has been developed to further improve accuracy and consistency, especially in complex sample matrices (Agilent Technologies, 2015). The function of the first quadrupole is to control the ions that pass through the ORS. The ORS is a temperature-controlled collision/reaction cell with an octupole ion guide and four cell gas lines to increase flexibility in collision and reaction modes. In the ORS the ions and the cell gases interact ensuring the removal of interference from the mass spectrum (Agilent Technologies, 2015). The second quadrupole filters the ions that emerge from the ORS leading to that only the target analyte ions can pass through to the detectors leading to improved peak separation (Agilent Technologies, 2015). This leads to that even for difficult elements, the background is essentially zero (Agilent Technologies, 2015). The detector converts the arriving ions to electrical signals that can be quantified (Wilschefski and Baxter, 2019).

2.5 Polycyclic Aromatic Hydrocarbons (PAHs)

Polycyclic aromatic hydrocarbons (PAHs) are semi-volatile compounds composed of at least two fused benzene rings containing only hydrogen and carbon atoms (Stout et al., 2015).

Sources of PAHs can be categorized into three groups: 1) Petrogenic, 2) Pyrogenic, and 3) Biogenic. Petrogenic PAHs are formed from organic matter in ancient rocks/sediments together with the formation of fossil fuels by geological processes (Stout et al., 2015).

Pyrogenic PAHs are generated by incomplete combustion or pyrolysis of different types of organic matter such as wood, petroleum, and coal. Lastly, biogenically derived PAHs are created by the transformations of biological precursors in the environment by chemical or biological processes (Stout et al., 2015).

PAHs in the atmosphere are mainly derived from pyrogenic sources (Balmer et al., 2019).

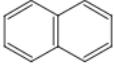
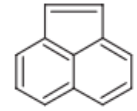
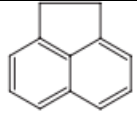

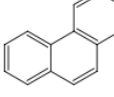
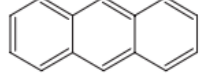
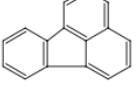
Pyrogenic sources can both be natural and anthropogenic. Natural pyrogenic sources include volcanic eruptions and forest fires while anthropogenic pyrogenic sources include the combustion of wood, coal, and fossil fuels in vehicles, industries, or houses for different purposes (Balmer et al., 2019). Many PAH congeners are toxic, mutagenic, and/or carcinogenic (Abdel-Shafy and Mansour, 2016). The U.S. EPA has therefore identified 16 of the PAH congeners as priority PAHs in 1976, see Table 2 (EPA, 2021). Priority pollutants are a set of chemicals that EPA regulates and has published analytical test methods for (EPA, 2021).

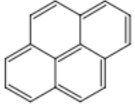
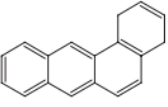
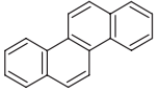
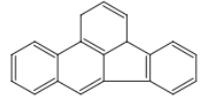
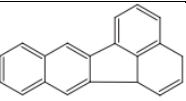
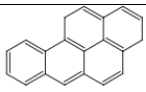
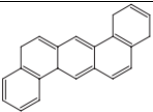
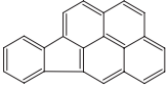
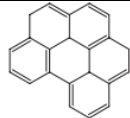
In general, PAHs are volatile to semi-volatile as they have high melting and boiling points, low vapor pressures, and low water solubility (Table 2). The volatility of the PAH congeners decreases with increasing molecular mass (Balmer et al., 2019). PAHs, especially those with three or four rings, are classified as semi-volatile, meaning that their vapor pressure is between 10^{-6} and 10^{-2} Pa (Balmer et al., 2019). According to models, PAHs with 3-5 rings have atmospheric half-lives of hours or days during which they are transported (Keyte et al., 2013). They are deposited either through wet or dry deposition, where their half-lives are up to the order of decades. Due to their semi-volatility, they can re-volatize from the terrestrial compartment or seawater and undergo further atmospheric transportation (Keyte et al., 2013).

PAHs can be emitted into the atmosphere, either in gas phase or adsorbed to particles. After emission, atmospheric PAHs in the gas phase can either remain in the gas phase or sorb to particles (Lammel et al., 2009). Simulations have shown that gas-particle partitioning has a substantial effect on long-range atmospheric transport (Lammel et al., 2009). PAHs adsorbed

to particles will deposit faster than PAHs that stay in the gas phase (Lammel et al., 2009). Gas-particle partitioning of a semi-volatile organic compound can be quantified by the gas-particle partitioning coefficient K_p ($\text{m}^3\mu\text{g}^{-1}$) (Keyte et al., 2013). Another partitioning coefficient that is often used for organic pollutants' adsorption to particles is the octanol-air partition coefficient K_{OA} (Friedman and Selin, 2012). Further, gas phase reactions can occur between PAHs and atmospheric oxidants, i.e. OH, NO₃ and O₃, leading to oxy-derivates and nitrated compounds (Keyte et al., 2013). These are not taken into consideration when measuring the targeted PAH analytes, which can create problems for receptor modeling methods (Keyte et al., 2013).

Table 2 PAH characteristics important for LRAT: Molecular structure, Molar mass (g mol^{-1}), Water solubility (mg L^{-1}), Log Kow, Log K_{OA}, Henry's law constant K_H ($\text{pa m}^3 \text{mol}^{-1}$) and particle/gas phase distribution (Ravindra et al., 2008; Tobiszewski and Namieśnik, 2012).

	Abbrev.	Molecular structure	Molar mass [g mol^{-1}]	Water solubility [mg L^{-1}] at 25°C	Log Kow at 25°C	Log K _{OA}	Henry's law constant K _H [$\text{pa m}^3 \text{mol}^{-1}$]	Particle/ gas phase distribution
2-ring PAHs								
Naphthalene	NAP		128.17	31	3.37	5.1	42.6	-
3-ring PAHs								
Acenaphthylene	ACY		152.20	16	4	6.36	12.7	Gas phase
Acenaphthene	ACE		154.21	3.8	3.92	6.3	18.5	Gas phase
Fluorene	FLU		166.22	1.9	4.18	6.7	9.8	-
Phenanthrene	PHE		178.23	1.1	4.46	7.5	4.3	Particle gas phase
Anthracene	ANT		178.23	0.04	4.49	7.3	4.45	Particle gas phase
4-ring PAHs								
Fluoranthene	FLT		202.26	0.2	8.9	8.6	1.96	-

Pyrene	PYR		202.26	0.13	8.8	8.6	1.7	Particle gas phase
Benzo[a]anthracene	BaA		228.29	0.011	5.8	9.5	1.22	Particle phase
Chrysene	CHR		228.29	0.0019	5.73	10.4	0.53	Particle phase
5-ring PAHs								
Benzo[b]fluoranthene	BbF		252.32	0.0015	5.78	-	0.05	Particle phase
Benzo[k]fluoranthene	BkF		252.32	0.0008	6.5	11.2	0.04	Particle phase
Benzo[a]pyrene	BaP		252.32	0.0015	6.35	10.8	0.07	Particle phase
Dibenzo[a,h]anthracene	DBA		278.35	0.0005	6.5	-	0.0075	Particle phase
6-ring PAHs								
Indeno[1,2,3-cd]pyrene	IND		276.33	0.00019	6.7	-	0.029	Particle phase
Benzo[ghi]perylene	BgP		276.33	0.00014	6.63	-	0.031	Particle phase

2.5.1 Relevant Previous Studies on PAHs

Only one study on PAH concentrations in snow on Svalbard was found (Vecchiato et al., 2018). In the study, snow in the area of Ny-Ålesund was collected to study local and long-range atmospheric contamination in the snow. Vecchiato et al. (2018) measured 16 PAH congeners in the snow and found concentrations varying between 2.6 and 299 ng L⁻¹. However, the authors noted that some of the samples were influenced by coal dust from previous mining activities. Further, they measured PAHs in a snow-pit on Austre Brøggerbreen and found concentrations ranging between 3 – 14 ng L⁻¹. Na et al. (2011) measured similar total concentrations in Fildes Peninsula, Antarctica, (52.15 – 272.29 ng L⁻¹) as Vecchiato et al. (2018). In addition to long-range atmospheric sources, they further state that local monitoring stations could contribute to local sources of PAHs in the snow. The main components of the total PAH concentration were 2-ring and 3-ring PAHs. Another study in Antarctica, Warszawa icefield, measured 9 PAH congeners and found generally lower concentrations (0.11 – 1.4 ng L⁻¹) than the other studies.

Further, 3 studies measuring PAHs in air were found (Drotikova et al., 2020; Garrido et al., 2014). Drotikova et al. (2020) studied the local emission of PAH from the Longyearbyen coal power plant, Svalbard, simultaneous as two other additional sample positions further away from the coal plant along a transect. The study showed that phenanthrene, fluorene, fluoranthene, and pyrene are the major congeners emitted from the coal powerplant, not including naphthalene. A dilution factor of 0.63 ± 0.14 ng m⁻³ was observed from the coal power plant to Adventdalen, located 6 km away from the power plant. Garrido et al. (2014), on the other hand, studied levels and trends of atmospheric PAHs in Europe, including measurements in Norway and Svalbard. In general, Garrido et al. (2014) found higher concentrations of PAHs during the colder months. Further, they found negative latitudinal gradients for 4 out of the 15 measured PAHs; PHE, FLT, PYR, and BgP. The mentioned studies are summarized in Table 3.

Table 3 Relevant previous studies on PAHs. Matrix they were measured in, location, congeners measured, the concentration range found, when the study was conducted and reference to the study are listed in the table.

Matrix	Location	PAH measured	Concentration	When	Reference
Snow	Ny-Ålesund	\sum_{16} PAH	2.6 – 299 ng L ⁻¹	2017	(Vecchiato et al., 2018)
Snow	Fildes Peninsula, Antarctica	\sum_{16} PAH	52.15 – 272.29 ng L ⁻¹	2009	(Na et al., 2011)
Snow	Warszawa Icefield, Antarctica	\sum_9 PAH	0.11-1.4 ng L ⁻¹	2017	(Szumińska et al., 2021)
Air	15 stations in Europe, including Birkenes, Norway, and Svalbard	\sum_{15} PAH	Birkenes: 0.2 – 0.5 ng m ⁻³ Svalbard: 0.05 – 0.2 ng m ⁻³	Birkenes: 2009-2011 Svalbard: 1994-2010	(Garrido et al., 2014)
Air	Adventdalen Longyearbyen, Svalbard	\sum_{16} PAH	279.0 – 454.5 pg m ⁻³	2018	(Drotikova et al., 2020)

2.6 Polychlorinated Biphenyls (PCBs)

Polychlorinated biphenyls (PCBs) are a group of 209 different congeners that are classified as persistent organic pollutants (POPs) (EPA, 2022). PCBs are man-made and characterized by a biphenyl main structure with varying positions and degrees of chlorinated substitutions. The domestic manufacturing of PCBs started in 1929 for the usage in hundreds of industrial and commercial products such as electrical products, hydraulic equipment, as plasticizers and in pigments and dyes (EPA, 2022). Manufacturing of these compounds was banned in 1979 due to the adverse health effects of PCBs in both humans and wildlife including cancer, and effects on the immune system, reproductive system, nervous system, and endocrine system (EPA, 2022). Even now, long after the ban, PCBs can still be released into the atmosphere for instance through leaks or releases from electrical transformers containing PCBs, poorly maintained hazardous waste sites, or dumping of PCB waste into landfills not designed for hazardous waste. Furthermore, PCBs do not break down readily in the environment and they, therefore, remain in the environment for a long time (EPA, 2022). PCBs have been found in all kinds of different matrixes in the environment (Arp et al., 2020; Cleemann et al., 2000;

Hermanson et al., 2020b; Polkowska et al., 2011). However, a decrease in PCB concentrations in arctic air has been detected during the last 25 years (Wong et al., 2021).

PCBs are in general lipophilic, and their lipophilicity increases with increasing degree of chlorination. On the other hand, their water solubility and volatility are low and they decrease with increasing degree of chlorination (Table 4) (World Health Organization, 2000).

Therefore, PCB congeners with a higher degree of chlorination are more frequently associated with particles. Trichlorobiphenyls, for instance, have a particulate percentage between 2-5%, while for octachlorobiphenyls it is > 90% at 10°C (Falconer and Bidleman, 1994). Further, Falconer and Bidleman (1994) proved that PCBs with fewer ortho-chlorines have higher particulate percentages than PCBs with higher amounts of ortho-chlorines within the same homolog. The degree of chlorination and their position affects the congeners partitioning characteristics and therefore their environmental fate.

A study by Agrell et al. (2002) showed that PCB concentration in precipitation decreased with increasing temperature, but the magnitude of the slope was dependent on the chlorination of the congener. Highly chlorinated congeners had a flatter slope than less chlorinated congeners, which the authors explain by the higher atmospheric concentrations of low chlorinated PCB congeners during low temperatures. Additionally, the study also found an increase with a factor of 2 in the wash-out ratio of PCBs during snow scavenging events. The deposition during winter in their study was dominated by low chlorinated congeners (Agrell et al., 2002).

Table 4 PCB characteristics important for LRAT. Structure, molar mass (g mol^{-1}), partitioning coefficients K_{OA} (Octanol-air) and K_{OW} (Octanol-water), and Henry's law constant K_H ($\text{Pa m}^3 \text{mol}^{-1}$) (Li et al., 2003; Mwanza et al., 2021).

Abbreviation	Name	Structure	Molar mass (g mol^{-1})	K_{OA}	K_{OW}	K_H ($\text{Pa m}^3 \text{mol}^{-1}$)
PCB-28	Trichlorobiphenyl 2,4,4N		257.54	7.85	5.66	1.48
PCB-52	Tetrachlorobiphenyl 2,2N,5,5N		291.99	8.22	5.91	1.40
PCB-101	Pentachlorobiphenyl 2,2N,4,5,5N		326.43	8.73	6.33	1.38
PCB-118	Pentachlorobiphenyl 2,3N,4,4N,5		326.43	9.36	6.69	1.16
PCB-138	Hexachlorobiphenyl 2,2N,3,4,4N,5N		360.88	9.66	7.22	1.48
PCB-153	Hexachlorobiphenyl 2,4,5,2',4',5'		360.88	9.44	6.87	1.30
PCB-180	Heptachlorobiphenyl 2,2N,3,4,4N,5,5N		395.32	10.16	7.16	0.93

2.6.1 Relevant Previous Studies on PCBs

Previously, a study on PCB concentrations in the snow on top of 4 different glaciers around Svalbard has been conducted (Hermanson et al., 2020a). In the study, they measured 209 different PCB congeners and found the highest total PCB fluxes in the western sites measured on Svalbard ($26.7 \text{ pg cm}^{-2} \text{ yr}^{-1}$). At all sites PCB-52, 70+74, 95, 101, and 110 were the most concentrated, comprising 32-39% of the total concentration (Hermanson et al., 2020a). Agrell et al. (2002) studied the annual and seasonal deposition fluxes in precipitation in 16 stations around the Baltic Sea. Generally, they did not find any statistically significant latitudinal trends, but showed that the wash-out ratio of PCBs increased by a factor of 2 during snow scavenger events.

Two studies on PCB concentrations in ice cores were found on Svalbard (Garmash et al., 2013; Hermanson et al., 2020b). Garmash et al. (2013) studied an ice core representing 1957-2009 and snow from 2009/2010. They measured 209 PCB congeners and found a prevalence of tetra- and pentachlorobiphenyls in all samples. Further, they found peak fluxes in 1957-1966, 1974-1983, 1998-2009. As PCB was phased out in 1983 the peak fluxes afterward indicate distribution processes that could include secondary sources to the atmosphere (Garmash et al., 2013). Similar to Garmash et al. (2013), Hermanson et al. (2020b) found that the PCB congeners with the highest concentrations of the triCB, tetraCB, and pentaCB in Holtedalsfonna in the ice core from 1953-2005. They divided the core into 6 segments and found concentrations ranging between $106\text{-}1230 \text{ pg L}^{-1}$. Surface snow on Holtedalsfonna in 2014 was 591 pg L^{-1} . However, they hypothesize that the low-molecular-mass PCB congeners that were found in higher concentrations in the snow compared to the ice, might evaporate back into the atmosphere during summer and not be incorporated into the ice (Hermanson et al., 2020b).

For Norway, only studies reporting measurements in the air were found (Lunder Halvorsen et al., 2021; Ubl et al., 2012). Ubl et al. (2012) investigated the source regions of atmospheric PCB concentrations of among others Zeppelin, Svalbard, and Birkenes, Norway. The study concluded that Western Russia was the dominant source region for PCB-28 and PCB-101 to the arctic, while PCB-180 mostly derives from central Europe. The study by Lunder Halvorsen et al. (2021) used passive samplers at 45 remote sites in Norway and 2 on Svalbard. In general, concentrations of the PCBs were low and a limited spatial variability was found, suggesting LRAT to be the dominating source of PCBs in Norway. The concentrations found in the different studies are summarized in Table 5.

Table 5 Relevant previous studies on PCBs. Matrix they were measured in, location, congeners measured, the concentrations found (as specified in the articles), when the study was conducted and reference to the study are listed in the table.

Matrix	Location	PCBs measured	Concentration	When	Reference
Snow	Holtedahlfonna, Kongsvegen, Lomonosovfonna, Austfonna (Svalbard)	\sum_{209} PCB	458 - 844 pg L^{-1}	2013-2014	(Hermanson et al., 2020a)
Precipitation	Around the Baltic Sea	\sum_{51} PCB annual mean	0.8-10.7 ng L^{-1}	1990-1993	(Agrell et al., 2002)
Ice core	Lomonosovfonna (Svalbard)	\sum_{209} PCB	5.75 - 19 $\text{pg cm}^{-2} \text{ year}^{-1}$	1957-2009	(Garmash et al., 2013)
Ice core	Holtedahlfonna (Svalbard)	\sum_{81} PCB	106 - 1230 pg L^{-1}	1953 - 2005	(Hermanson et al., 2020b)
Air	Zeppelin (Svalbard)	PCB-28 PCB-101 PCB-180	2 – 4 pg m^{-3} 0.3 – 0.5 pg m^{-3} 0.04 – 0.06 pg m^{-3}	1998-2009	(Ubl et al., 2012)
Air	Birkenes (Norway)	PCB-28 PCB-101 PCB-180	1.2 - 1.5 pg m^{-3} 0.6 – 0.8 pg m^{-3} 0.07 – 0.2 pg m^{-3}	2004-2009	(Ubl et al., 2012)
Air	At 45 remote sites in Norway + 2 on Svalbard	\sum_6 PCB	1.03 - 5.72 pg m^{-3}	2016	(Lunder Halvorsen et al., 2021)

2.7 Sample Pretreatment and GC-MS Analysis for PAHs and PCBs

Organic pollutants can usually not be analyzed in environmental water samples without preliminary sample preparations, as the analytes in the sample are too diluted and the matrix too complex (Barcelo, 2000). Large volumes of the sample need to be concentrated and cleaned before analysis to overcome the limit of detection and to achieve efficient separation of the compounds in the sample. The pretreatment of the sample generally involves one or more of the following steps: 1) extraction 2) concentration and 3) clean-up (Barcelo, 2000).

Several different techniques can be used to extract the analytes from the sample. Generally, the techniques can be divided into liquid-liquid extraction and liquid-solid extraction (Barcelo, 2000). Solid-phase extraction (SPE) has since the 1980s revolutionized the extraction and clean-up techniques, making the procedure less time-consuming and more reliable, in addition to reducing the consumption of expensive and sometimes harmful solvents (Hübschmann, 2015). SPE methods are both efficient at cleaning up the sample and at concentrating the analytes, which is often required to reach detectable concentrations of the analyte (Hübschmann, 2015).

For SPE a sorbent is packed into either a disposable cartridge, a column, or enmeshed in an inert matrix of a membrane-based extraction disk. About 100 to 2000 mg of the sorbent is used and it is retained between two porous frits (Barcelo, 2000). Before the sample can be added to the SPE cartridge, the cartridge needs to be activated by wetting the sorbent with a suitable solvent and by conditioning it with water. The sample is then percolated through the sorbent, which can be aspirated by vacuum (Barcelo, 2000). If the interactions between the analytes and the solid phase packing material are higher than the interactions of the analyte with the solvent or the matrix components the extraction is successful. This leads to the analytes adsorbing to the sorbent in the cartridge, while the other sample components pass through the column unhindered (Hübschmann, 2015). Elution of the analyte from the sorbent is achieved by changing to a solvent that interacts more strongly with the analyte than the SPE sorbent (Hübschmann, 2015). As mentioned, SPE simultaneously carries out the extraction and concentration of many organic compounds in water samples, however, the eluate can be further concentrated by gentle evaporation to increase the enrichment factor (Barcelo, 2000).

The main problems with extraction procedures are the risk of contamination of the sample, degradation of the sample, insufficient extraction, and evaporation loss (Jacob, 1995). To avoid sample contamination, all glassware used should be cleaned carefully by using a freshly

redistilled solvent. Degradation of the sample can occur by for example photooxidation of photosensitive analytes such as many PAHs (Jacob, 1995). Exposure of the samples to sunlight should therefore be avoided. The efficiency of the extraction depends on the extraction method, the solvents chosen, and on the matrix (Jacob, 1995).

The concentrated eluate can then be analyzed by gas chromatography mass spectrometry (GC-MS). GC is a chromatographic technique using gas as the mobile phase and a stationary phase consisting of a liquid with a high boiling point coated onto an inert solid support to separate gases or volatile analytes before being detected in a mass spectrometer (Welch, 2000). A calibrated microsyringe is used to measure and transport the specified sample volume from the sample container to the vaporization chamber, where it is injected through a self-sealing silicone rubber (Welch, 2000). The sample can be injected splitless or with split, which means that either the full injected sample volume is analyzed, or the initial sample volume is split and only a small fraction is analyzed to avoid overloading of the column. In the vaporization chamber, the sample is vaporized by heating the sample 50°C above the lowest boiling point of the sample. The sample is then mixed with the carrier gas and transported into the column (Welch, 2000). The column is placed in an oven with a thermostat which serves to control the temperature of the column. There are two different ways to use the column oven, either the temperature is set in the middle of the boiling point range of the sample (isothermal programming), or the temperature is either increased continuously or in steps as the separation progresses (temperature programming). If the sample contains a wide range of boiling points, temperature programming is better suited for the separation (Welch, 2000).

At the end of the column, the samples will be eluted into the detector, which provides quantitative measurements of the components of the mixture as they elute. A mass spectrometer (MS) is one type of detector that measures the abundance of ions according to their masses (Shrader, 2013). As an MS operates under a high vacuum, the analyte needs firstly to be transferred from atmospheric pressure to the high vacuum. Then the sample is ionized, for which many different techniques have been developed such as electron ionization, chemical ionization, and photoionization (Shrader, 2013). Electron ionization uses a high-energy electron beam to excite molecules, which leads to ejections of electrons from the molecule leaving a positively charged ion. The ions are then separated depending on their mass to charge (m/z) ratio, using for example a quadrupole described in chapter 2.4.2.

To be able to quantify the analytes separately each analyte should have different retention times, meaning that the time it takes for the different analytes to pass through the column differs. The retention time of a compound can be identified by analyzing an external standard of the same analyte under the same conditions (Budde et al., 1995). Further, the concentration of the compound can be measured by relating the response of the MS from the sample to the response of the MS from different concentrations of the external standard (calibration curve) (Budde et al., 1995). For more accurate quantification, internal standards can be used to account for losses during sample preparation steps and potential differences in the injected sample volume into the GC (Sparkman et al., 2011). An internal standard is a pure analyte that is added in known amounts to samples, extracts, and/or external standards to measure the relative responses. The internal standard should chemically resemble the target analyte but differ in retention time and should not be a sample component (Budde et al., 1995; Sparkman et al., 2011). Calibration curves, consisting of different known concentrations of the target analytes and the internal standards, are created for each target analyte by plotting the relative response of the MS against the concentration of the analyte (Asimakopoulos et al., 2014). The limit of detection and the limit of quantification can be calculated using the signal-to-noise ratio (S/N), meaning the intensity of the signal compared to the background noise of the instrument. The limit of detection is usually set as 3 times the signal-to-noise ratio, while the limit of quantification is set as 10 times the signal-to-noise ratio (Equation 1, Equation 2) (Lundanes et al., 2014).

$$\text{Equation 1:} \quad LOD = 3 \times \frac{S}{N}$$

$$\text{Equation 2:} \quad LOQ = 10 \times \frac{S}{N}$$

During several steps of the sample pretreatment losses of analyte can occur e.g., during the extraction or concentration (Fajgelj et al., 1999). Recovery studies are therefore used to validate the method and to correct for biases. The recovery of a method can be measured by adding a known amount of analyte (spiking) to either a matrix blank or to an aliquot of a sample before extraction or post extraction (Asimakopoulos et al., 2014; Fajgelj et al., 1999). This is called a surrogate recovery study (Fajgelj et al., 1999). The absolute recovery (%) is the response of the pre-extraction spiked sample ($Area_S$) minus the response of the method blank ($Area_B$) divided by the post-extraction spiked sample ($Area_P$) minus the response of the method blank ($Area_B$):

$$\text{Equation 3:} \quad AR = \frac{(Area_S - Area_B)}{(Area_P - Area_B)} \times 100$$

As mentioned before, an internal standard can be used to determine concentrations more accurately. If an internal standard is used in the recovery test, the relative recovery (%) can be calculated using equation 4, where $Area_{IS}$ is the area of the internal standard in the pre-extraction spiked sample (S), blank (B), and post-extraction sample (P) (Asimakopoulos et al., 2014).

Equation 4:

$$RR = \frac{\left(\frac{Area_S}{Area_{IS,S}} - \frac{Area_B}{Area_{IS,B}}\right)}{\left(\frac{Area_P}{Area_{IS,P}} - \frac{Area_B}{Area_{IS,B}}\right)} \times 100$$

2.8 Principal Component Analysis (PCA)

Principal component analysis (PCA) is a type of multivariate data analysis, used to interpret large datasets. PCAs reduce the dimensionality of a dataset while preserving as much variability as possible. It is mainly used as an exploratory tool for data analysis. The objective of using a PCA is usually to find relationships between objects (Wold et al., 1987). In the field of environmental chemistry, PCAs can be used for emission source identification, depending on the grouping of the compounds (Ravindra et al., 2008).

PCAs take datasets with p numerical variables (e.g. measurements such as different concentrations) for n entities or individuals (e.g. samples) and it creates p n -dimensional vectors (Jolliffe and Cadima, 2016). These vectors are called score vectors. From these score vectors, a direction coefficient is comprised giving each sample or entity a loading vector (Wold et al., 1987). Linear combinations of the score vectors are compared to find the highest variance between them. These linear combinations are called the principal components of the dataset (Jolliffe and Cadima, 2016). The principal component showing the maximum amount of variance is called PC1. PC2 is the highest variance that is perpendicular to PC1 (Ringnér, 2008). Usually, the data is centered using the mean of the column to move the coordinate system to the middle of the dataset. Further, the data set is scaled so each column has a variance of 1 to avoid bias in the dataset (Wold et al., 1987).

3 Method

3.1 Sampling Sites

In total, 16 different glaciers were sampled from the 15th of April to the 22nd of August 2021. The glaciers are distributed from the south of Norway (Rembesdalskåka 60.54°N) up to the Arctic Archipelago Svalbard (Midtre Lovénbreen 78.87°N). Ten glaciers were sampled on mainland Norway: Austdalsbreen (1), Storbreen (2), Gråsubreen (3), Hellstugubreen (4), Juvfonne (5), Nigardsbreen (6), Engabreen (7), Rembesdalskåka (8), Langfjordjøkelen (9), and Ålfotbreen (10) (See Figure 1). All these glaciers were sampled by or with the help of the glacier department of the Norwegian Water Resources and Energy Directorate (NVE). On Svalbard, six glaciers in total were sampled. Austre Brøggerbreen (13.1), Edithbreen (15), and Kongsvegen (16) were sampled during spring by the Norwegian Polar Institute (NPI) and during the summer Austre Brøggerbreen (13.2) was sampled again in addition to Midtre Lovénbreen (14), Platåbreen (11) and Linnébreen (12) by this author. The positions of the glaciers are shown in Figure 1, and Table 6 shows the date of sampling, the coordinates, the altitude, and the distance to the nearest fjord. Each sample point's position on the glaciers can be found in Appendix A.

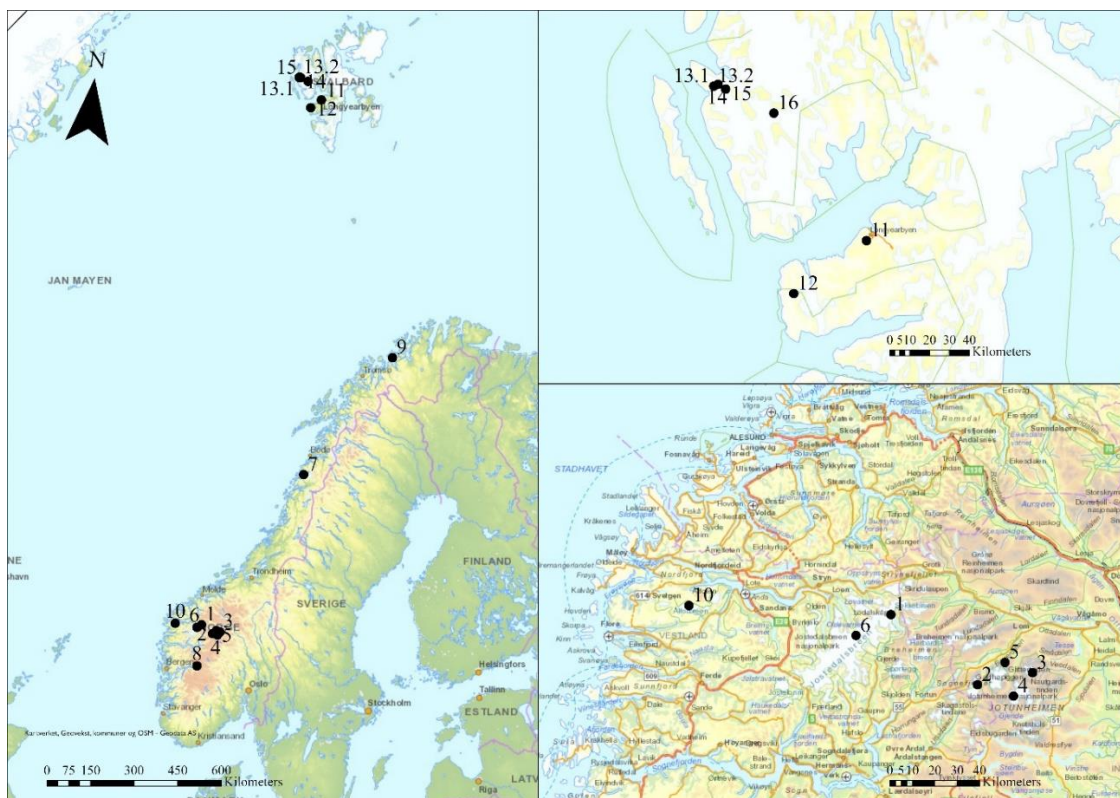


Figure 1 Position of the 16 glaciers sampled. Austdalsbreen (1), Storbreen (2), Gråsubreen (3), Hellstugubreen (4), Juvfonne (5), Nigardsbreen (6), Engabreen (7), Rembesdalskåka (8), Langfjordjøkelen (9) and Ålfotbreen (10), Platåbreen (11), Linnébreen (12), Austre Brøggerbreen (13), Midtre Lovénbreen (14), Edithbreen (15) and Kongsvegen (16).

Table 6 The sample date of the glaciers, the coordinates (dd), the altitude (masl) and the distance to the closest fjord (km). Glaciers marked with (S) were sampled during summer.

Glacier	Date	Latitude (dd)	Longitude (dd)	Altitude (masl)	Distance to fjord (km)
1. Austdalsbreen	2021-04-15	61.82	7.35	1500	30
2. Storbreen	2021-04-27	61.58	8.14	1700	30
3. Gråsubreen	2021-04-28	61.65	8.59	2200	56
4. Hellstugubreen	2021-04-29	61.55	8.45	2000	45
5. Juvfonne	2021-05-12	61.68	8.35	1900	45
6. Nigardsbreen	2021-04-30	61.72	7.08	1700	20
7. Engabreen	2021-05-26	66.65	13.85	1200	9
8. Rembesdalskåka	2021-05-28	60.54	7.37	1700	14
9. Langfjordsjøkelen	2021-05-04	70.13	21.74	710	4
10. Ålfotbreen	2021-04-28	61.75	5.65	1200	7
11. Platåbreen (S)	2021-06-27	78.19	15.46	730	6
12. Linnébreen (S)	2021-08-01	77.95	13.88	450	7
13.1 Austre Brøggerbreen	2021-04-30 2021	78.87	11.92	490	3
13.2 Austre Brøggerbreen (S)	2021-08-20	78.87	11.92	210	5
14. Midtre Lovénbreen (S)	2021-08-22	78.88	12.02	320	4
15. Edithbreen	2021-04-30	78.86	12.20	670	4
16. Kongsvegen	2021-04-28	78.76	13.34	700	22

3.2 Back Trajectory Analysis

The Hybrid Single Particle Lagrangian Integrated Trajectory (HYSPLIT) model by the National Oceanic and Atmospheric Administration (NOAA) was used to establish back trajectories of air masses passing the different glaciers (Stein et al., 2015). The models' starting point was the day before sampling at 23.00 UTC and traced the air 120 h back in time. A new trajectory was started every 3 h for 30 days before sampling. From these trajectories a frequency plot was made, showing the frequency of the trajectories passing over a specific grid on the map. The coordinates of the sample for PAH and PCB analysis on each glacier was used as well as the altitude of that point. The used input variables are shown in Table 7.

Table 7 Input parameters used for the NOAA HYSPLIT trajectory model.

Input parameters	
Type of trajectory	Frequency
Trajectory direction	Backwards
Vertical Motion	Model vertical velocity
Total run time (hours)	120
Number of days to calculate trajectory frequencies	30
Trajectory frequency grid solution	1.0 deg.
Trajectory starting interval	3 hrs
Trajectory model	Trajectory 1: #endpoint grid squares/#trajectories (%)

3.3 Sampling Technique

The majority of the samples were collected using a snow scooter for transportation to the site. The samples were taken 50 m upwind from the snow scooter and the top layer of snow was removed to avoid potential contamination of the sample. Longfjordjøkelen and Jufvonne were sampled using skis for transportation, while the glaciers sampled in the summer on Svalbard; Linnébreen, Platåbreen, Austre Broggerbreen, and Midtre Lovénbreen; were sampled by foot.

At five different positions on the glaciers, one sample for element analysis was taken by scraping of the top 2 – 5 cm of the snow with a 50mL sampling tube (Appendix B), rinsing

the bottle 3 times with the snow, and then filling the tube with the snow. These samples were then stored in a -20°C freezer upon return until analysis.

Approximately 4 – 5 L of snow were sampled in slider zip bags (Appendix B) on each glacier for the analysis of PAHs and PCBs. On the 10 glaciers sampled by NVE and the 3 samples taken by NPI, the snow was taken from a transect of approximately the top 1.5 m of snow on the glacier. On the glaciers sampled during the summer on Svalbard instead of a transect, 4 – 5 L of snow were gathered after removing the top layer, as the snow layer was too thin for a transect. The samples were taken with a metal scoop to avoid potential contamination from the scoop. The snow samples were kept at room temperature after sampling until melted and then transferred to aluminum flasks for transport and storage in a -20°C freezer. On Austre Brøggerbreen, Edithbreen, and Kongsvegen only one big sample was collected which was divided into 2 aluminum flasks for PAH and PCB analysis and one 50 mL sample tube for element analysis. For specifications on the material used see Appendix B.

3.4 Analytical Method

3.4.1 Element Analysis

The samples for the element analysis were filtered using a syringe and a 0.45 µm polyethersulfone membrane syringe filter (Appendix B). Approximately 2 mL of the sample was used to rinse the syringe between each sample. Then the syringe was filled with the sample. The filter and the vial were then rinsed 3 times with about 2 mL of the sample before filling the vial with 10 mL of the sample. The syringe was exchanged before measuring samples from the next glacier, and the filters were changed in between each new sample. After filtering, 3 drops of ultra-pure nitric acid (14.4 M) were added to each of the samples. Three method blanks were prepared by following the procedures using Milli-Q water (Purelab flex 3, ELGA). Additionally, three blanks were made for the ICP-MS.

All samples and blanks were analyzed using the Agilent 8800 Triple Quadrupole inductive coupled plasma mass spectrometry system (Agilent, USA) equipped with prepFAST M5 autosampler (ESI, USA). System parameters used during the analysis are listed in Table 8. In total 62 selected elements were analyzed. The accuracy of the analysis was determined using certified freshwater reference material (SLP 2129) and the obtained concentrations in the samples were corrected for the concentrations found in the blank samples.

Table 8 ICP-MS settings used for the analysis of the 62 elements.

General parameters	
RF Power	1600 W
Nebulizer Gas	0.77 - 0.80 L min ⁻¹
Makeup Gas	0.40 L min ⁻¹
Sample depth	8.0 mm
Ion lenses	s-lens
H₂ mode	
H ₂ gas flow	6.0 mL min ⁻¹
He gas flow	1.5 mL min ⁻¹
O₂ mode	
O ₂ gas flow	0.675 mL min ⁻¹
He gas flow	1.0 mL min ⁻¹

3.4.2 PAH and PCB Analysis

Around 1 L of the melted snow was used for the analysis of the 16 U.S. EPA priority PAHs and 7 PCBs. The exact amount used in each sample is listed in Appendix C and was accounted for when calculating the concentration. For the extraction, empty propylene Solid Phase Extraction (SPE) tubes with a volume of 12 mL were filled with 1g bondesil-C18 sorbent and a polyethylene frit (20 µm porosity) was put on top of the sorbent. The cartridges were preconditioned using 10 mL dichloromethane (DCM), 10 mL methanol, and 10 mL Milli-Q water (Purelab flex 3, ELGA). The samples were spiked with 10 µL of three different internal standards: 3'-F-PCB-28, 5'-F-PCB-118, and the mixture of F-PAH 'All in One Cocktail, Window 1-4' (see Table 9), all dissolved in ethyl acetate with the concentration 1 µg mL⁻¹. The unfiltered samples were sucked through the cartridge by a vacuum pump at a flow rate of approximately 3 mL min⁻¹. After the sample, 10 mL of Milli-Q water (Purelab flex 3, ELGA) was passed through the cartridge. The cartridges were then dried using a strong vacuum. When dry, the cartridges were eluted into 15 mL polypropylene tubes using 5 mL of

acetone and 8 mL of DCM. The eluents were dried under a gentle nitrogen stream at 35°C to approximately 1 drop and then redissolved in ethyl acetate to 0.2 mL.

Snow from the surrounding of Trondheim was used to test the recovery of the method. The extraction was performed on three method blanks (Milli-Q water (Purelab flex 3, ELGA)), three samples spiked with 10 µL of the target analytes (see Table 9) dissolved in ethyl acetate with the concentration of 1 µg mL⁻¹ before extraction, and three snow samples that were spiked with 10 µL of the target analytes after extraction. All samples were spiked with 10 µL of internal standard. The absolute recovery and the relative recovery were calculated using Equation 3 and Equation 4 (Chapter 2.7).

Table 9 Calibration standards used for the analysis of PAHs and PCBs.

Calibration Standards	Specifications
Internal Standards	
3'-F-PCB-28	100 µg mL ⁻¹ in isooctane
5'-F-PCB-118	10 µg mL ⁻¹ in isooctane
F-PAHs 'All in One Cocktail, Window 1-4'	1-Fluoronaphthalene, 4-Fluorobiphenyl, 3-Fluorophenanthrene, 1-Fluoropyrene and 3-Fluorochrysene, each 200 µg mL ⁻¹ in toluene
Target analytes	
'Dutch Seven' PCBs, ISO 10382 multicomponent stock solution	7 compounds (PCB-28, PCB-52, PCB-101, PCB-118, PCB-138, PCB-153, PCB-180) each 100 µg mL ⁻¹ each in isooctane
16 U.S. EPA priority pollutant PAHs	NAP, ACY, ACE, FLU, PHE, ANT, FLT, PYR, BaA, CHR, BbF, BkF, BaP, DBA, BgP and IND each 100µg mL ⁻¹ in toluene

The extracts of the recovery test and the samples were analyzed using the Agilent 7890A gas chromatogram with a GC Pal autosampler coupled to an Agilent 5975 single quadrupole mass spectrometer. The column used in the analysis is Thermo Scientific™ TraceGOLD™ TG-5MS GC Column (5% diphenyl/95% dimethyl polysiloxane, 30 m x 0.25 mm inner diameter x 0.5 µm film thickness). From the sample, 1 µL was injected in spitless mode. The carrier

gas, helium, was kept at a flow of 1 mL min⁻¹ and the transfer line and the injection port temperature were kept at 290°C. The temperature program starts at 50°C for 2 min and is then increased at a rate of 25°C min⁻¹ to 250°C and held for 1 min, followed by an increase of 3°C min⁻¹ to 286°C and held for 3 min, then the temperature is increased by 8°C min⁻¹ to 308°C and held for 1 min. Finally, the temperature was increased by 1°C min⁻¹ to 310°C and held for 3 min, resulting in an overall analyzing time of 34.75 min. Selected ion monitoring (SIM) mode using electron ionization (EI) set at 70 eV was used on the mass spectrometer. The peaks were integrated using the program Agilent MassHunter Quantitative Analysis (for GCMS) and quantified using calibration curves. Calibration solutions made from the standard solution “16 U.S. EPA priority pollutant PAH mixture” and ‘Dutch Seven’ PCB standard (see Table 9) dissolved in ethyl acetate were analyzed ranging in concentration from 0.5 ng mL⁻¹ to 200 ng mL⁻¹, to establish a calibration curve. The calibration solutions also contained 10 ng of the internal standards F-PAHs and 3’-F-PCB-28 and 5’-F-PCB-118. The limit of detection (LOD) and lowest limit of quantification (LOQ) were calculated from the calibration curve according to Equation 1 and Equation 2 (Chapter 2.7).

3.5 Data Analysis

To visually present the results of the concentration of elements, PAHs, and PCBs on maps the program ArcGIS Pro was used. For further investigation of the datasets, PCAs were plotted using the program Aspen unscrambler for all the elements that were above the detection limit in most samples and for which the RSD looked acceptable. A PCA was also made for the PAHs including all PAHs that had 3 or more values above LOQ. Half the LOD/LOQ was used for samples that were below the limit. All values were centered with the mean of the compound in all samples and scaled with the standard deviation.

Lastly, the dataset was tested for normality using a Shapiro-Wilk test. The glaciers were put in three different groups depending on the latitude, 3 groups depending on their altitude, and 3 groups depending on how far from the fjord they are located (Table 10). Differences between the groups were tested with one-way ANOVA if the data were normally distributed and with Kruskal Wallis if the data were not. The point of significance was set to p<0.05. Differences between the first and the third group were calculated if there was a significant difference between the groups and if the difference in the mean either increased or decreased in one direction. The difference was calculated by using the equation 5:

Equation 5:
$$\text{Percent change} = \frac{(\text{Final}-\text{Initial})}{\text{Initial}} \times 100$$

To compare spring and summer concentrations in the snow on Svalbard the data were also first tested for normality using the Shapiro-Wilk test and then either compared with a student t-test if the data was normally distributed and a Mann-Whitney U test if the data were not normally distributed.

Table 10 Criteria used for grouping the 13 glaciers sampled in spring depending on the latitude (dd), altitude (masl), and distance to fjord (km).

	Group 1		Group 2		Group 3	
	Criteria	Samples (nr)	Criteria	Samples (nr)	Criteria	Samples (nr)
Latitude (dd)	60-62	8	66-71	2	78-79	3
Altitude (masl)	400-1000	4	100-1400	3	1500-2300	6
Distance to fjord (km)	0-50	6	100-140	3	150-170	4

4 Results and Discussion

4.1 Quality of the Dataset

All glaciers sampled on mainland Norway are either in a national park or in a nature reserve, except for Langfjordjøkelen (9). This makes them suitable for measuring LRAT as the impact of local sources is neglectable (background areas). Langfjordjøkelen was included to cover the northern part of Norway. Even though the glacier is not located in a protected area, it is located far from bigger cities and highways. On Svalbard, only Linnébreen is partly inside a national park. However, the archipelago in general does not have a lot of local pollution. Therefore, glaciers close to local pollution such as cities, coal mines, and scooter tracks were avoided, but accessibility needed to be taken into consideration.

4.1.1 Quality of the Element Analysis

To ensure not to contaminate the sample, the syringe was first rinsed with approximately 2 ml of the sample, and the filter and the vials were rinsed 3 times with approximately 2 ml. One sample on Austdalsbreen (1) and one sample on Hellstugubreen (4) were too small to rinse the filter and the vial three times, therefore they were only rinsed twice. On Storbreen (2) the sample was only sufficient to rinse the filter and the vial once. No effect of this was seen in the dataset.

The detection limit of the analyzed elements varies between $1.62 \text{ E}^{-7} \mu\text{g L}^{-1}$ (Ta) to $0.713 \mu\text{g L}^{-1}$ (Cl) (see Appendix E). Hg, Pt, and Au were below the detection limit in all samples. Tl, Th, Ta, Hf, Lu, Yb, Tm, Er, Ho, Tb, Gd, Eu, Sm, Cs, In, Ga, Mn, Sc, and Be were below the detection limit in most samples. The recovery test using the freshwater reference material showed a recovery varying from 83% (Cu) to 108% (Cl), proving sufficient recovery of the analytes.

4.1.2 Quality of the PAH and PCB Analysis

The regression line fitted to the calibration samples fitted well to the data (R^2 : 0.994-0.9996). The LOD and LOQ of the different compounds vary between $0.211\text{-}2.56 \text{ ng mL}^{-1}$ and $0.729\text{-}8.53 \text{ ng mL}^{-1}$ (Table 11). The 5-ring and 6-ring PAHs had the highest LOD and LOQ. The absolute recovery (AR) varies between 31-74% (Figure 2). The AR was especially low for many of the PCBs (31-47%). For the PAHs, the AR varies between 42-74%. The AR of the compounds should be improved, especially for the measured PCBs. Changes in the volume of the sample, the volume of the packing material, type of packing material, flowrate, or solvent should be tested to improve the recovery of the analytes (Jacob, 1995).

The relative recovery (RR) varies between 79-117%, except for the relative recovery of ACE which is -132%. The negative RR is due to the high concentrations of ACE in the blank sample, which when standardized with the internal standard was higher than in the spiked sample. Due to the high concentrations in the blank and the negative RR, ACE was removed from the results.

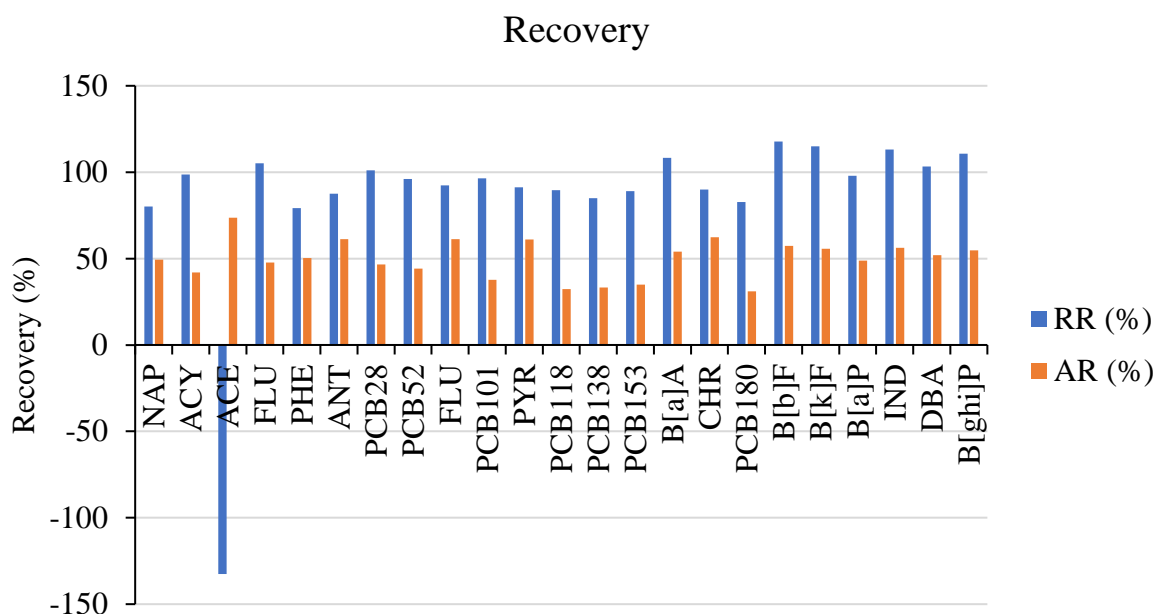


Figure 2 Absolute recovery (AR) (orange) and relative recovery (RR) (blue) of the target analytes added to snow samples for testing the recovery of the method.

Table 11 Limit of detection (LOD) and limit of quantification (LOQ) (ng mL⁻¹) of the target analytes in GC-MS, using the extracts of the calibration curve and calculated with equation 1 and equation 2 (chapter 2.7).

	LOD (ng mL⁻¹)	LOQ (ng mL⁻¹)
NAP	0.228	0.759
ACY	0.332	1.11
ACE	0.875	2.92
FLU	0.474	1.58
PHE	0.282	0.94
ANT	0.448	1.50
FLT	0.229	0.764
PYR	0.246	0.821
BaA	0.709	2.36
CHR	0.529	1.76
BbF	1.79	5.98
BkF	1.55	5.18
BaP	2.56	8.53
IND	2.17	7.24
DBA	2.15	7.15
BgP	2.18	7.26
PCB28	0.283	0.942
PCB52	0.278	0.926
PCB101	0.211	0.703
PCB118	0.261	0.871
PCB138	0.219	0.729
PCB153	0.229	0.762
PCB180	0.261	0.872

4.1.1 Quality of the Seasonal Dataset

It is important to stress that different glaciers were sampled in spring than in summer. This is due to covid-related travel restrictions. Only Austre Brøggerbreen (13) could be sampled during both seasons. Therefore, local differences could affect the concentrations in the samples in addition to seasonal differences. Nevertheless, Austre Brøggerbreen, which was sampled during both seasons, shows similar trends to the rest of the dataset. Therefore, a discussion of the differences in spring and summer concentrations seems relevant but can only reveal potential trends that need to be confirmed in more comprehensive studies.

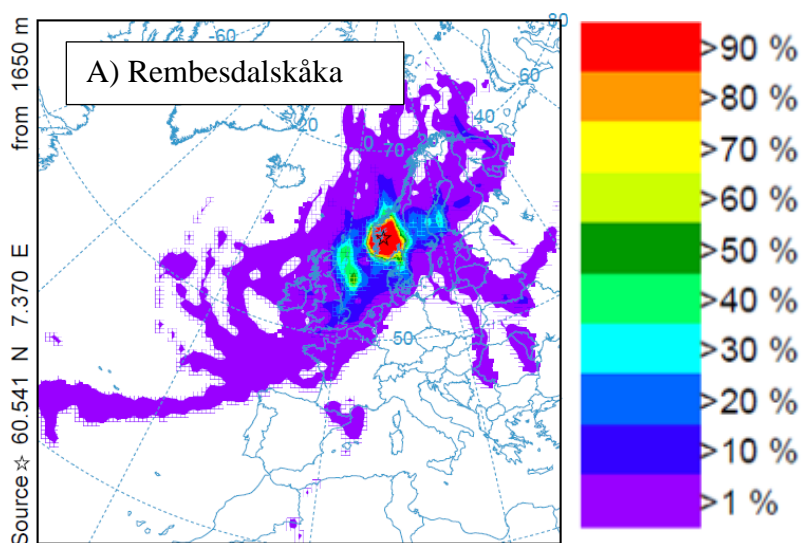
4.2 Airmass Back Trajectories

Back trajectory models were plotted for each of the glaciers (see Appendix D and Figure 3). Many of these resemble each other as they were taken in similar areas close in time, therefore only 6 out of the 17 back trajectories are shown in Figure 3. Storbreen (2) represents the glaciers Austdalsbreen (1), Gråsubreen (3), Hellstugubreen (4), Juvfonna (5), Nigardsbreen (6), and Ålfotsbreen (10). Austre Brøggerbreen (13.1) represents the glaciers Edithbreen (15) and Kongsvegen (16). Linnébreen (12) represents Platåbreen (11) and lastly, Austre Brøggerbreen (13.2) represents Midtre Lovénbreen (14). The different colors in the trajectory models show the frequency of the trajectory passing over the grid of the in total 240 trajectories that were made every 3h starting from 30 days before sampling to the sampling day.

Starting with Rembesdalskåka (8), which is the most southern glacier sampled, it receives 90% of its air from a large area in southern Norway (see Figure 3). 10-40% of the air masses come from mid-Sweden, the Gulf of Bothnia, and outside the coast of Great Britain in the North Sea. About 1% comes from Great Britain, northern France, Belgium, Netherlands, northern Germany, Finland, Sweden, Lithuania, Belarus, and a little bit from west Russia. The air passing Storbreen (2) compared to Rembesdalskåka (8) comes mainly from closer regions. About 20-90% originate from southern Norway or the Norwegian sea close to the coast. About 1% comes from Iceland, the coast of Greenland, northern Great Britain, Sweden, Finland, Estonia, and a little from west Russia. Engabreen (7) located at 66.7°N receives most air masses (30-90%) from mid-Norway and mid-west Sweden. 1% of the air passed southern Great Britain, Belgium, Netherlands, Denmark, Estonia, Latvia, Lithuania, Belarus, west Russia, Finland, Novaya Zemlya Island, and Svalbard. The trajectory model of Langfjordsjøkelen (9), located at 70.1°N, shows that 30-90% of the air derives from northern Norway. 10-20% derived from the east coast of Norway, from northern Sweden and the

Barents Sea between Norway, and Svalbard. Further, 1% derives from Iceland, southern Norway, mid-Sweden, southern Finland, the north and east coast of Greenland, Svalbard, and the Norwegian-, Barents- and Arctic Oceans. Lastly, the trajectory model for Austre Brøggerbreen (13.1) sampled in spring shows that 10-90% of the air derives from Svalbard. The remaining air derives from northern Russia, eastern Greenland, the Barents Sea, the Greenland Sea, and the Arctic Ocean. Linnébreen (12) and Austre Brøggerbreen (13.2) were sampled in summer. Both samples receive air masses from mainly Svalbard. 10% of the air masses to the glaciers come from a transect going from Iceland to Svalbard. Further, 1% of the air comes from the surrounding oceans, Greenland, and northern Russia. Comparing the air masses deriving to Austre Brøggerbreen during spring and summer, the source area in spring appears to be bigger than during summer.

Drotikova *et al.* (2021) compared the origin of the air mass to Svalbard with a 10-day backward trajectory probability map. As the time for the backward trajectory is twice the time used in this study, more potential source areas were identified. The winter concentrations of polycyclic aromatic compounds (PAC) were in this study mainly influenced by northwestern Eurasia, similar to this study. Further, Drotikova *et al.* (2021) concluded that winter concentrations were mainly influenced by LRAT while summer concentrations were dominated by local emissions. Similar to this study, the source area of LRAT was bigger in spring than during summer in Svalbard.



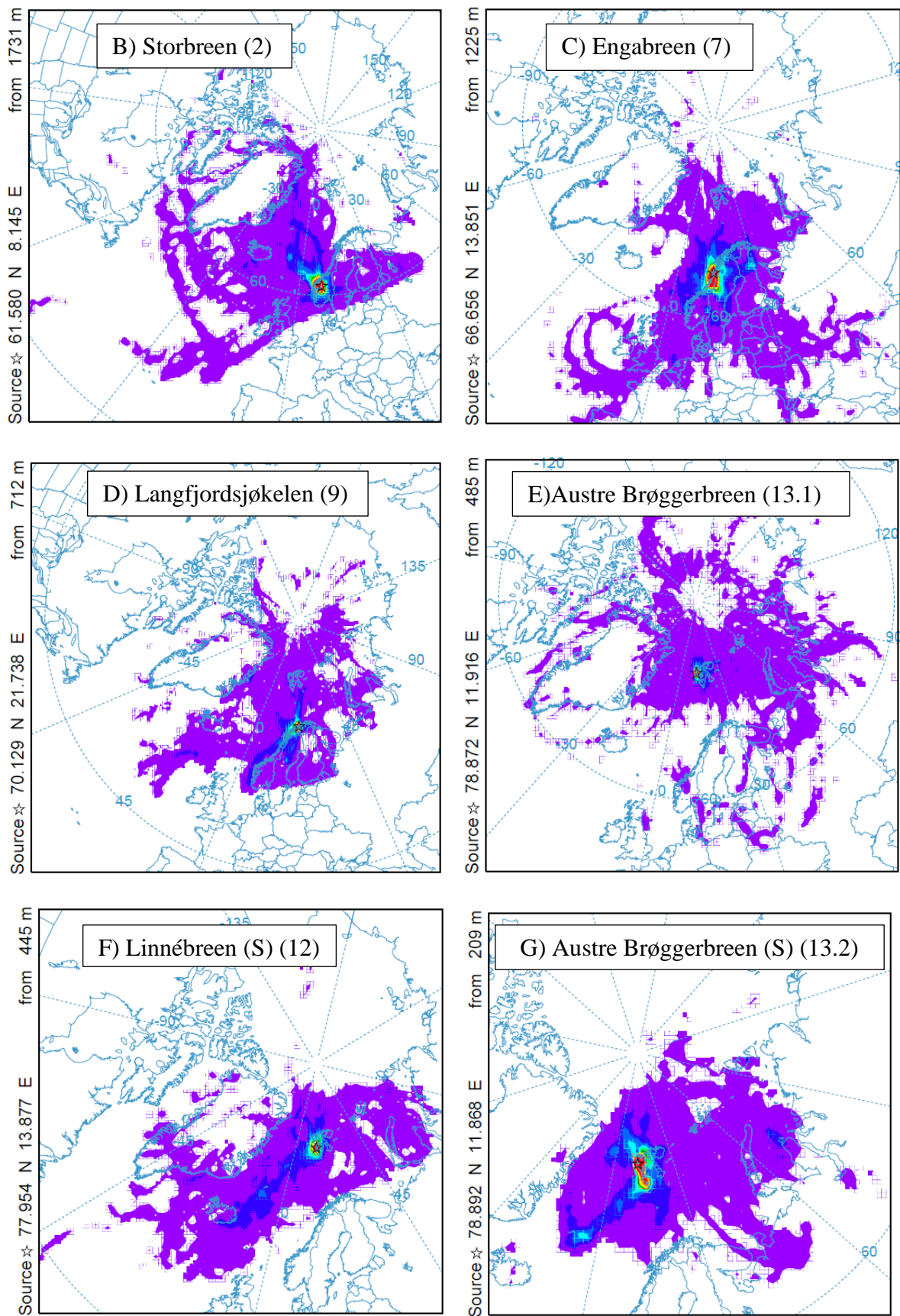


Figure 3 NOAA HYSPLIT atmospheric back trajectory models of the glaciers A) Rembesdalskåka (8), B) Storbreen (2), C) Engabreen (7), D) Langfjordsjøkelen (9), E) Austre Brøggerbreen (13.1), F) Linnébreen (S) (12), and G) Austre Brøggerbreen (S) (13.2) (Stein et al., 2015). Glaciers marked with (S) are sampled in summer.

4.3 Element Composition and Distribution

Langfjordsjøkelen (9) has the highest total concentration of elements ($12181 \mu\text{g L}^{-1}$), while Rembesdalskåka (8) has the lowest total concentration ($262 \mu\text{g L}^{-1}$). No latitudinal trends of the total concentration of the elements can be found ($p > 0.05$) (Figure 4). However, trends of some element groups and some individual compounds can be seen and are discussed in the next chapters.



Figure 4 Total element concentration ($\mu\text{g L}^{-1}$) on the 16 measured glaciers: Austdalsbreen (1), Storbreen (2), Gråsbreen (3), Hellstugubreen (4), Juvfonne (5), Nigardsbreen (6), Engabreen (7), Rembesdalskåka (8), Langfjordjøkelen (9), Ålfotbreen (10), Platåbreen (11), Linnébreen (12), Austre Brøggerbreen (13), Midtre Lovénbreen (14), Edithbreen (15) and Kongsvegen (16).

The 62 elements measured in this study were separated into four groups: Major elements, Trace elements, Lanthanides, and Heavy metals (see Table 12). The definitions of the groups are specified in Chapter 2.4 and the allocation of the 62 measured elements in this study to these groups are shown in Table 12. The total element concentrations in the glaciers consist predominantly of the major element group (97.1-99.7%). The heavy metal group contributes 0.032- 2.419% of the total element concentration, trace elements to 0.19-0.52%, and lanthanoids to 1.14 E^{-5} - $1.06 \text{ E}^{-3} \%$. The exact concentrations of the different groups and the individual elements in the different glaciers are shown in Appendix E. The trend of the total

element groups: major elements, trace elements, and heavy metals will be discussed in chapters 4.1.1-4.1.3. Due to the low concentrations of lanthanoids in the samples, the group will not be further investigated. Further, the 2 elements with the highest concentrations in the major and trace element group will be discussed individually, while the 6 highest elements in concentrations will be discussed for the heavy metals, as this group is mostly related to anthropogenic sources.

Table 12 Element groups: Major elements, Trace elements, Lanthanides and Heavy metals.

Major elements	Trace elements	Lanthanides	Heavy metals
Si	Ba	La	As
Al	Sr	Ce	Cd
Fe	Zr	Pr	Cr
Ca	Rb	Nd	Cu
Mg	Co	Pm	Hg
Na	Nb	Sm	In
P	Li	Eu	Mn
Ti	Sc	Gd	Mo
Cl	Ga	Tb	Ni
S	Th	Dy	Pb
K	Hf	Ho	Sb
	U	Er	Se
	Be	Tm	Sn
	B	Yb	Tl
	Br	Lu	V
	Y		Zn
	Cs		
	Ta		
	W		
	Pt		
	Au		
	Bi		

4.3.1 Major Elements Composition and Distribution

The total concentration of the major elements in the samples is dominated by the elements Cl and Na followed by K, S, and Ca, similar to the studies by De Caritat et al. (2005), Koziol et al. (2021), and Spolaor et al. (2021) (Figure 5). Na concentrations varied between 0.06 – 3.9 mg L⁻¹, and Cl concentrations varied between 0.09 – 6.8 mg L⁻¹ in this study, which is similar to the mean values and ranges found in the three previously mentioned studies.

The spatial distribution of the total concentration of the major elements in the samples taken in spring is shown in Figure 6, and Figure 7 shows the Na and Cl individually. There is no latitudinal deposition trend for the major element group ($p > 0.05$). Instead, a decreasing concentration trend from the coast of Norway (10 Ålfotsbreen) towards inland Norway (towards 3 Gråsubreen) is indicated. Longfjordsjøkelen (9) and the three glaciers on Svalbard (13, 15, 16) are all located close to the shore and have higher concentrations of major elements compared to Rembesdalskåka (8) and the other glaciers located further inland (2, 3, 4, 5, 6, and 1). Kongsvegen (16), located further inland on Svalbard, also has a slightly lower concentration than Austre Brøggerbreen (13) and Edithbreen (15), which are located closer to the coast. De Caritat et al. (2005) found that the major element concentrations in their study in the arctic snow are consistent with a diluted seawater composition, which indicates that sea spray is the main source of major elements in the snow. Enriched Na and Mg concentrations in coastal areas have further been observed in natural surface soil in Norway, following a similar decreasing trend inland (Steinnes and Lierhagen, 2018). The authors contribute this to marine input as well, as these elements are common in seawater. Sea spray could therefore be a potential explanation for the increased concentration of the major element group in samples located closer to the shore.

However, Engabreen (7), which is located close to the coast, has the next lowest concentration of major elements, and does thereby not follow this trend (Figure 5). Engabreen (7) and Rembesdalskåka (8) were the last two glaciers sampled in Norway, on the 26th of May and 28th of May, respectively. Rembesdalskåka (8) has the lowest concentration of major elements followed by Engabreen (7). Kakareka et al. (2022) measured newly fallen snow and old snow in Marguerite Bay Island, Antarctica, and found the lowest concentrations of major elements in old snow. Additionally, Spolaor et al. (2021), studied the dynamics of ionic species mobility in Austré Brøggerbreen, Svalbard, and found that the elements Na, K, Ca, and Mg generally decrease throughout the spring season. As the snow on Engabreen (7) and Rembesdalskåka (8) was sampled late in spring, lower concentrations of the major elements

due to snow redistribution and post-depositional processes, evaporation, and leaching of the compounds might be the reason for the lower concentrations in the snow (Kakareka et al., 2022; Spolaor et al., 2021).

The rest of the samples were taken earlier in the spring, from the 15th of April to the 12th of May. Removing the two glaciers sampled later in spring a significant marine gradient can be detected ($p < 0.05$). The mean concentration in the group closest to the fjord (0 – 50 km) is 5.3 times higher in major elements than the mean of the group furthest from the fjord (150 – 170 km). Na and Cl individually also showed a significant increase ($p < 0.05$) in concentration in glaciers closer to the fjord, when removing the glaciers 7 and 8. The concentrations were 7.6 and 7.5 times higher, respectively, in the glaciers close to the fjord.

A significant decrease with altitude was further detected for the total major element concentration ($p < 0.05$). As these most likely derive from sea spray aerosols, it is likely that they deposit at lower latitude. However, this trend could also be due to the fact that the two factors altitude and distance to fjord co-vary in this dataset, because in Norway, generally, the altitude increases with distance to the ocean. As Na and Cl, that dominate the composition of the major elements, are typical of marine origin, the distance to the fjord is most likely the most important factor.

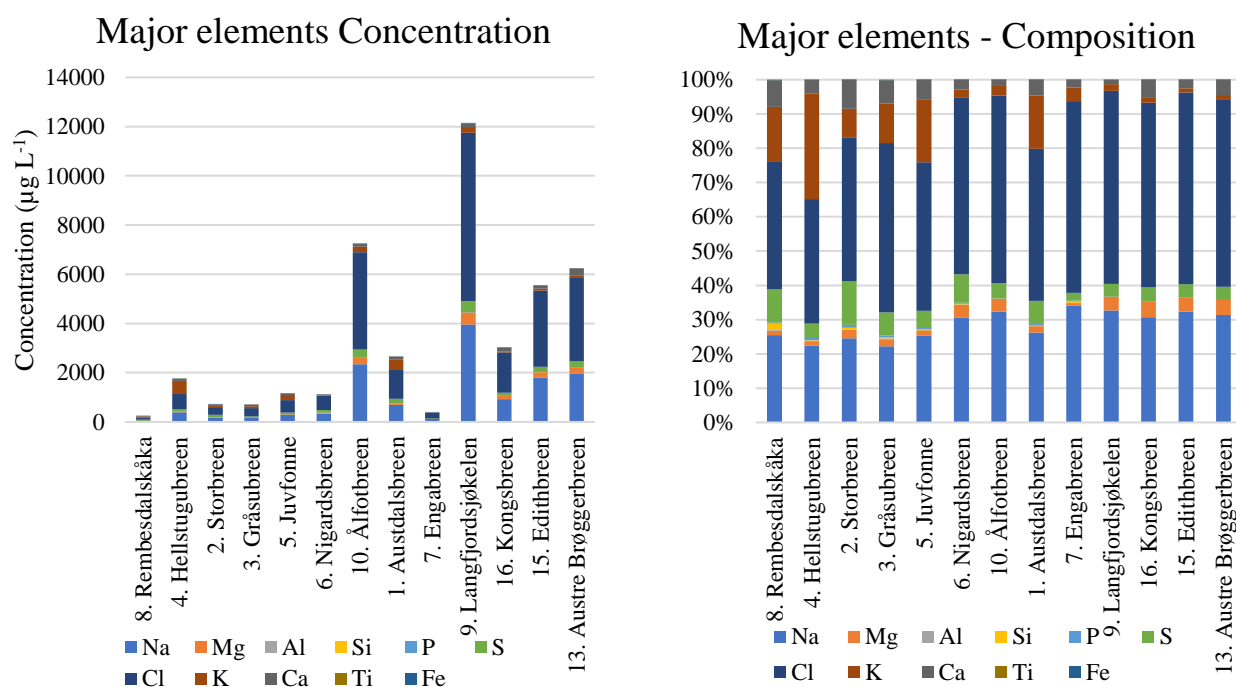


Figure 5 Major elements concentration ($\mu\text{g L}^{-1}$) (left) and composition (%) (right) in snow samples collected from the glaciers indicated.



Figure 6 Major element concentration ($\mu\text{g L}^{-1}$) in the snow on the glaciers: Austdalsbreen (1), Storbreen (2), Gråsubreen (3), Hellstugubreen (4), Juvfonne (5), Nigardsbreen (6), Engabreen (7), Rembesdalskåka (8), Langfjordjøkelen (9), Ålfotbreen (10), Austre Brøggerbreen (13), Edithbreen (15) and Kongsvegen (16).

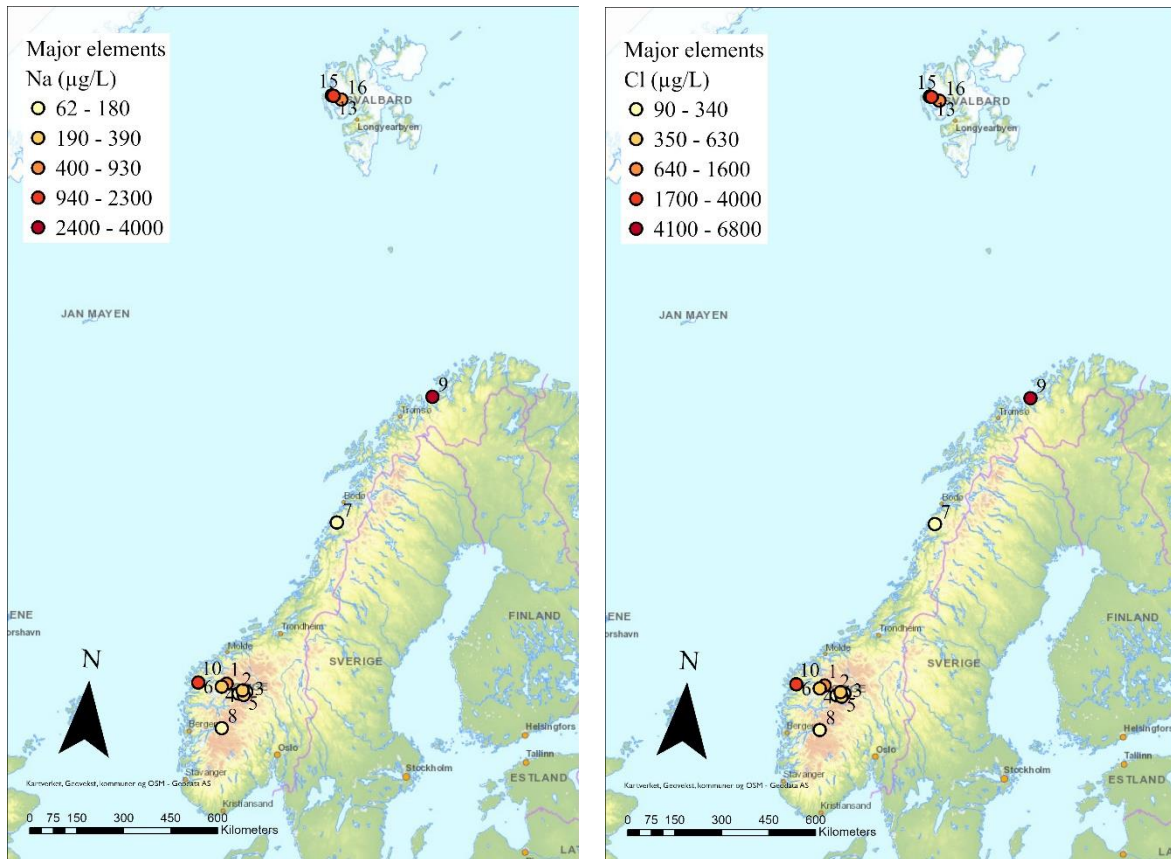


Figure 7 Na (left) and Cl (right) concentration ($\mu\text{g L}^{-1}$) in the snow on the glaciers: Austdalsbreen (1), Storbreen (2), Gråsübreen (3), Hellstugubreen (4), Juvfonne (5), Nigardsbreen (6), Engabreen (7), Rembesdalskåka (8), Langfjordjøkelen (9), Ålfotbreen (10), Austre Brøggerbreen (13), Edithbreen (15) and Kongsvegen (16).

4.3.2 Trace Elements Composition and Distribution

Trace elements seem to be similarly distributed spatially as the major elements, with increasing concentrations closer to the coast (Figure 9). The trace elements are dominated by Br followed by Ba, B, Sr, and Rb (Figure 8). Bromine concentrations varied between 0.36 and $21 \mu\text{g L}^{-1}$. The concentrations found are similar to, but slightly higher than what was measured by Spolaor et al. (2021) on Austre Brøggerbreen.

Steinnes and Lierhagen (2018) measured trace elements in soil in Norway and detected higher concentrations of Br and Sr closer to coastal areas, which according to their study was due to the marine influence. As Br is dominating in all samples, the concentration trend of the total trace element group is similar to the major element concentration distribution showing a marine gradient (Figure 9, Figure 6). Removing the two glaciers 7 and 8, due to the reasons explained in chapter 4.3.1, a significant increase in the total trace elements and Br was detected towards marine influences ($p < 0.05$) (Figure 9, Figure 10). Total trace element

concentrations on the glaciers closest to the fjord (0 – 50 km) are 2.8 times higher than on the glaciers located furthest away (150 – 170 km). Bromine individually is 5.6 times higher.

Barium concentration, on the other hand, decreased significantly by 77% towards the coast (Figure 10). Depletion of Ba towards the coast was also detected by Steinnes and Lierhagen (2018) in surface soil. They suggest that the depletion could be due to the potential cation exchange of Ba by marine cations in the soil, leading to depletion in the surface soil. The Ba concentration on the glacier could, therefore, potentially reflect the Ba concentration in the surrounding surface soil. The concentration of Ba further decreases significantly with latitude ($p < 0.05$) (Figure 10). The mean concentration of Ba is 78% lower on Svalbard (78-79°N) than the mean concentration in southern Norway (60-62°N). This could be both due to local differences in the bedrock or due to a potential LRAT of Ba. Anthropogenic Ba sources to the atmosphere are mining, refining, and production of barium and barium chemicals, fossil fuel combustion, entrainment of soil and rock dust, and coal ash (Gad, 2014).

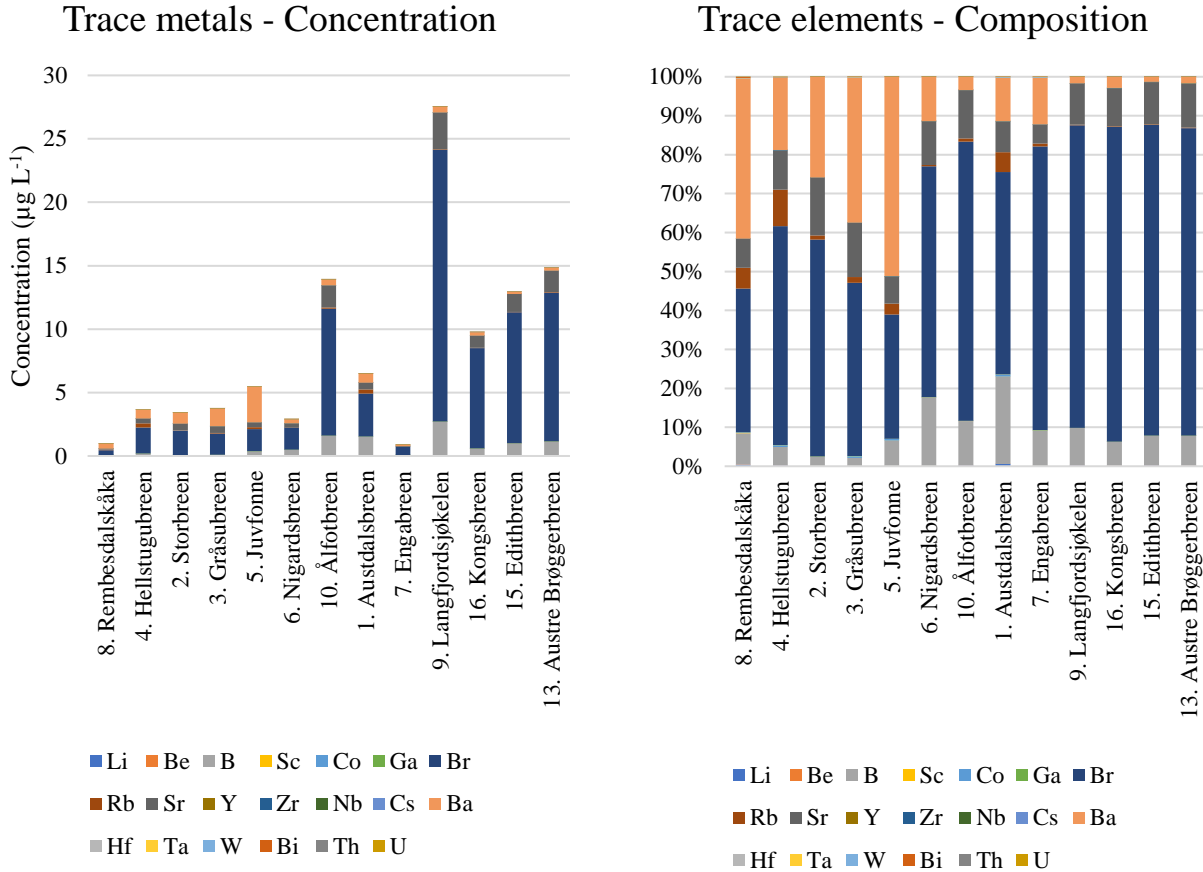


Figure 8 Trace element concentration ($\mu\text{g L}^{-1}$) (left) and composition (%) (right) in snow samples collected from the glaciers indicated.

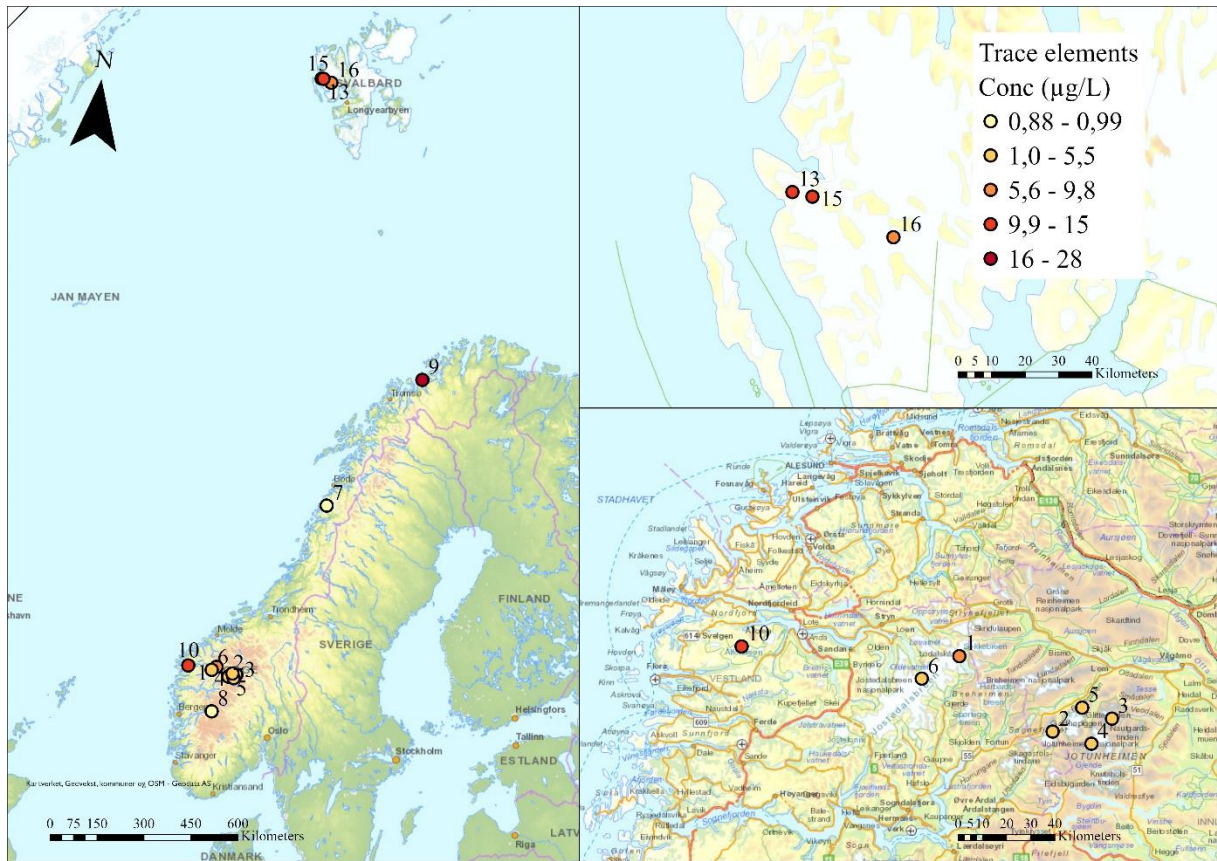


Figure 9 Trace element concentration ($\mu\text{g L}^{-1}$) in the snow on the glaciers: Austdalsbreen (1), Storbreen (2), Gråsubreen (3), Hellstugubreen (4), Juvfonne (5), Nigardsbreen (6), Engabreen (7), Rembesdalskåka (8), Langfjordjøkelen (9), Ålfotbreen (10), Austre Brøggerbreen (13), Edithbreen (15) and Kongsvegen (16).

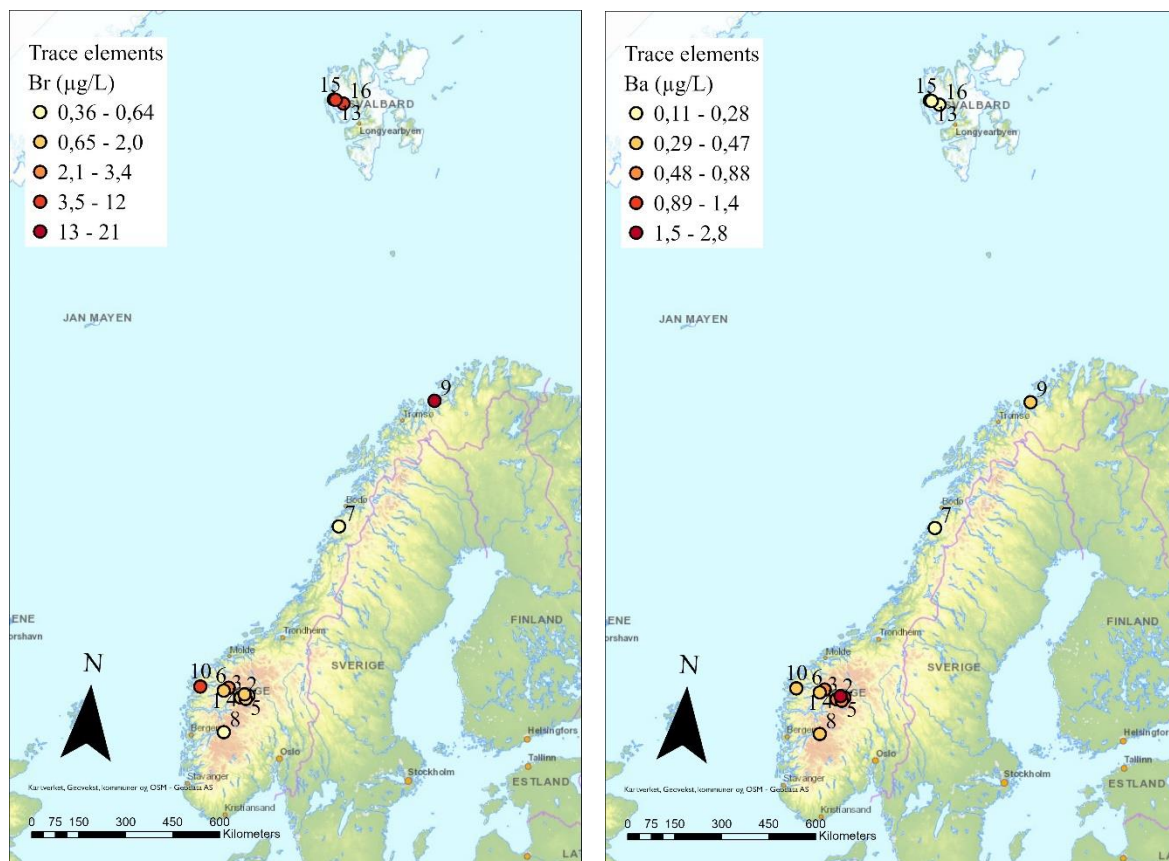


Figure 10 Br and Ba concentration ($\mu\text{g L}^{-1}$) in the snow on the glaciers: Austdalsbreen (1), Storbreen (2), Gråsubreen (3), Hellstugubreen (4), Juvfonne (5), Nigardsbreen (6), Engabreen (7), Rembesdalskåka (8), Langfjordjøkelen (9), Ålftobreen (10), Austre Brøggerbreen (13), Edithbreen (15) and Kongsvegen (16).

4.3.3 Heavy Metals Composition and Distribution

Total heavy metal concentration decreases significantly with latitude ($p < 0.05$) (Figure 12).

The highest sum of heavy metal concentrations ($59 \mu\text{g L}^{-1}$) was found in the snow on Austdalsbreen (1) followed by Ålftobreen (10) ($35 \mu\text{g L}^{-1}$), both located in southern Norway.

The lowest sum of heavy metal concentrations ($1.9 \mu\text{g L}^{-1}$) was found in Kongsvegen (16) on Svalbard. The mean concentration decreases significantly by 89% from southern Norway ($60\text{--}62^\circ\text{N}$) to Svalbard ($78\text{--}79^\circ\text{N}$). The total heavy metal concentration mainly consists of Cu and Zn (Figure 11), which individually also decreased significantly with latitude ($p < 0.05$); 99% and 80%, respectively (Figure 13).

A study on element concentrations in lake sediments in Norway shows increased concentrations in surface sediments of Cu and Zn in southeast Norway, which they assume to be due to either atmospheric deposition, chemical reactions occurring after sediment deposition, or release from the catchment due to an increased mobilization (Fjeld and Rognerud, 2001). As the elemental composition of snow mainly depends on atmospheric

composition and deposition, the increased concentrations in southern Norway, in this study, are assumed to be due to atmospheric deposition.

Around 70% of anthropogenic sources of Cu and Zn to the atmosphere derive from non-ferrous metal production (AMAP, 2005). In Norway, there are 121 metal industry companies producing mainly aluminum and ferroalloys, but also iron, steel, magnesium, nickel, and zinc (Regjeringen, 2001). Norway is the largest producer of aluminum in western Europe and one of the world's largest producers of ferrosilicon and silicon metal (Regjeringen, 2001). Most of these industries are located in southern Norway along the coast, which could contribute to the generally higher concentrations of Cu and Zn in southern Norway. Ålfotbreen (10) is located approximately 20 km away from Elkem Bremanger a ferrosilicon metallurgical industry, which could potentially explain why it has the next highest concentrations of Cu and Zn (Thorsnæs and Askheim, 2022). Additionally, a smelter is located close to the border between Norway and Russia close to the town Nickel, Russia, producing Ni-Cu (Šillerová et al., 2017). A study on Ni and Cu isotopes in snow, soil, and lichen showed a general increase of these elements in the whole area, highlighting the impact of the smelting activity (Šillerová et al., 2017). Compared to the other glaciers sampled further north, Langfjordsjøkelen has a slightly higher total heavy metal concentration ($13 \mu\text{g L}^{-1}$) (Figure 11). The airmass back trajectory of Langfjordjøkelen (9) includes the area of the smelter, which therefore might have contaminated the area with predominantly Cu. The spatial distribution of Cu and Zn are shown individually in Figure 13.

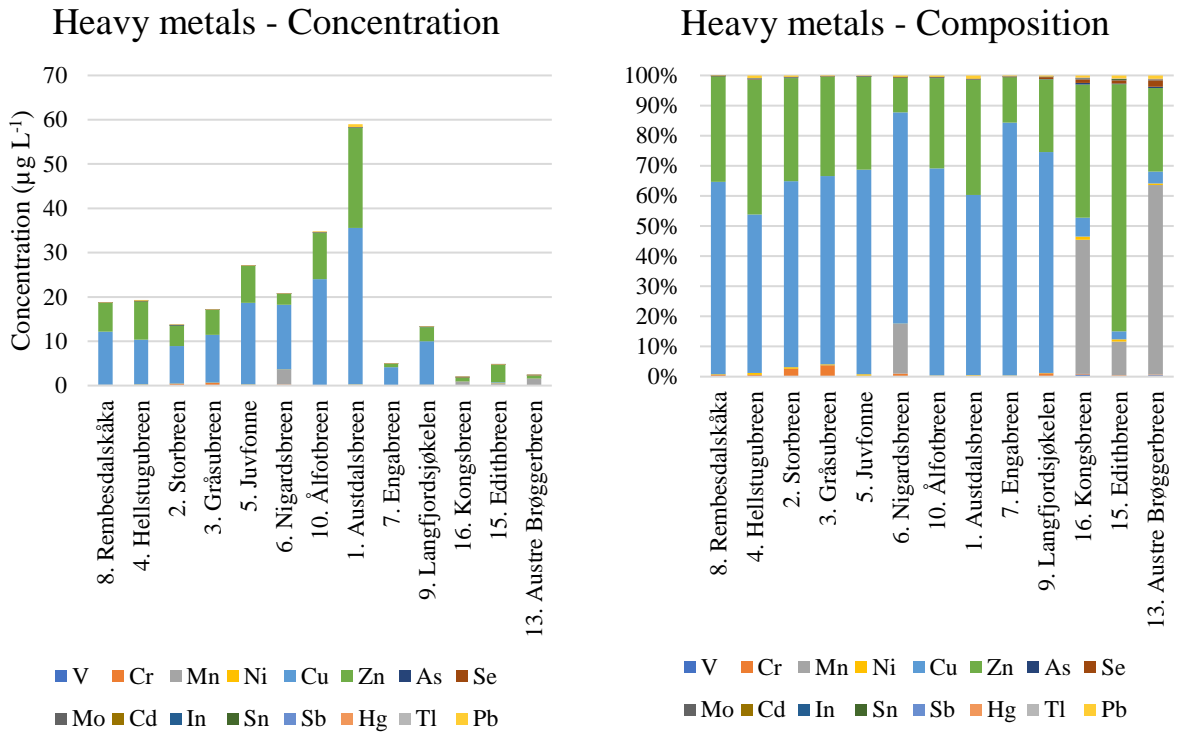


Figure 11 Heavy metal concentration ($\mu\text{g L}^{-1}$) (left) and composition (%) (right) in snow samples collected from the glaciers indicated.

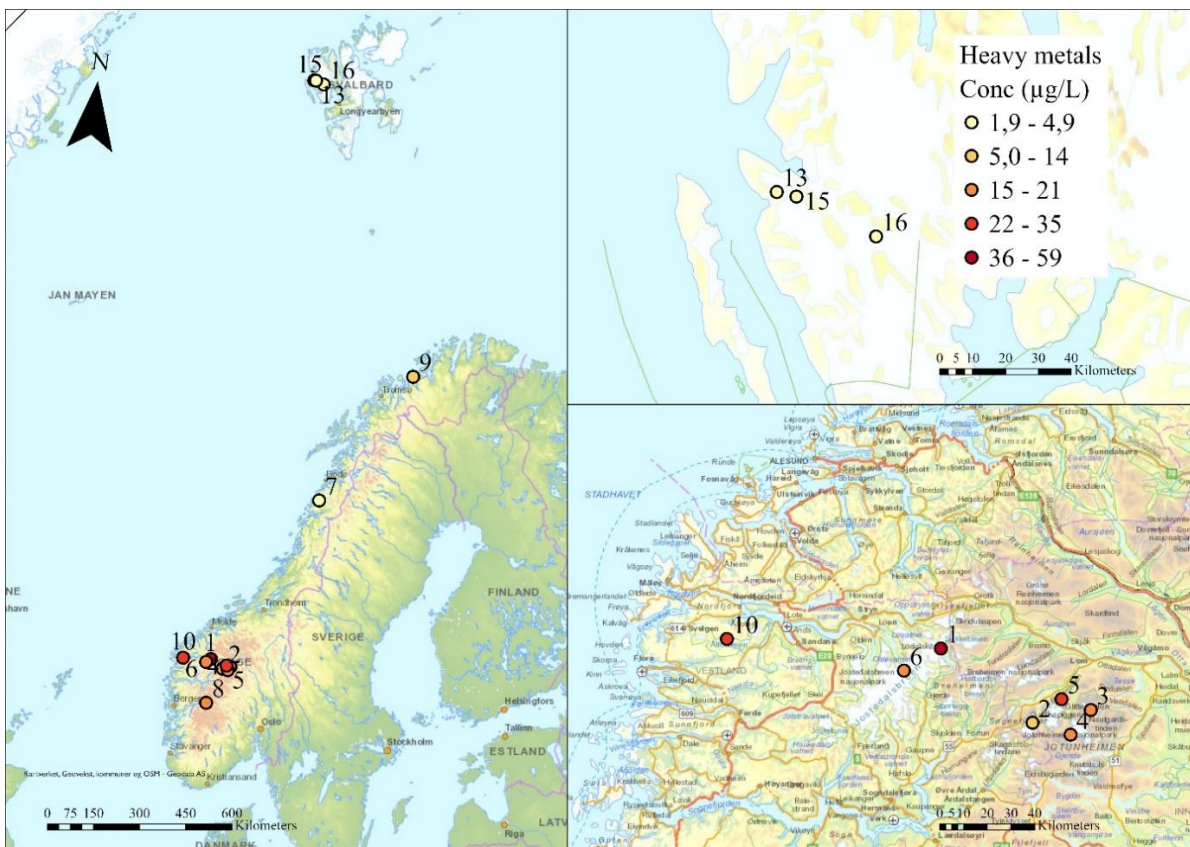


Figure 12 Heavy metal concentration ($\mu\text{g L}^{-1}$) in the snow on the glaciers: Austdalsbreen (1), Storbreen (2), Gråsubreen (3), Hellstugubreen (4), Juvfonne (5), Nigardsbreen (6), Engabreen (7), Rembedalskåka (8), Langfjordjøkelen (9), Ålfotbreen (10), Austre Brøggerbreen (13), Edithbreen (15) and Kongsvegen (16).

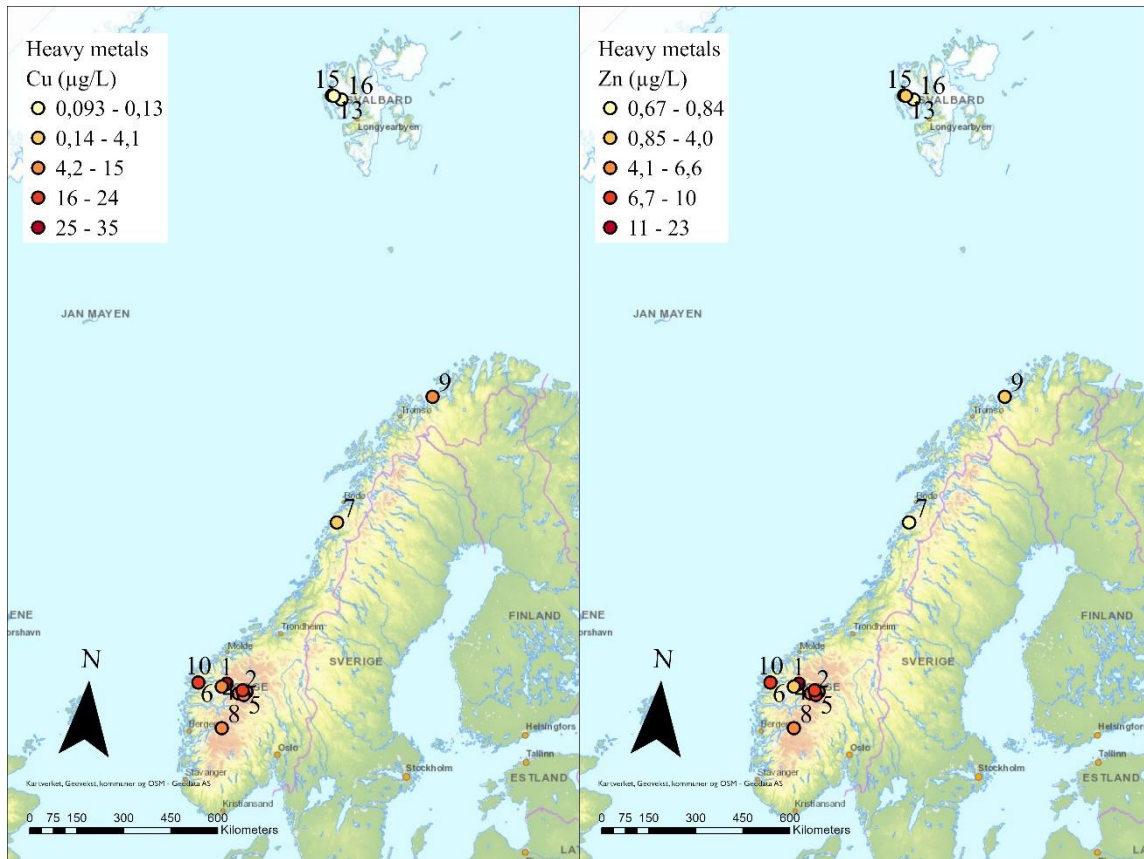


Figure 13 Cu and Zn concentrations ($\mu\text{g L}^{-1}$) in the snow on the glaciers: Austdalsbreen (1), Storbreen (2), Gråsubreen (3), Hellstugubreen (4), Juvfonna (5), Nigardsbreen (6), Engabreen (7), Rembesdalskåka (8), Langfjordjøkelen (9), Ålfotbreen (10), Austre Brøggerbreen (13), Edithbreen (15) and Kongsvegen (16).

Further, heavy metals such as Mn, Cr, Ni, and Pb were detected in the samples (Figure 14). Coal combustion is responsible for 85% of Mn and 69% of Cr emissions to the atmosphere (AMAP, 2005). The highest Mn concentrations ($3.4 \mu\text{g L}^{-1}$) were found in the snow on Nigardsbreen (6) and the glaciers on Svalbard ($0.54 - 1.5 \mu\text{g L}^{-1}$). Cr on the other hand is highest in Gråsubreen (3) ($0.64 \mu\text{g L}^{-1}$) followed by Storbreen (2) ($0.35 \mu\text{g L}^{-1}$) and Nigardsbreen (6) ($0.22 \mu\text{g L}^{-1}$). The lowest concentrations of Cr are found in Svalbard and closer to the coast in Norway (Figure 15). Coal combustion contributes in addition to Cr and Mn to 66% of Hg, 47% of Sb, 89% of Se, 89% of Sn, and almost 100% of Tl to atmospheric emissions (AMAP, 2005). Mercury was under the detection limit in all samples and thallium was either close to the detection limit or below. In general, no similar trends in the distribution of these elements could be seen. Therefore, it is uncertain if coal combustion is the source of Mn and Cr in the snow.

A study by Steinnes (1995) on moss in Norway found higher concentrations of Mn further inland than in coastal regions. However, as the concentrations in the moss are higher than

what can be explained by air pollution, they suggest Mn in the moss derives from the soil by root uptake (Steinnes, 1995). Differences in Mn concentration in the snow in this study could, therefore, also be due to differences in Mn concentration in the surrounding bedrock of the glaciers. Chromium significantly decreases in concentration towards Svalbard (-96%). Indicating LRAT to be the main source of Cr to the glaciers. In the study by Christensen et al. (2018) Cr was, however, categorized to derive from geogenic sources to moss in Norway.

Lead is highest in the snow from the glaciers in southern Norway such as Austdalsbreen (1), Hellstugubreen (4), and Ålfotbreen (10) ($0.63 \mu\text{g L}^{-1}$, $0.17 \mu\text{g L}^{-1}$, and $0.14 \mu\text{g L}^{-1}$ respectively) (Figure 14). The mean concentrations of Pb on Svalbard are 82% lower compared to the mean of the glaciers in southern Norway, however, the decrease in concentration was not statistically significant ($p = 0.073$). Vehicle traffic and oil combustion in general are typical sources of Pb (AMAP, 2005). In surface soil in Norway a latitudinal gradient was found, which strongly correlated to atmospheric deposition rates (Steinnes and Lierhagen, 2018).

Lastly, Cd is usually also associated with long-range atmospheric transport. Steinnes and Lierhagen (2018) for instance found similar decreasing concentrations with latitude as Pb, where Cd concentrations also strongly correlated with atmospheric deposition rates. In the snow, the highest concentrations were found on Austdalsbreen (1) and generally the concentrations in southern Norway were higher than on Svalbard. A significant decreasing trend was found for Cd ($p < 0.05$) showing that the mean concentration in Svalbard is 60% lower than in southern Norway.

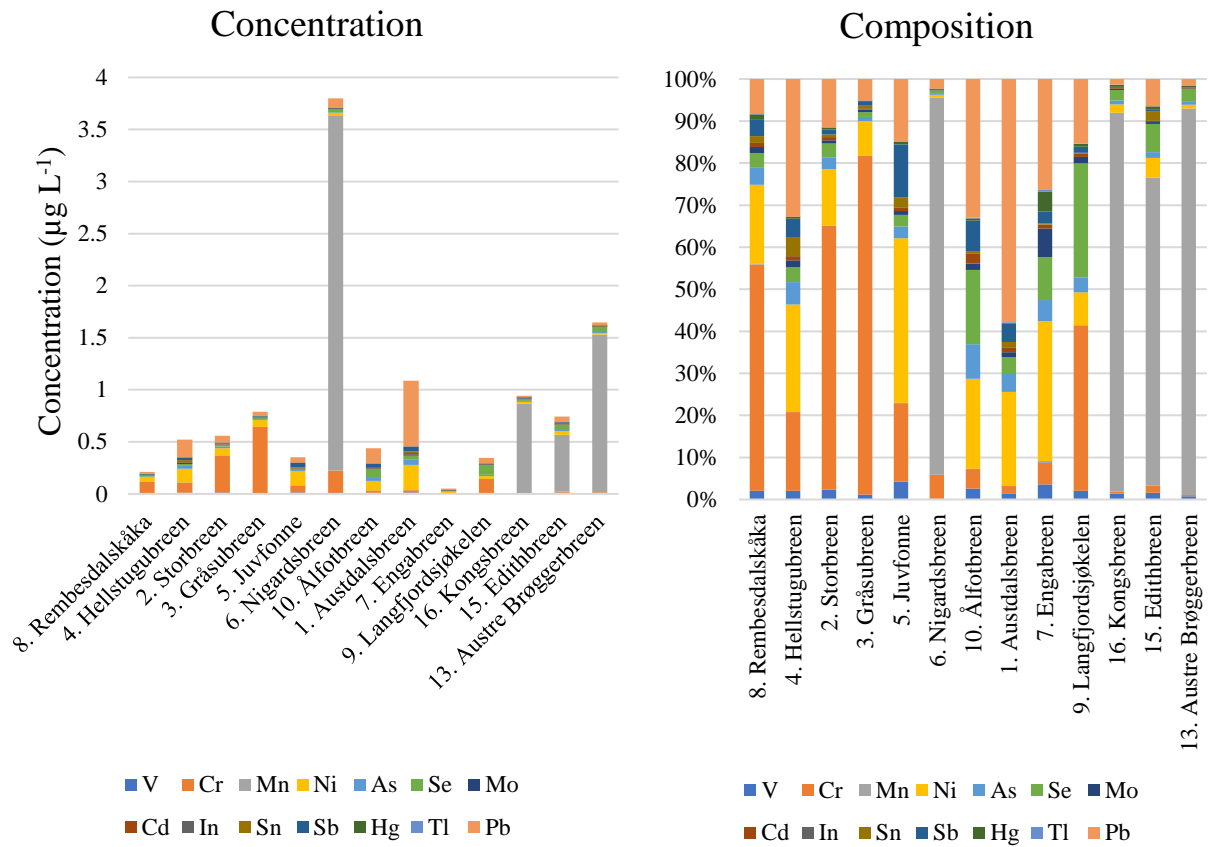


Figure 14 Heavy metal concentration ($\mu\text{g L}^{-1}$) (left) and composition (%) (right) without Cu and Zn in snow samples collected from the glaciers indicated.

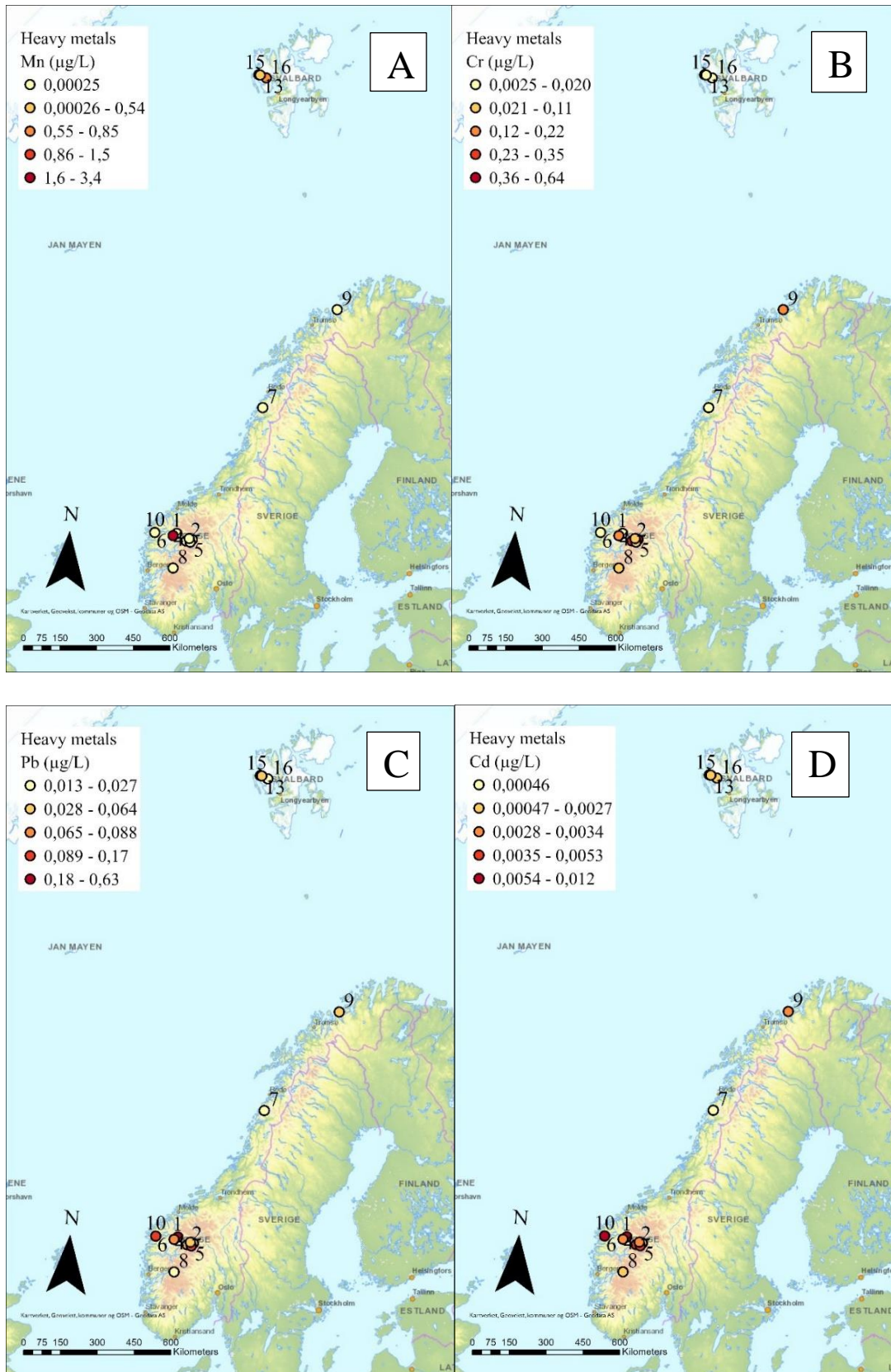


Figure 15 Concentrations of A) Mn, B) Cr, C) Pb and D) Cd ($\mu\text{g L}^{-1}$) in the snow on the glaciers: Austdalsbreen (1), Storbreen (2), Gråsubreen (3), Hellstugubreen (4), Juvfonne (5), Nigardsbreen (6), Engabreen (7), Rembesdalskåka (8), Langfjordjøkelen (9), Ålftobreen (10), Austre Brøggerbreen (13), Edithbreen (15) and Kongsvegen (16).

4.3.4 Source Identification of Elements using PCA

The principal component analysis of the element concentrations in the glaciers is shown in Figure 16. In the loading graph (Figure 16 A), two different groups of elements can be identified. Along PC1, the elements Co, Sb, P, Ni, Zn, Cu, Pb, Mo, K, Cd, and As are grouped, meaning that 35% of the differences in the glaciers can be explained by the different concentrations of these compounds. Along PC2, the elements Mg, Br, Sr, Ca, Na, Cl, S, Se, B, and Li are forming a second group explaining 31% of the differences. As these two groups are on a right angle in respect to each other they do not correlate.

The group along the PC1 axis consists mainly of heavy metals, except for K and P which are major elements. The highest concentrations of these groups were found on Austdalsbreen (Figure 16 B). According to AMAP (2005), the elements Cd, Cu, Zn, and As typically derive from non-ferrous metal production. Sb, Ni, and Mo typically derive from stationary fossil fuel combustion, Sb and Ni can, however, also be emitted by non-ferrous metal production. Pb's main anthropogenic source to the environment has traditionally been through vehicle traffic, but stationary fossil fuel combustion and non-ferrous metal production are also potential sources (AMAP, 2005). As most of the elements in this group can be associated with non-ferrous metal production an influence of this source on the glaciers appears likely. However, no non-ferrous metal production could be found close to the glacier with the highest concentrations of these compounds, Austdalsbreen (1). Instead, as mentioned in chapter 4.3.3, a non-ferrous metal production industry is located close to Ålfotsbreen (10), which is the glacier with the third highest loading score of these compounds (Figure 16).

The second group along the PC2 axis consists mainly of major and trace elements (Figure 16 A). As mentioned before, Na, Cl, and Br that are part of this group are typical in seawater and so are Ca, Mg and S (Duxbury et al., 2020). The glacier that has the highest concentration of this group is Langfjordsjøkelen, which is located close to the coast (Figure 16 B). Comparing the distance of the glaciers from the closest fjord to the loading of these elements, a gradient along PC2 can be observed, where the glaciers closest to the fjord (marked with 1) are lowest on the axis and glaciers furthest from fjords are the highest up (marked with 3) (Figure 17). This shows that the influence of marine sea spray seems to explain 31% of the variance in the glaciers.

The glaciers were also categorized according to their latitudinal location and their altitude (Figure 17). The scores of the glacier along the PC1 axis do not seem to be affected by

latitude, altitude, or distance to the fjord. The difference in concentration of the glaciers, therefore, seems to derive from local sources. Along PC2 the clearest trend is shown for the distance to the fjord, which as mentioned is the most likely explanation. However, latitude and altitude also seem to show a slight trend along PC2. The glaciers with the lowest latitudes appear to be located at the top of the graph, while the higher latitude seems to be located in the lower part of the graph. On the other hand, glaciers with low altitudes are located in the lower part of the graph, and glaciers located at higher altitudes are at the top of the graph. The three chosen factors, latitude, altitude, and distance to fjord seem to covariate with each other. As a lot of high mountains in southern Norway are located further inland it also means that they are further from a fjord, making it hard to distinguish between the factors. For the elements, the trend for distance to the fjord is the clearest and the compounds affecting the scores are typical for marine influence making it the most likely influencing factor. Lastly, the glaciers on Svalbard are grouped, while the glaciers on mainland Norway seem to be more spread out, indicating potential local sources that could affect the concentrations in mainland Norway (Figure 17).

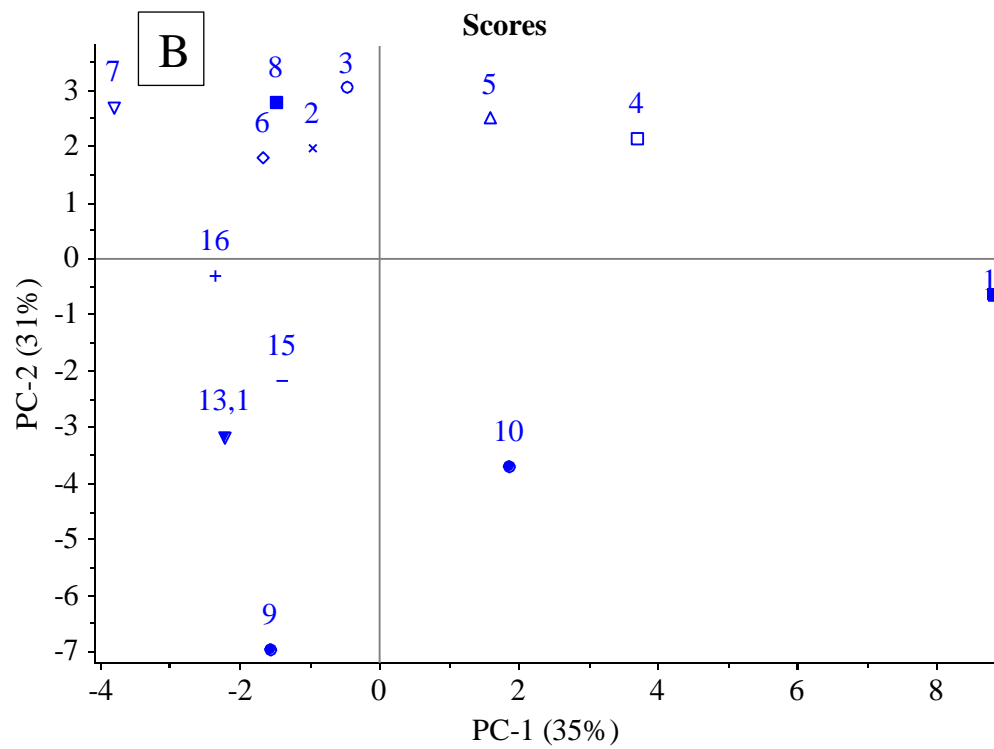
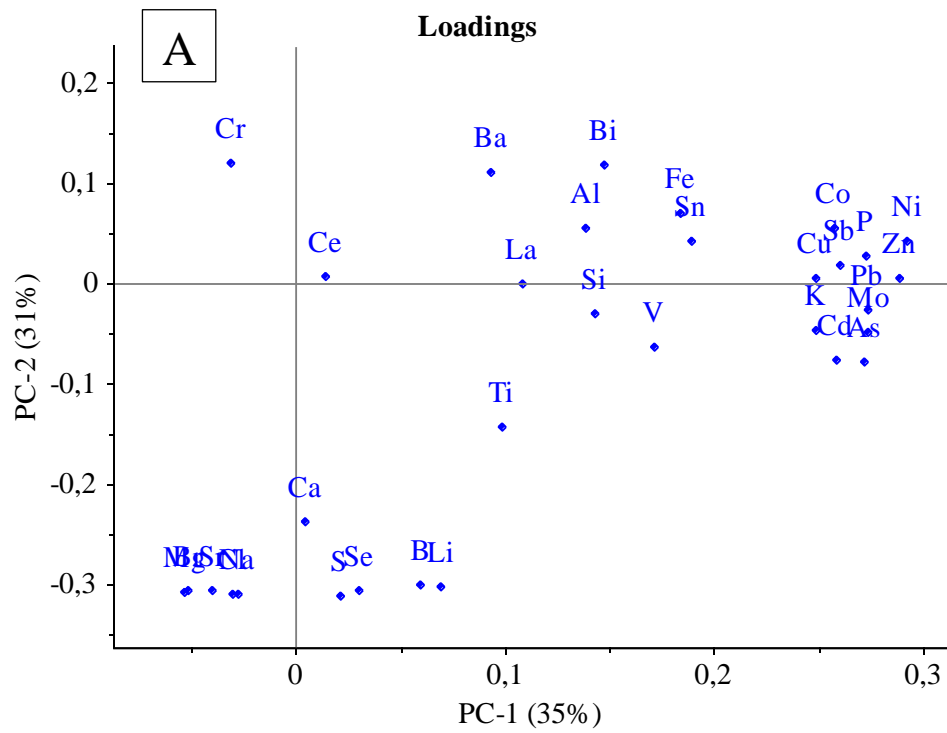
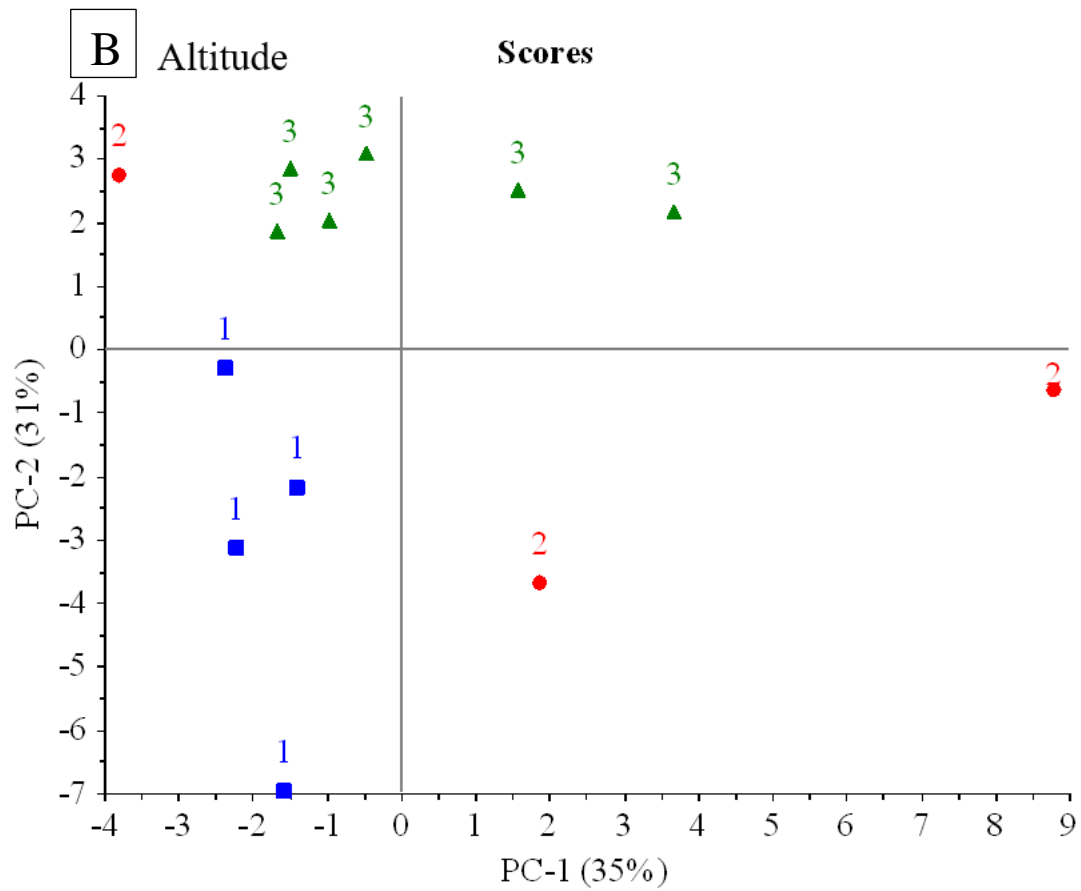
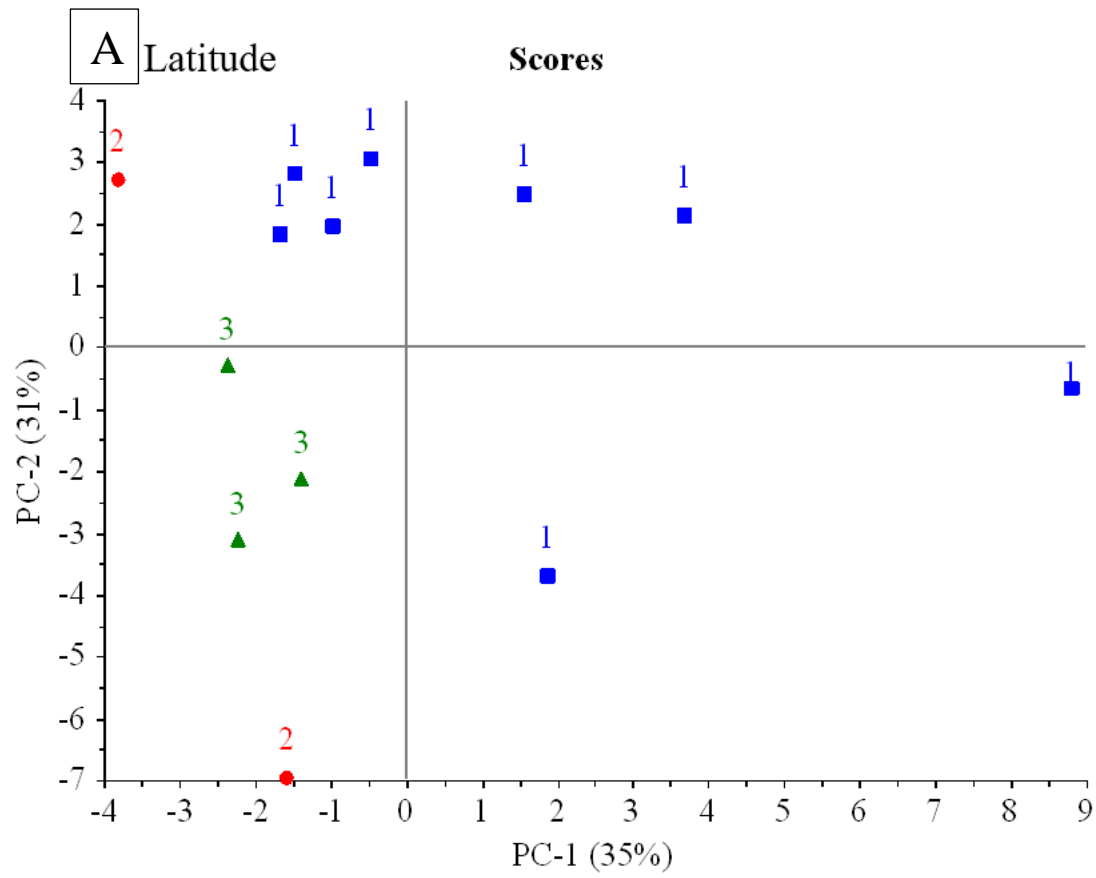


Figure 16 PCA plot of the element composition of the glaciers: Austdalsbreen (1), Storbreen (2), Gråsubreen (3), Hellstugubreen (4), Juvfonne (5), Nigardsbreen (6), Engabreen (7), Rembesdalskåka (8), Langfjordjøkelen (9), Ålftobreen (10), Austre Brøggerbreen (13), Edithbreen (15) and Kongsvegen (16). Factor loading (A) and score of the samples (B).



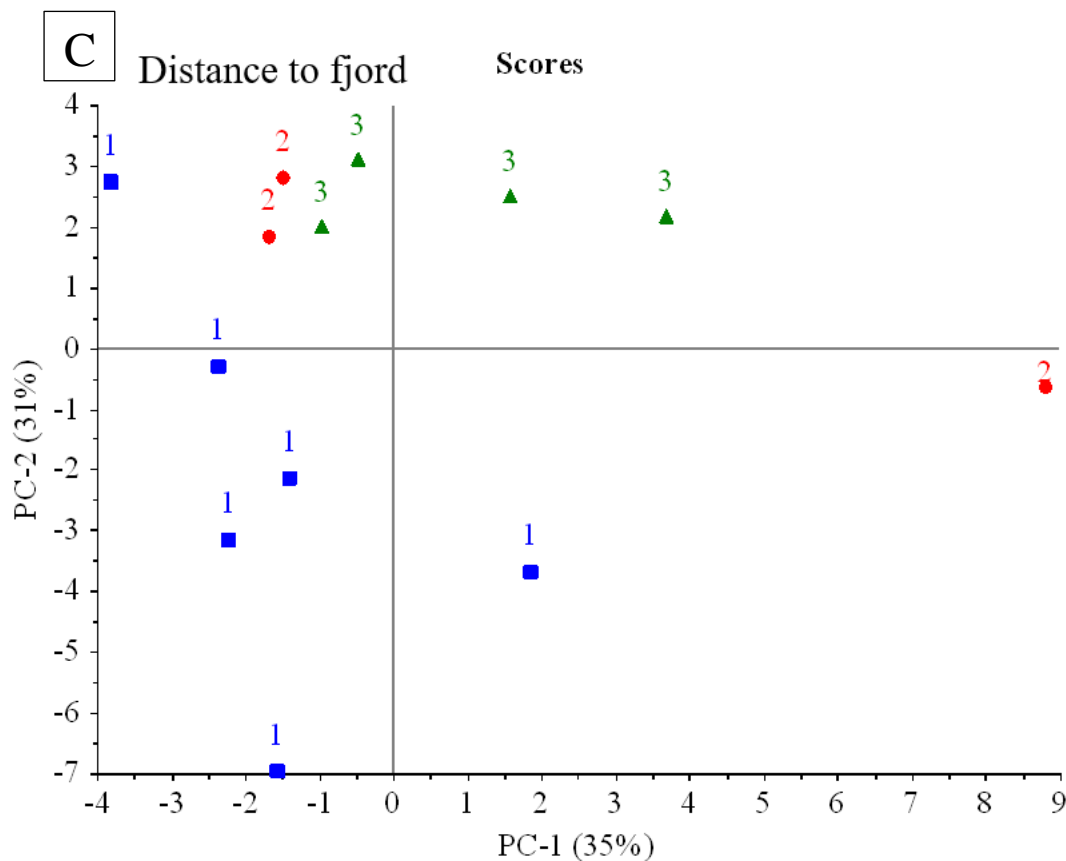


Figure 17 PCA plots of the element concentrations showing 3 groups of the glaciers for each factor: Latitude (A), Altitude (B), Distance to fjord (C). The glaciers are grouped into 3 groups. Latitude 1: 60-62°N, 2: 66-71°N, 3: 78-79°N. Altitude 1: 400-1000masl, 2: 1000-1400 masl, 3: 1500-2300 masl. Distance to fjord: 1. 0-50km, 2. 100-140km, 3. 150-170km.

4.3.5 Seasonal Changes in Element Concentration in Snow on Svalbard

Samples taken in summer on Svalbard are significantly lower in the concentration of major elements and trace elements. The total concentration decreased by 77% and 79%, respectively (Figure 18). The concentration of heavy metals, on the other hand, is similar in both seasons.

As mentioned in chapter 4.3.1, trace and major elements were measured in fresh and old surface snow in Marguerite Bay Islands, Antarctic Peninsula (Kakareka et al., 2022), and on Austre Brøggerbreen from early spring to late spring (Spolaor et al., 2021). Both studies saw a decrease in Na, Mg K, and Ca concentrations, Kakareka et al. (2022) from new to old snow and Spolaor et al. (2021) over the spring season. Further, Kakareka et al. (2022) found the lowest average concentrations of Fe, Cr, Se, Ba, As, and Tl in old snow. The decreases in concentrations of the mentioned elements are according to the authors connected to snow redistribution and post-depositional processes, evaporation, and leaching (Kakareka et al., 2022). The study also found an increase in the concentration of Al, Mn, Mo Ag, Th, and U in old snow. No increase in the concentration of these elements was found in this study. Spolaor

et al. (2021) found that Cl stays at an almost constant concentration and that Br increases during the spring season, which is the opposite of what was found in this study, where both Cl and Br seem to decrease from spring to summer. The study of Spolaor et al. (2021) started on the 27th of March and ended on the 31st of May, while the snow in this study was sampled on the 28th/30th of April the first time and then in the summer again between the 27th of June to 22nd of August. As the second measurements were taken later than the last samples by Spolaor et al. (2021), further processes leading to the decline in Cl and Br might have occurred. However, further research is needed on the snow concentrations covering the period spring to summer to explain the processes occurring during this period in further detail.

A study on air particles (PM₁₀) close to Ny-Ålesund, Svalbard, found that the particles had higher concentrations of geogenic and anthropogenic elements in March and April when the ground was almost entirely covered with snow and ice, suggesting that these particles were transported there by long-range atmospheric transport (Conca et al., 2019). Emissions of anthropogenic metals related to ship emissions (i.e. Co, Ni, and V) peaked in late spring and summer, due to increased ship activity in the fjord. In this study, no difference in the heavy metal concentration between spring and summer was observed. This might be due to that the sampled snow in the summer was old snow deposited in the spring that had not yet melted, instead of newly fallen snow which might represent the concentrations in the air in summer better. Furthermore, the cruise ship activity around Ny-Ålesund was less during 2021 than in previous years due to the Covid-19 virus, which most likely reduced the impact of this source on the snow concentrations measured in this study (MOSJ, 2022).

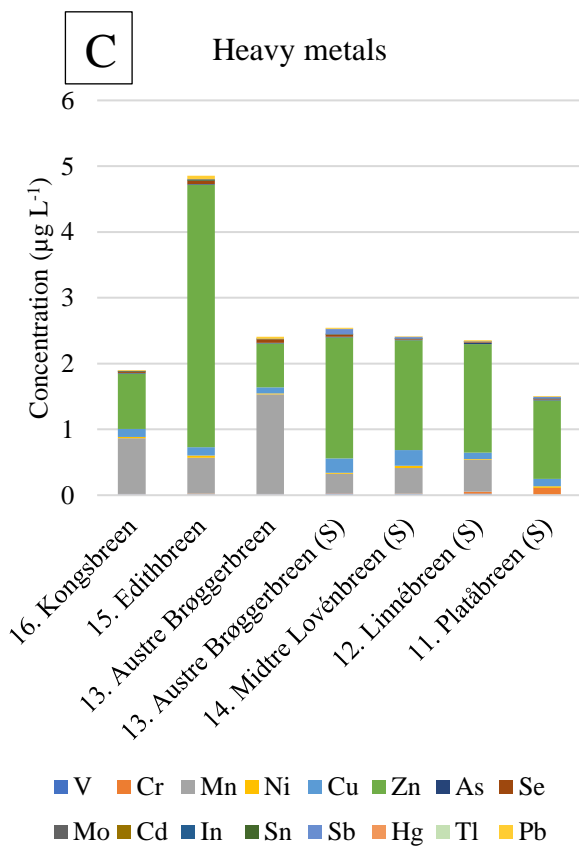
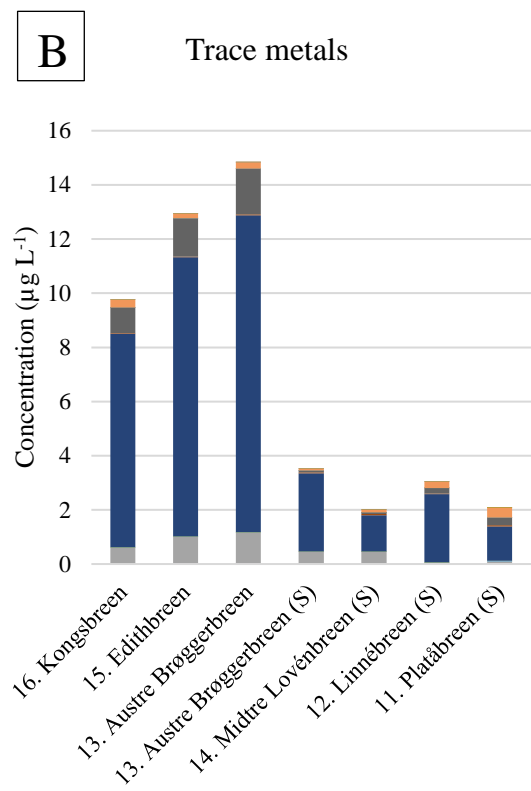
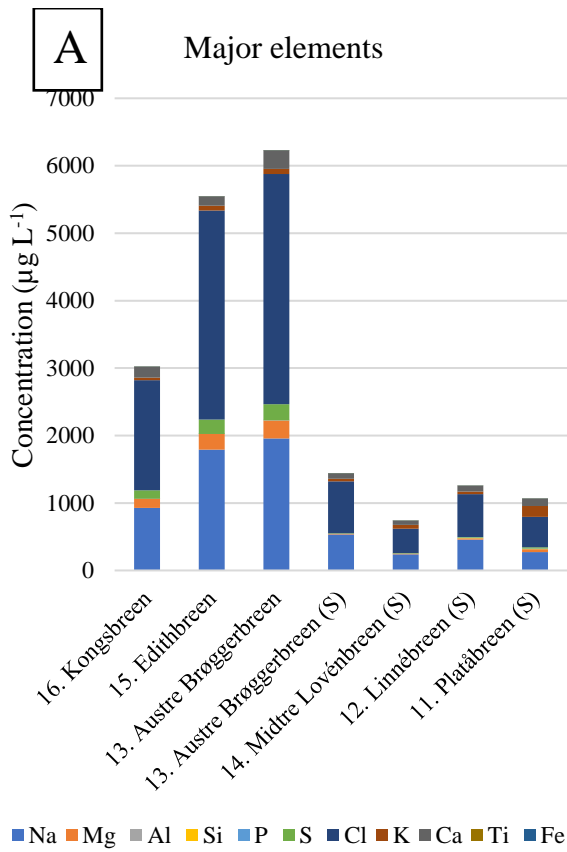


Figure 18 Trace elements (A), Major elements (B), and heavy metal (C) concentration ($\mu\text{g L}^{-1}$) in the snow on the glaciers sampled on Svalbard.

The seasonal differences were additionally analyzed using principal component analysis. PC1 explains 50% of the variance and PC2 20%. Along PC1, the elements Na, Br, Cl, S, Mg, Sr, Li, Cd, Ti, Pb, Mo, Bi, and Ca are grouped, and they negatively correlate with P (Figure 19). The glaciers sampled in spring are higher in Na, Br, Cl, S, Mg, Sr, Li, Cd, Ti, Pb, Mo, Bi, and Ca than the glaciers sampled in summer. Out of the three glaciers sampled in spring, Kongsvegen (16) had the lowest concentration of these elements. This might be either because it is the furthest from the fjord, which leads to less marine influence (Na, Cl, Br, Mg), but it is also located the furthest from Ny-Ålesund, which might be a potential local source of elements such as Pb and Cd.

Ionic compounds such as Na, Cl, Br, Mg, S, Sr, Ca, and Li can depress the freezing point of water, which leads to snow melting at lower temperatures (Atkins et al., 2018). These ions were, thus, possibly lost by runoff, leading to lower concentrations in the snow in summer in comparison to the samples in spring.

Higher concentrations of Cd, Ti, Pb, Mo, and Bi were found in spring than in summer. At the weather station in Zeppelin Observatory, Ny-Ålesund, the atmospheric concentrations of e.g. Cd and Pb have been measured since 1994 (Platt et al., 2022). The observations show that Cd and Pb decrease in atmospheric concentration during the summer season (Platt et al., 2022). This means that the addition to the snow by dry deposition or rain during the summer is limited. In addition, the compounds could run off, leading to a lower concentration in the snow sampled in spring.

The glaciers sampled in the summer have a mean concentration of P that is 4.6 times higher than in the snow sampled in spring ($p < 0.05$). Phosphorous is an essential nutrient for all organisms. On most of the glaciers sampled in the summer, snow algae were observed. A study on snow algae revealed that mineral dust facilitates algal blooms by supplying P to the algae on the snow (Mccutcheon et al., 2021). A higher deposition of mineral dust is likely in the summer as the surroundings of the glaciers are not covered by snow, however, P does not correlate with lanthanides, which would be expected in mineral dust. However, some microorganisms, such as algae, can also take up and store P beyond what is necessary for immediate growth, called luxury uptake (Keenan and Auer, 1974). Mccutcheon et al. (2021) found in their study a delay in phosphorous addition to snow algae, which according to the authors suggests a mechanism of phosphate storage in snow algae. The increased P

concentration in the summer could therefore potentially be due to the storage of P in snow algae from melting snow leading to higher concentrations in the snow that remains.

Along PC2 Cr, Co, K, Ba, As and Si are grouped on the opposite side of La, Ce, Fe, Sb, Cu and V meaning they negatively correlate (Figure 19). The glaciers sampled in the spring all have low loadings on the PC2, meaning that they are not affected by this component.

Platåbreen (11) is the most affected by the group Cr, Co, K, Ba and is therefore located far up in the graph, followed by Linnébreen (12), while Austre Brøggerbreen (13.2) and Midtre Lovénbreen (14) are located further down in the graph towards La, Ce, Fe and Sb. Platåbreen (11) and Linnébreen (12) are located about 100km further south than the rest of the glaciers sampled in Svalbard. La and Ce are both lanthanides and are most likely connected to mineral dust from the surrounding area. Local geological differences could therefore be a potential explanation for the differences in the summer concentrations. Anthropogenic atmospheric Cr is, on the other hand, typically connected to coal combustion (AMAP, 2005). Further, one of the primary ways that Ba is released into the atmosphere is through coal ash (Gad, 2014). Platåbreen (11) is about 5km away from a coal power plant and Linnébreen (12) is 13 km away from the coal power plant in Barentsburg. Therefore, coal combustion might be a potential source of Cr and Ba. Other metals typically connected to coal combustions such as Sb, Se, and Sn are, however, not correlating with Cr (AMAP, 2005).

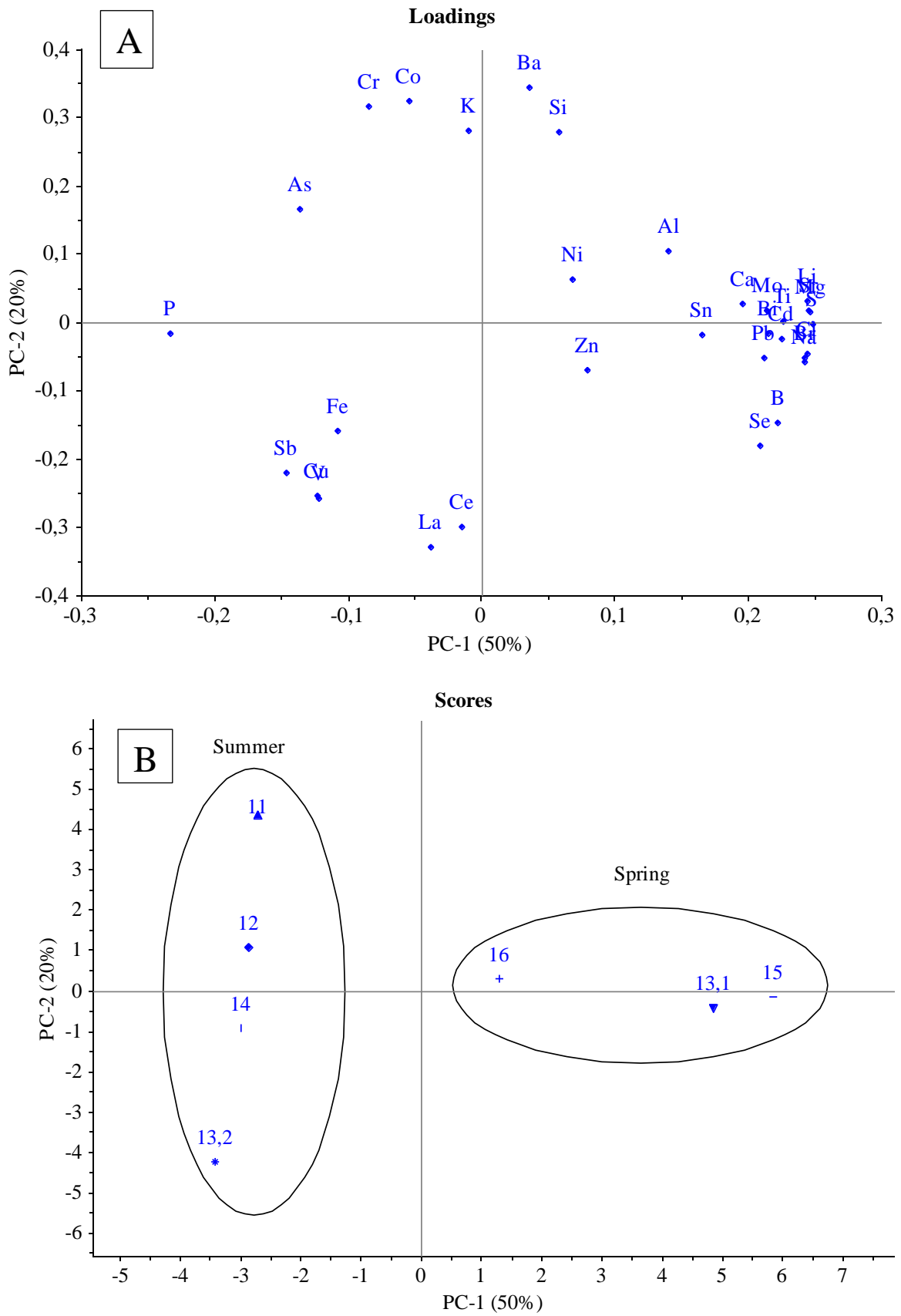


Figure 19 PCA plots on glaciers from Svalbard sampled in spring and summer: Platåbreen (11), Linnébreen (12), Summer Austre Brøggerbreen (13.2), Spring Austre Brøggerbreen (13.1), Midtre Lovénbreen (14), Edithbreen (15) and Kongsvegen (16). Loadings of the elements (A) and score of the glaciers (B).

4.4 Polycyclic Aromatic Hydrocarbon (PAH) Composition and Distribution

The total PAH concentration on the glaciers varies between 18 – 89 ng L⁻¹ (Figure 20). Auldalsbreen (1) has the highest total concentration, while Langfjordsjøkelen (9) has the lowest. A study on 16 PAHs in the vicinity of Ny-Ålesund found concentrations ranging from 2.6 – 299 ng L⁻¹ (Vecchiato et al., 2018). The high concentration of PAHs in the study was explained by local sources of coal dust. Contrary to the study by Vecchiato et al. (2018), this study only measures the concentrations of PAHs in background areas. It is, therefore, reasonable that the concentrations found in this study are in the lower range of what was found in Vecchiato et al. (2018) snow samples. A study (Levshina, 2019) on 13 PAHs in the urban and nature reserve areas of southern far east Russia showed similar concentrations in the nature reserve areas (38.92-79.80 ng L⁻¹) as was found for the background areas in this study.

In most of the samples, NAP has the highest concentration, followed by PHE, FLT, and PYR (Figure 20). NAP, ACY, FLU, PHE, FLT, and PYR were quantifiable in all samples. IND, DBA, and BgP, on the other hand, were in all samples, below either LOD or LOQ. All except 1 sample was below LOD/LOQ for the compound BbF, and 2 for BkF (Appendix F). This means that all the 6-ring PAHs and most of the 5-ring PAHs did not get transported in high enough concentrations to be quantifiable to the background areas. As these are the least volatile PAHs, they are likely deposited before reaching the glaciers. Important to point out, however, is that these compounds also had the highest LOD and LOQ. Na et al. (2011) studied the PAH composition in the snow in Fildes Peninsula, Antarctica. They found that NAP accounts for 60.57% of the total concentration, followed by FLU (21.61%) and PHE (9.80%). Similar to this study, Na et al. (2011) showed that NAP dominates in the samples as it has the highest potential for LRAT, followed by 3-ring PAHs, which have the next highest potential for LRAT (Figure 20).

No latitudinal trend for the total PAH concentration was found ($p > 0.05$) (Figure 21). Visually looking at individual compounds in the snow on the glaciers a potential decreasing trend with latitude can be seen for the compounds ACY, PHE, FLT, and PYR (Figure 22). However, grouping the glaciers into 3 latitudinal groups a significant decrease could only be found for PHE and FLT ($p < 0.05$). PYR is close to being significant ($p = 0.068$). Garrido et al. (2014) studied PAH in the atmosphere in Europe, including Svalbard, and found an overall decreasing trend in the total PAH concentration, contradictory to this study. This might be due

to that NAP was not included in the Garrido et al. (2014) study, while it is the dominating compound found in the arctic in this study. Further, they found significant decreasing trends for four individual PAHs: PHE, FLT, PYR, and BgP (Garrido et al., 2014). The same trends can be seen in this study, except for BgP, which was in all samples below either LOD or LOQ, and PYR, for which no significant decrease was detected. PHE decreases by 59% and FLT by 80%. As PHE is a 3-ring PAH, it has higher LRAT potential than FLT, which has 4 benzene rings. This might explain the lower decrease of PHE towards the arctic region in comparison to FLT. However, these differences could potentially also be caused by local sources. Drotikova et al. (2020) showed that the composition of the 16PAHs emitted by Longyearbyen's coal powerplant is dominated by PHE (54%), followed by FLU (15%), FLT (14%), PYR (9%) and ACY (4%). NAP and FLU show high concentration in both southern Norway and on Svalbard and no significant difference in the latitudinal groups could be found ($p > 0.05$) (Figure 22).

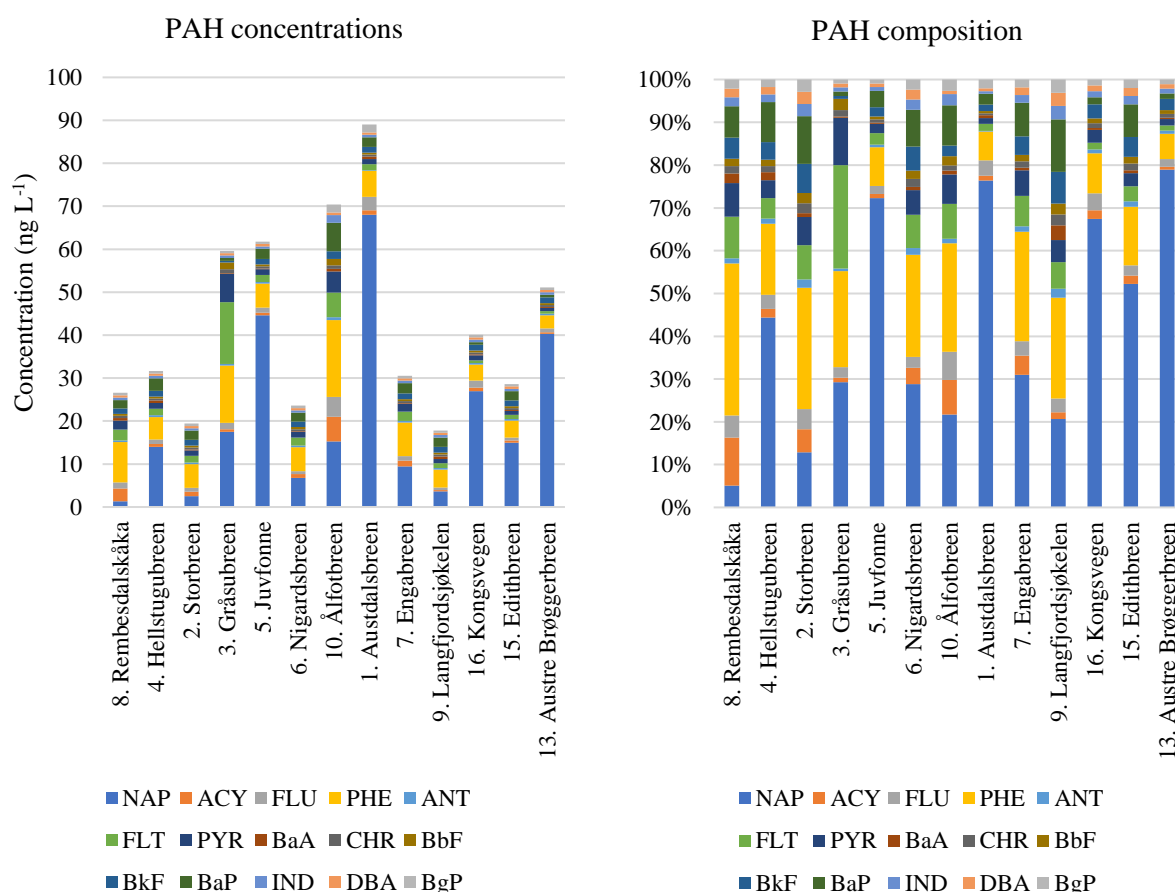


Figure 20 PAH concentrations (ng L⁻¹) (left) and composition (%) (right) in snow samples collected from the glaciers indicated.

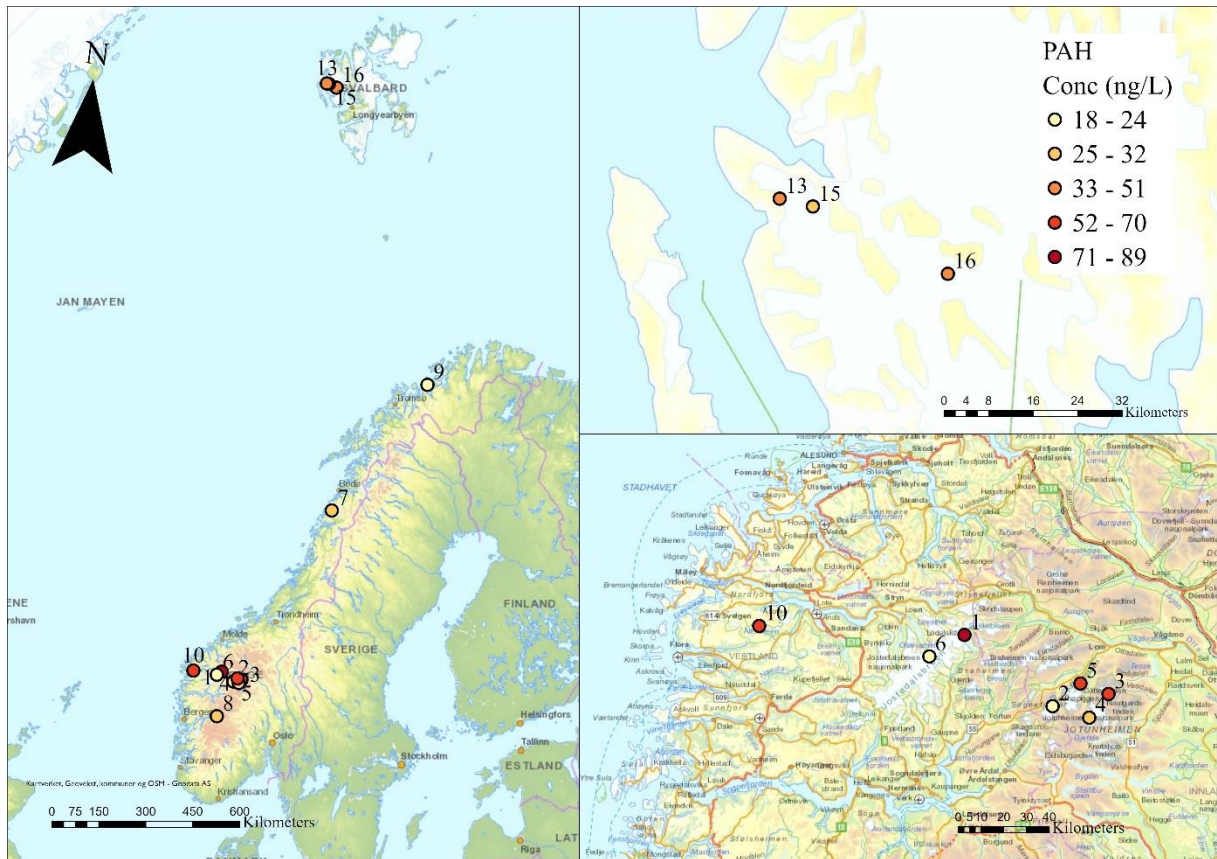
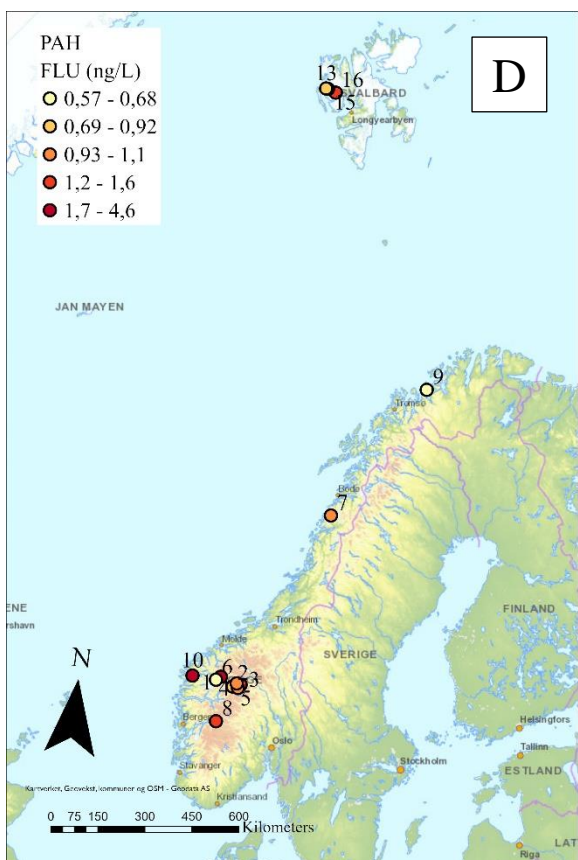
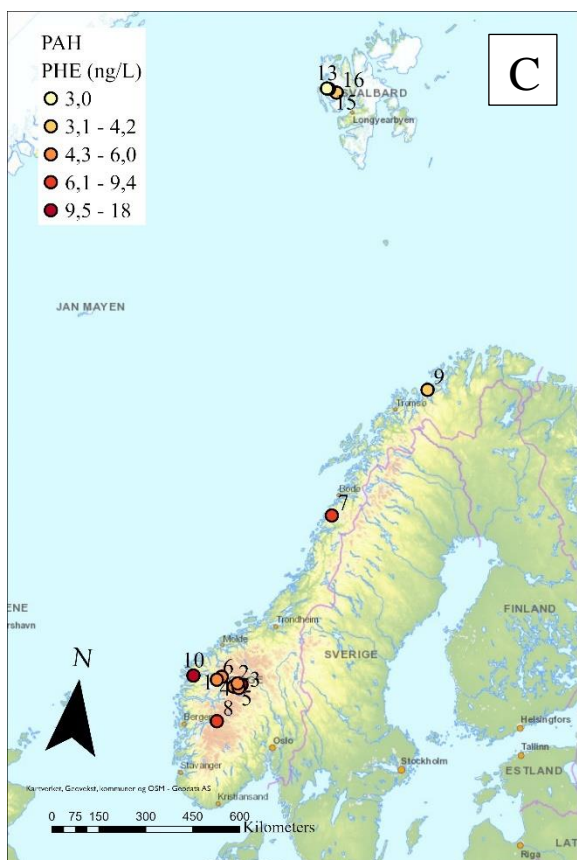
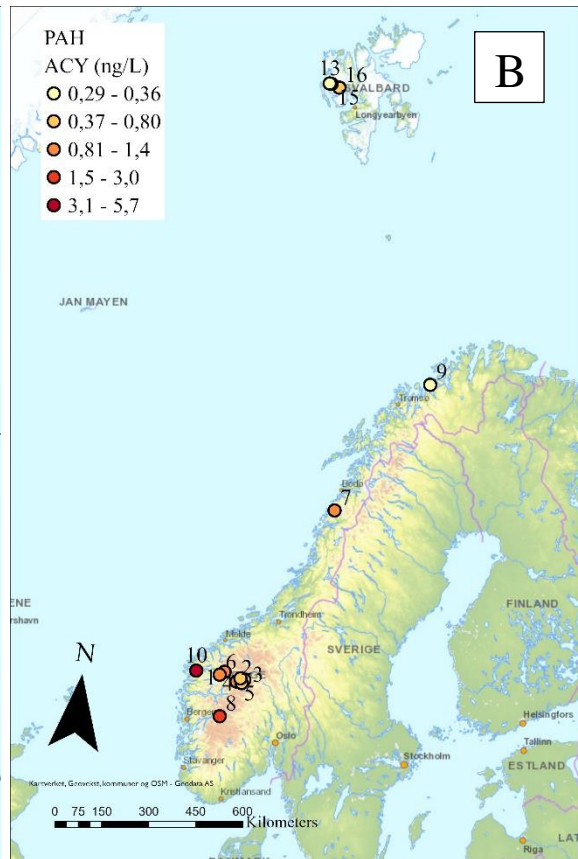
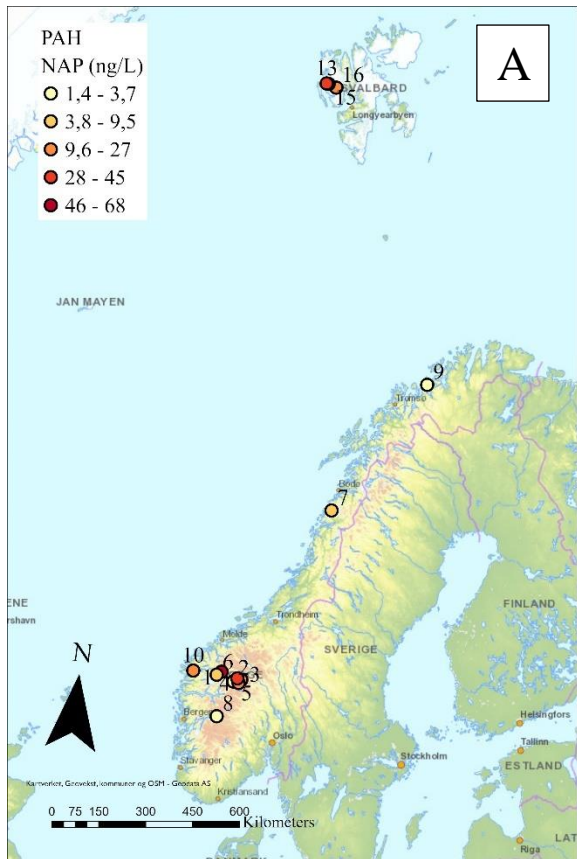


Figure 21 Total PAH concentration (ng L⁻¹) in the snow on the glacier: Austdalsbreen (1), Storbreen (2), Gråsúbreen (3), Hellstugubreen (4), Juvfonne (5), Nigardsbreen (6), Engabreen (7), Rembesdalskåka (8), Langfjordjøkelen (9), Ålfotbreen (10), Austre Brøggerbreen (13), Edithbreen (15) and Kongsvegen (16).



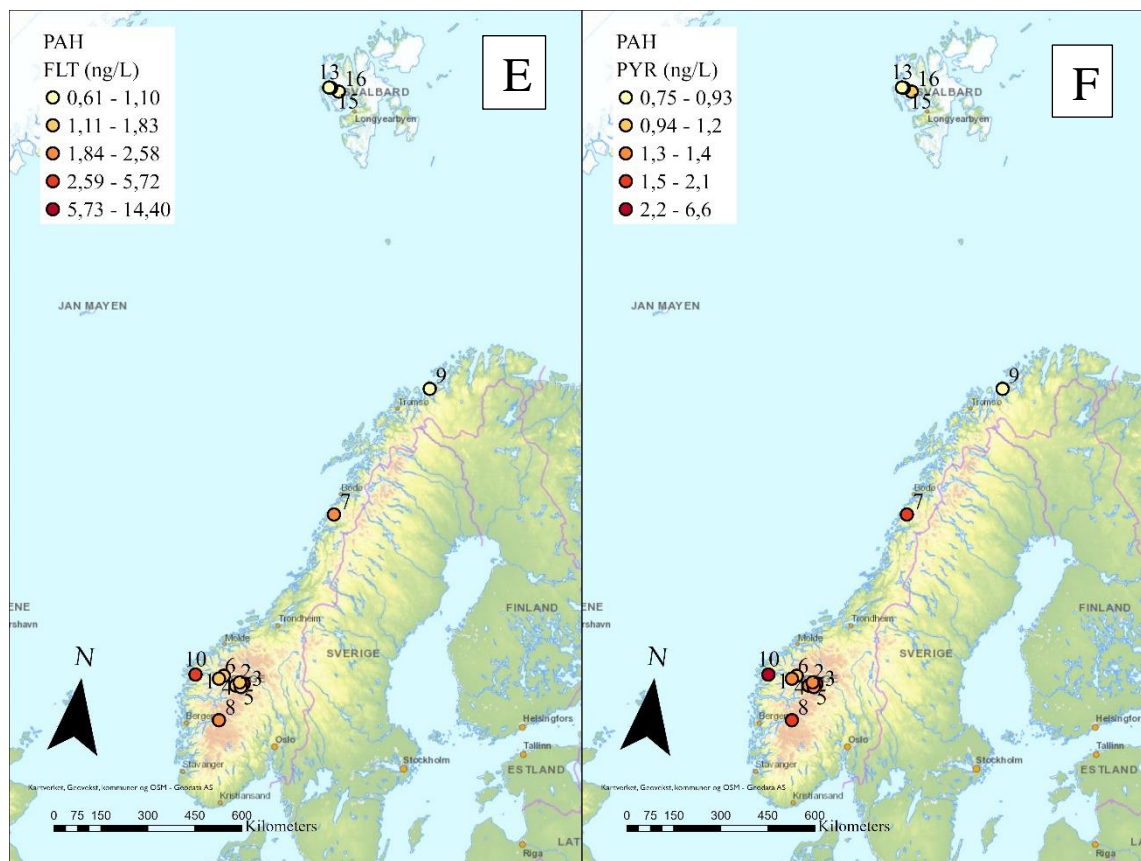


Figure 22 NAP (A), ACY (B), PHE (C), FLU (D), FLT (E), and PYR (F) concentration (ng L^{-1}) in snow on the glaciers: Austdalsbreen (1), Storbreen (2), Gråsubreen (3), Hellstugubreen (4), Juvfonne (5), Nigardsbreen (6), Engabreen (7), Rembesdalskåka (8), Langfjordjøkelen (9), Ålfotbreen (10), Austre Brøggerbreen (13), Edithbreen (15) and Kongsvegen (16).

4.4.1 Source Identification of PAHs using PCA

Only PAH congeners that were quantifiable in at least 3 samples were included in the PCA. The loadings of the different compounds and the scores of the glaciers are shown in Figure 23. NAP and PHE are positioned on opposite sites along PC1, which explains 58% of the variance. Further BaP, ACY, FLU, ANT, CHR, PYR, and FLT are located on the left side of the graph together with PHE, meaning that NAP, which is the most volatile congener, is negatively correlating with these less volatile congeners. Austre Brøggerbreen is located furthest to the right in the graph, which means that it has the highest NAP concentration in comparison to the rest of the compounds. Ålfotbreen (10) is located the furthest to the left meaning it has the highest concentration of the heavier PAHs, in comparison to NAP, of the different glaciers.

PC2 explains 20% of the variance in the dataset. BaP, ACY, FLU, and ANT are located at the top of the PCA, and CHR, PYR, and FLT are at the bottom. Most of the glaciers are located around 0 meaning that they are not influenced by this factor, except for Ålfotbreen (10) and Gråsubreen (3). Ålfotbreen is located in the upper part of the graph, meaning it has higher

concentrations of BaP, ACY, FLU, and ANT, while Gråsubreen (3) is located at the bottom of the graph, being influenced by the factors CHR, PYR, and FLT. A Hotelling's T² distribution ellipse is shown in Figure 23, showing that all samples inside the ellipse are normally distributed. Gråsubreen (3) and Åfotbreen (10) are outside the ellipse and can, therefore, be classified as outliers. This might be due to local sources of PAHs or contamination of the sample. The closest possible contamination source to Gråsubreen (3) is a tourist cabin located 4 km away with a diesel generator. According to Ravindra et al. (2008), high factor loading for FLT, PHE, ANT, and PYR in atmospheric samples indicate diesel emissions. Gråsubreen has high factor loadings of FLT, PHE, and PYR, but it negatively correlates with ANT. The glacier might be influenced by the diesel generator, however, contamination during sample handling could also be the reason. The aluminum bottles of the sample broke in the freezer at the field site and had to be put into regular plastic trash bags for transportation to the laboratory. In the laboratory, the sample was thawed completely in the same plastic bags that were also used for transportation and then transferred to new aluminum bottles. PAHs can leach out of plastic and could have, therefore, contaminated the sample as these bags are not designed for sampling (Khaustov et al., 2022). This did not happen to the sample on Åfotbreen (10). Therefore, local sources are assumed to be affecting the concentration.

High factor loading of ANT, PHE, BaP, BgP, and CHR has been suggested to derive from the steel industry (Ravindra et al., 2008). Out of these compounds, Åfotbreen (10) had high factor loadings of ANT, PHE, and BaP. However, BgP was not included in the PCA, as all samples were below LOD or LOQ. CHR was not included in the factor group and did instead correlate negatively with the group. Åfotbreen (10) is located close to a ferrosilicon metallurgical industry, which may constitute a local source of these PAHs. Other likely sources of PAHs to Åfotbreen are the offshore oil rigs located close to the glacier (Hylland, 2006; "Interactive map - Norwegianpetroleum.no," n.d.).

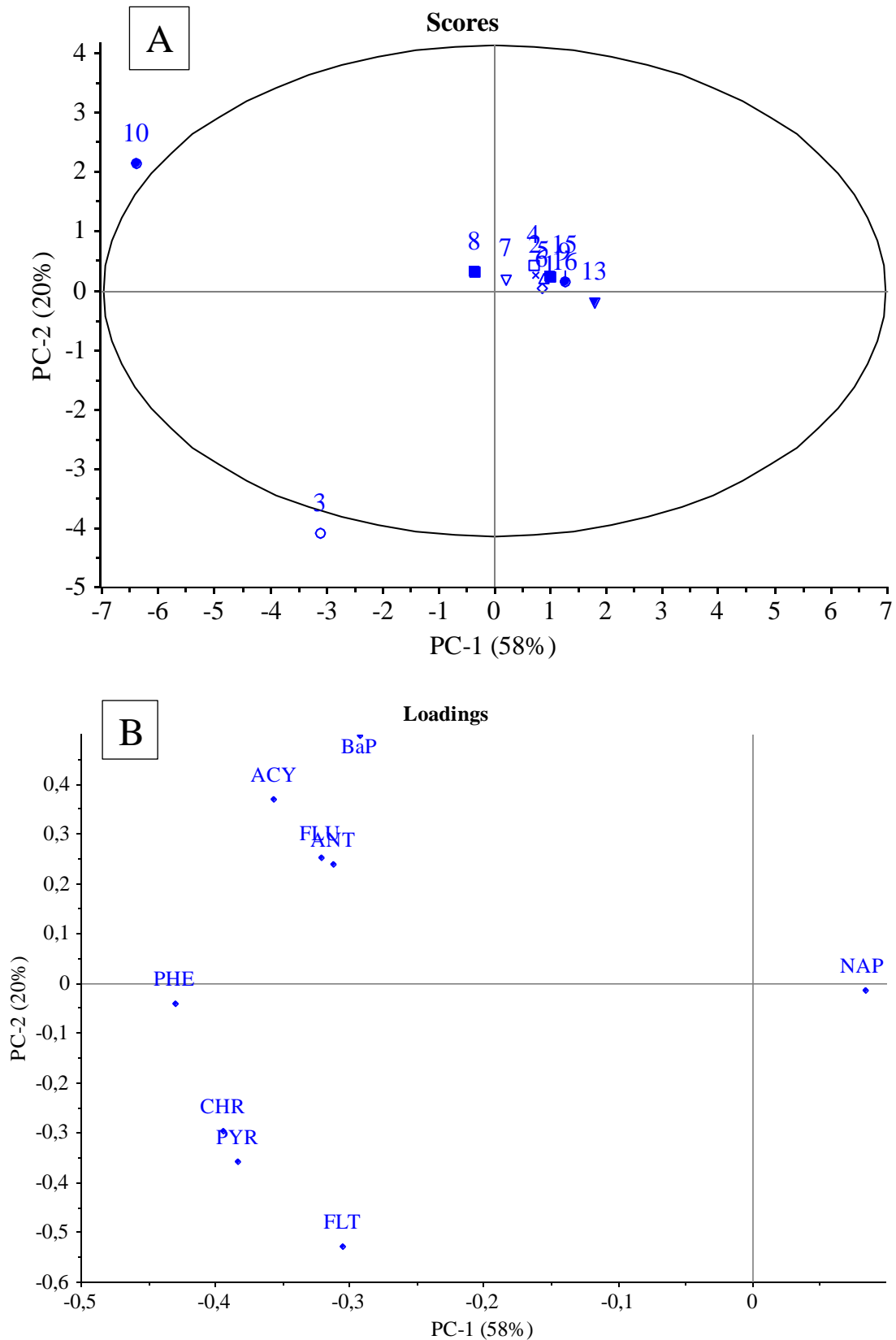
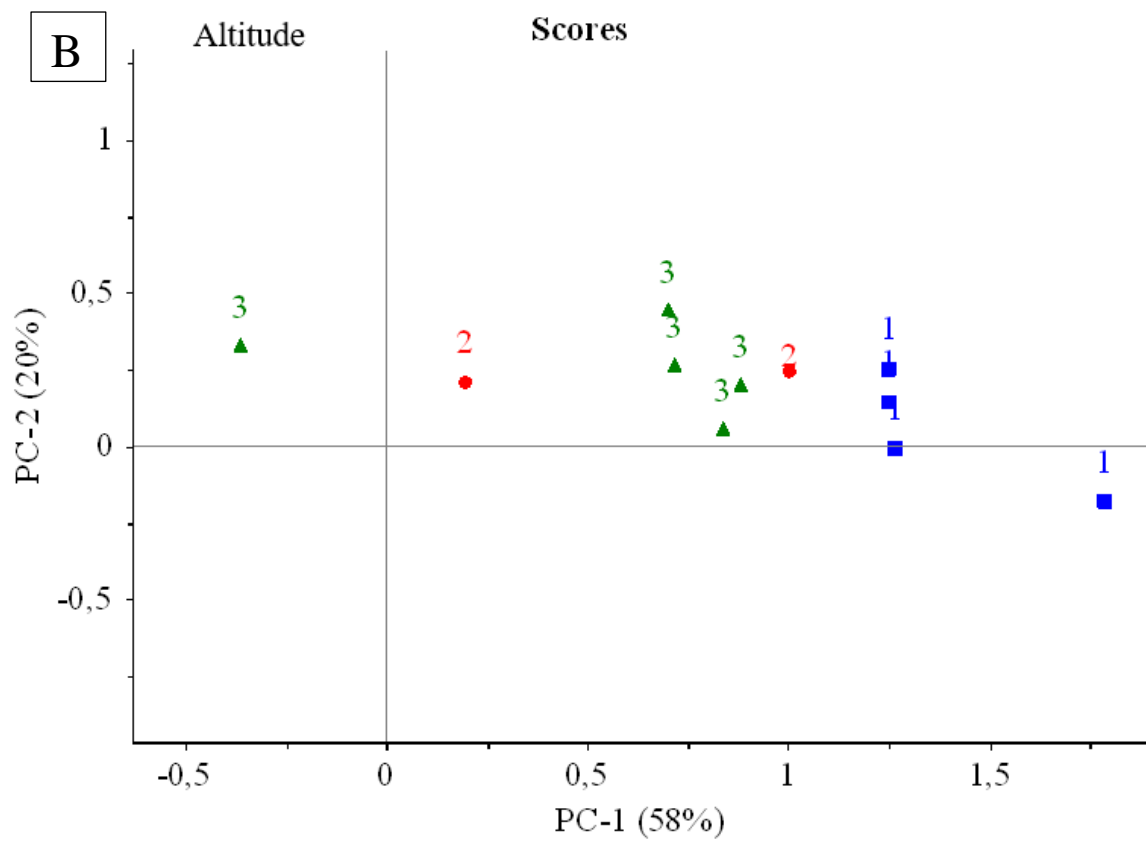
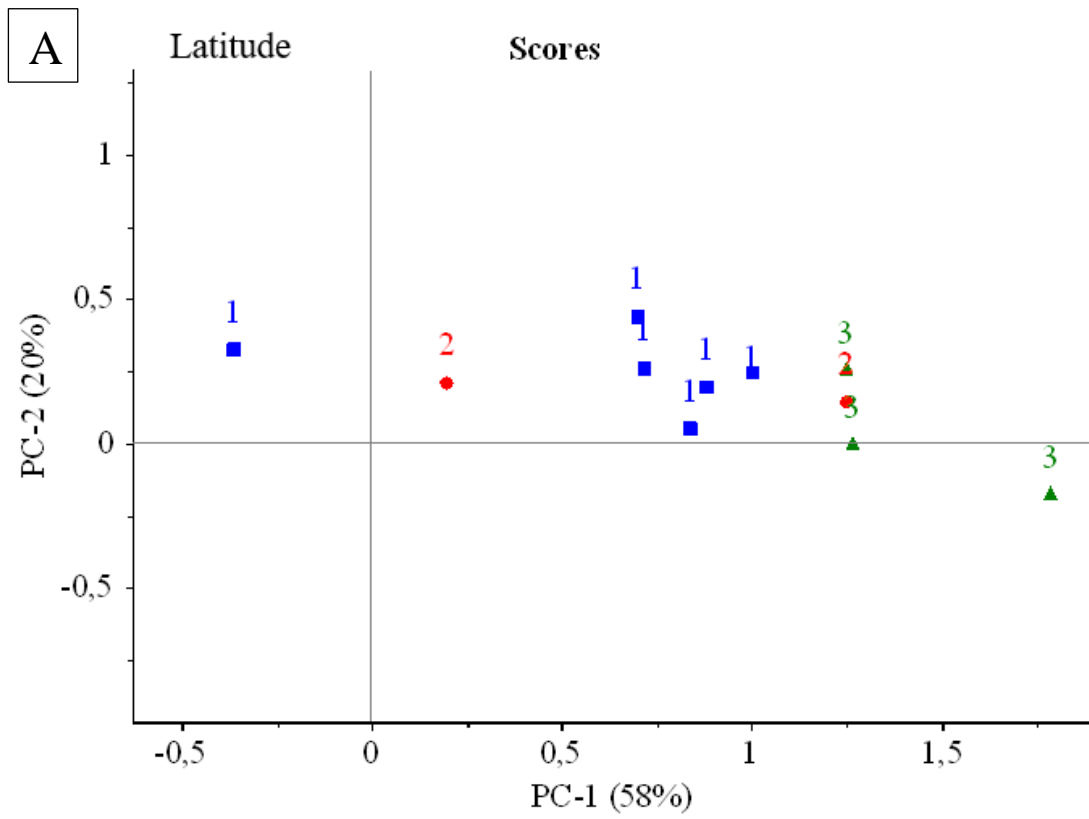


Figure 23 PCA of the PAH concentration of the glaciers: Austdalsbreen (1), Storbreen (2), Gråsubreen (3), Hellstugubreen (4), Juvfonne (5), Nigardsbreen (6), Engabreen (7), Rembesdalskåka (8), Langfjordjøkelen (9), Ålfotbreen (10), Austre Brøggerbreen (13), Edithbreen (15) and Kongsvegen (16). Loading of the elements (A) and score of the glaciers (B).

Grouping the glaciers according to latitude shows a latitudinal gradient along PC1 meaning that 58% of the variance of the PAH concentrations in the samples can be explained by the latitude from which the sample was taken (Figure 24). Glaciers at the highest latitude (3) have higher factor loading of NAP and lower factor loading of the heavier compounds such as PHE, CHR, PYR, ANT, FLU, and FLT. The PAHs with more rings than two seem to deposit at a higher degree at lower latitudes. As mentioned in chapter 4.4, this corresponds to the findings of Garrido et al. (2014) measured in the atmosphere. All samples taken on Svalbard are located furthest to the right of the plot (Figure 24).

The distance to the fjord does not seem to influence the concentrations, but altitude seems to show a slight trend going from high altitude on the left side to low altitude on the right side of the graph. This means that glaciers at lower altitudes have higher factor loading of NAP and glaciers at higher altitudes have higher factor loading of the less volatile PAH compounds PHE, CHR, PYR, ANT, FLU, and FLT. As more volatile compounds, such as NAP, have higher potential for long-range atmospheric transport, they should also be transported to higher altitudes to a higher degree than less volatile compounds. Giannarelli et al., (2019) studied the effect of altitude on PAH concentration in snow and found a 40% decrease in PAH concentration at higher altitude, with significant decreases in high molecular weight PAHs. Comparing the 3 groups statistically, no PAH compounds decrease significantly. As mentioned in chapter 4.3.4 latitude and altitude seem to negatively covariate in this study, meaning the higher in latitude the glaciers are the lower they are in altitude. The trend seen in the PCA in this study could therefore also be due to the covariance of the factors.



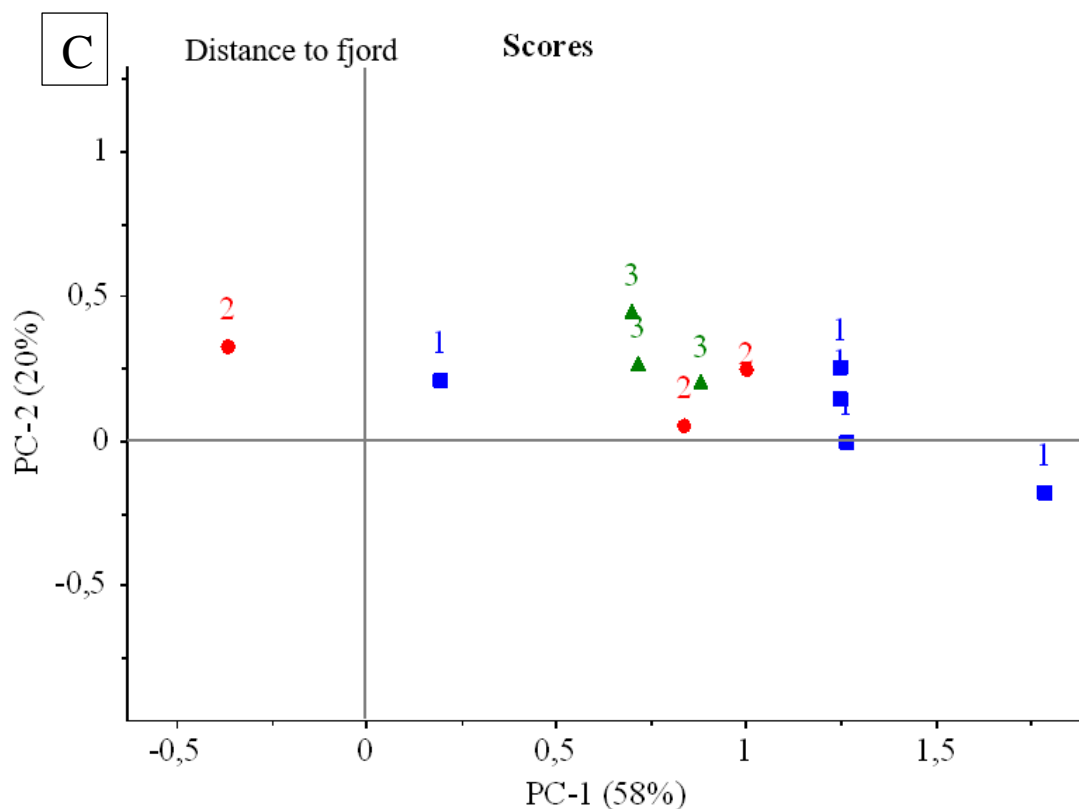


Figure 24 Grouping of the glaciers into Latitude (A), Altitude (B), and distance to the fjord (C). Latitude: 1: 60-62°N, 2: 66-71°N, 3: 78-79°N. Altitude 1: 400-1000 masl, 2: 1000-1400, 3: 1500-2300 masl. Distance to fjord 1. 0-50km, 2. 100-140km, 3. 150-170km.

4.4.2 Seasonal Changes in PAH Concentration in Snow on Svalbard

In total, no differences in concentration can be seen between the spring and summer samples on Svalbard (Figure 25). However, PHE increased significantly by 41% from spring to summer. The increase in PHE is most likely due to local differences between the glaciers. Linnébreen and Platåbreen are both close to coal power plants, which potentially could affect the PAH concentrations (Stout et al., 2015). Linnébreen has the highest total concentration of PAH of the samples taken on Svalbard, including the glacier sampled in spring. Platåbreen, on the other hand, has the next lowest concentration of PAHs, which is surprising but might be due to local meteorological regimes, leading to that the exhaust from the Longyearbyen coal power plant does not reach the glacier. Additionally, Abramova et al. (2016) studied PAHs in snow particulates around Longyearbyen and Barentsburg settlements and found significantly higher total concentrations in Barentsburg than in Longyearbyen. As the emission of 16PAHs from the coal powerplant in Longyearbyen and Barentsburg is dominated by PHE, the differences in spring and summer concentration could be because

different glaciers were sampled in summer than in spring which are located closer to potential local sources (Abramova et al., 2016; Drotikova et al., 2020).

In Austre Brøggerbreen (13), which was sampled during both seasons, the total PAH concentration decreased from spring to summer, where especially NAP decreased in concentration. Garrido et al. (2014) found lower concentrations of 3-ring, 4-ring, 5-ring, and 6-ring PAHs in the atmosphere during the summer. The snow sampled from the glaciers in the summer in this study was old snow from earlier that season, meaning that it was deposited in spring and should therefore mainly represent changes in the snowpack since the deposition, and not the current atmospheric concentrations. Potential processes leading to changes in concentration could be additional dry deposition, runoff, reemission, and photodegradation. However, no studies measuring and explaining changes in PAH concentrations in snow from spring to summer were found to compare the results in this study to.

On the PCA no separation of glaciers sampled in summer and spring can be observed (Figure 26). Linnébreen and Midtre Lovénbreen differ the most from the other glaciers, showing higher concentrations of PYR and FLT. Midtre Lovénbreen is further higher in ACY, BaP, and FLU, while Linnébreen is higher in PHE, ANT, and CHR. PHE dominates the emission from the coal power plants in Svalbard, and CHR was found to compose 2-5% of the emission (Abramova et al., 2016; Drotikova et al., 2020). The coal power plant in Barentsburg is located approximately 12 km from Linnébreen and could potentially affect the PAH concentrations. Platåbreen, which is located approximately 5 km from the powerplant in Longyearbyen does, however, not show increased concentrations of these PAHs, which as mentioned might be due to less emission and/or local meteorological regimes affecting the transportation of the exhaust.

Potential local sources of PAHs to Midtre Lovénbreen could be the diesel power plant in Ny-Ålesund. However, typical factor loadings representing diesel emissions are FLT, PHE, ANT, and PYR according to Ravindra et al. (2008), which are not the compounds in the factor loading group. More samples should be taken at each location to confirm the concentrations and potential sources of PAHs in the snow on the glaciers.

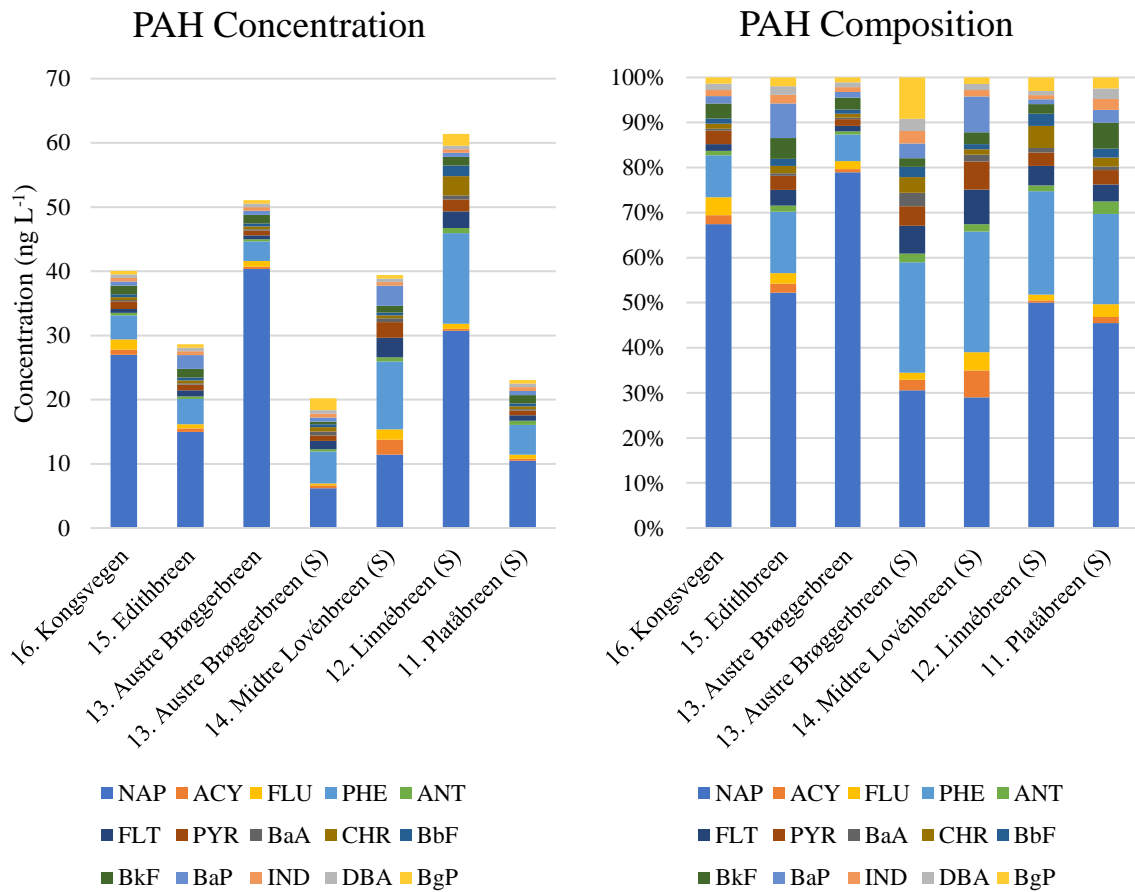


Figure 25 PAH concentration (ng L⁻¹) (left) and composition (%) (right) in the glaciers taken in spring and summer on Svalbard.

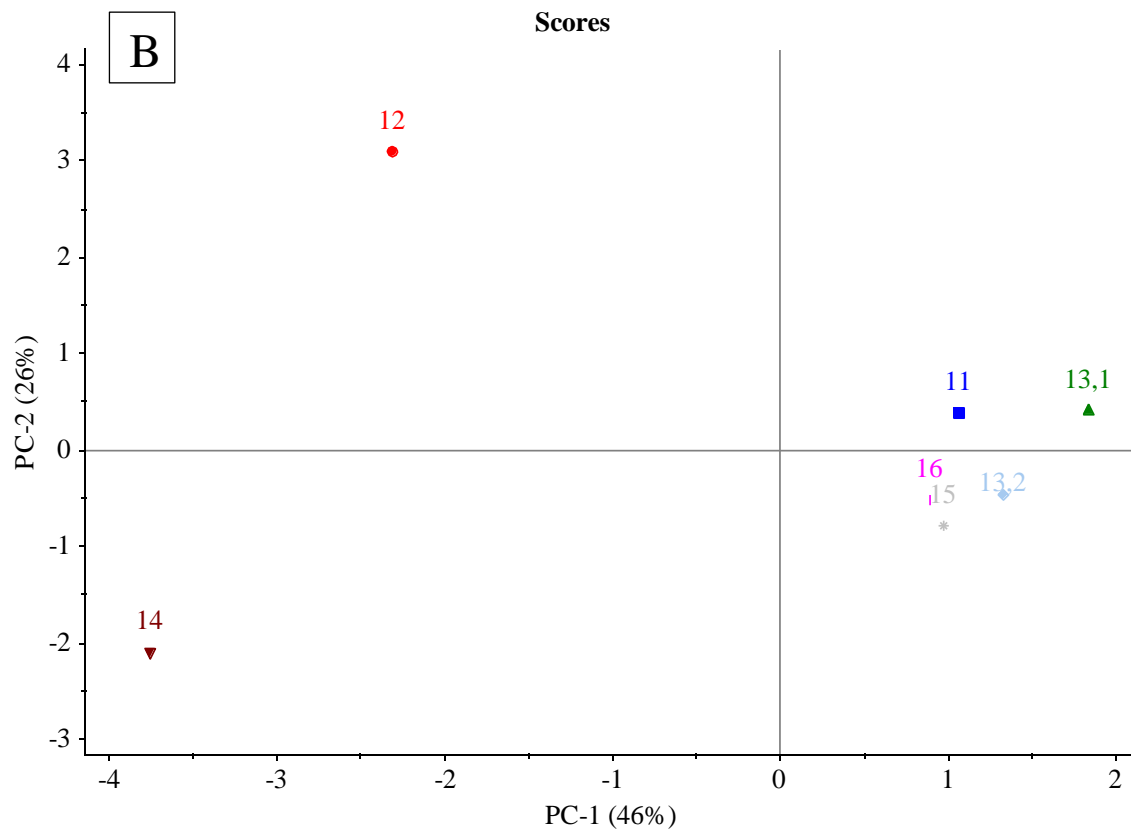
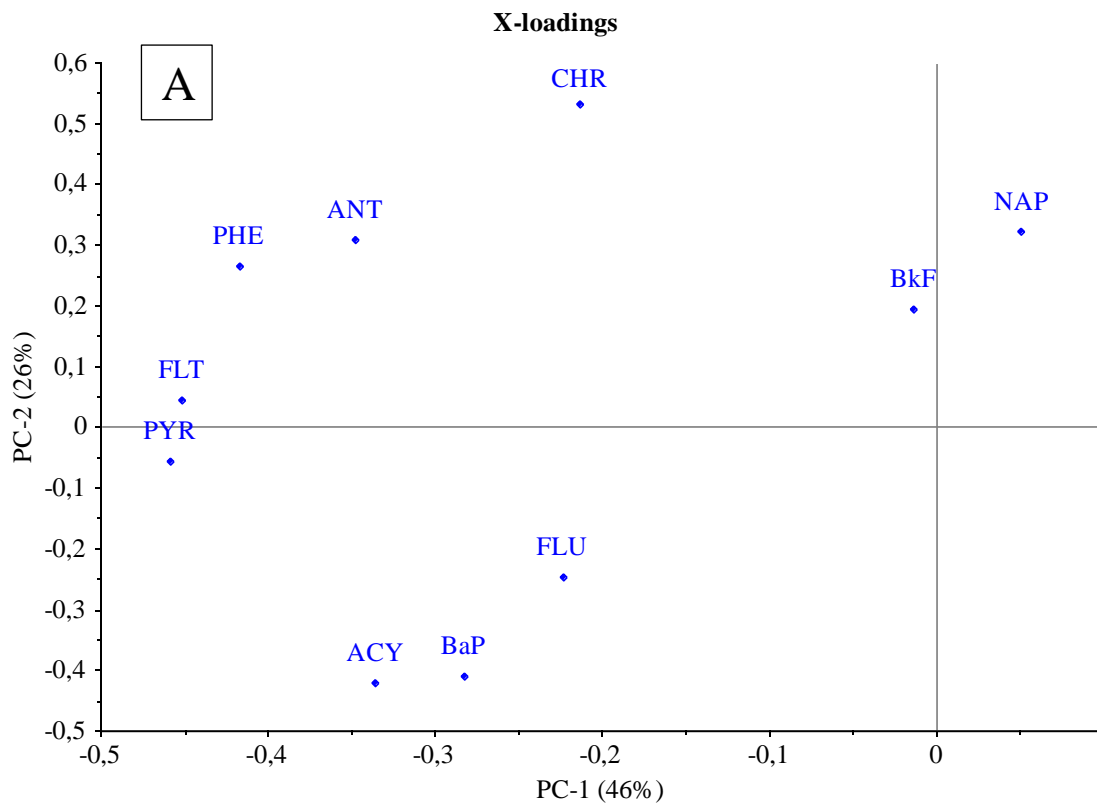


Figure 26 PCA of PAH concentration on glacier sampled in spring and summer in snow on Svalbard. In graph A the factor loading is shown and in graph B the scores of the glaciers are shown.

4.5 Polychlorinated biphenyls (PCB) Concentrations

None of the PCB congeners measured were detected in the samples, which might be due to the low absolute recovery, too low sensitivity of the GC-MS, and/or too small sample size (Appendix G). Hermanson et al. (2020) studied PCB concentrations in snow on four glaciers on Svalbard. They measured 209 different congeners and found total concentrations of 0.458 - 0.844 ng L⁻¹ in the snow, dominated by tetra- and penta- congeners. About 20 L of snow was used for the analysis and XAD columns were used for the extraction of the PCBs. Further, instead of using GC-MS, the study measured the PCB-congeners with isotope dilution gas chromatography high-resolution mass spectrometry (GC-HRMS)(Hermanson et al., 2020a). To summarize, a larger volume of snow needs to be used to extract high enough concentrations of PCBs to be measurable, changing the extraction method to using for example XAD columns might improve the recovery of the PCBs, and a more sensitive analytical method than GC-MS, such as GC-HRMS, might additionally be necessary to achieve measurable peaks.

Agrell et al. (2002) studied PCBs in precipitation in the Baltic Sea region. They found decreasing PCB concentrations with increasing temperature. However, latitudinal trends (54-65°N) could not be significantly proven in the study. Further, they found seasonal variation in deposition of PCBs being the highest in fall. Overall, the total PCB concentration of 51 congeners in the precipitation varied between 0.8–10.7 ng L⁻¹ with a mean concentration of 2.3 ng L⁻¹. The total concentrations of 52 PCBs found by Agrell et al. (2002) in the Baltic region are higher than the total concentration of 209 congeners found in the snow by Hermanson et al. (2020) on Svalbard. This might suggest that PCB concentrations decrease latitudinal towards the arctic, but no study measuring the same PCB congeners with the same method along this latitudinal gradient can be found to prove this.

4.6 Future Studies

To be able to see more and clearer deposition trends of elements, PAHs and PCBs, additional sampling points should be added, especially in the mid and northern part of Norway. Replicates for the PAH and PCB samples should be added to establish the accuracy of the measured concentrations on the glaciers. As the timing of sampling after a snow event and timing in the season seems to affect the concentrations of especially major and trace elements, this should be taken into consideration when sampling to avoid these differences when

studying spatial trends. For future studies of seasonal changes, the same glaciers should be sampled during both seasons to exclude potential local differences in for instance local bedrock, distance to marine influences, atmospheric pathways, and potential anthropogenic local sources.

As mentioned in chapter 4.5, with the method used in this study PCBs could not be detected in the samples. To establish a deposition pattern of PCBs in snow, higher volumes of samples need to be used to reach concentrations above the detection limit in addition to improving the extraction method by for example changing to the method used by Hermanson et al. (2020a). The current method should further be tested for compounds bound to particles to establish if, and to what extent, these were extracted.

Although the study could be further improved, there is still a lot more to explore in the current data set. For instance, more of the individual element trends should be explored, as the general trend of the group does not seem to represent the trend for the individual compounds. Barium, which was analyzed as part of trace elements, showed, for example, a significant decreasing trend towards the ocean, while the total trace element group showed an increase. Therefore, individual trends might be missed when only looking at the trends of the element groups. Further, enrichment factors of the elements could be calculated to confirm the anthropogenic influence of the different elements similar to the study by Singh et al. (2015). For the PAH congeners, diagnostic ratios used to identify sources could be calculated as described by Ravindra et al. (2008) or Tobiszewski and Namieśnik (2012). Lastly, the measured concentrations of the elements and PAHs could be compared to toxicity levels in, for instance, drinking water to quantify potential risks of the atmospheric deposition in the snow.

5 Conclusion

This study achieved the first analysis of snow samples over a larger latitudinal range in Norway. Latitudinal trends were found for the total heavy metal group, specifically Cu, Zn, Cd, and Cr, and for the trace element Ba. Most of these metals are associated to the emissions of non-ferrous metal productions. Airmasses to the glaciers generally derive from northwester Eurasia, with increasing influence the further south the glacier is located. Several non-ferrous metal productions are located along the coast in southern Norway, which is part of the identified source area of the airmasses reaching the glaciers. Non-ferrous metal production is, therefore, defined as the most likely source of these elements to the snow on the glaciers. Decreasing latitudinal trends were also found for 2 out of 16 PAHs, PHE and FLT. The most volatile congener, NAP, had the highest concentrations in all samples, including in the arctic, while 5- and 6- ring PAHs did not reach the glaciers in high enough concentrations to be quantifiable. These results support the theory of global fractionation.

In addition to latitudinal trends, a marine gradient was found for both the major and trace element groups. Since the elements Na, Cl, Br, Mg, B, and Li that are abundant in seawater, sea spray aerosols are identified to transport the elements to the glaciers. This demonstrates the importance of natural sources of elements sampled in the snow on glaciers.

Seasonal changes were detected for major and trace elements in the snow from Svalbard. The concentrations of the two groups were significantly lower in summer compared to spring. Salts, such as NaCl, lower the melting point of snow, presumably leading to earlier runoff of these compounds, potentially explaining the found reduction. Phosphorous concentrations increased from spring to summer, which might be connected to P storage in snow algae during the summer. These seasonal changes appear to be independent of reemission processes, therefore no proof of the grasshopper effect was found in this study.

References

- Abdel-Shafy, H.I., Mansour, M.S.M., 2016. A review on polycyclic aromatic hydrocarbons: Source, environmental impact, effect on human health and remediation. *Egypt. J. Pet.* 25, 107–123. <https://doi.org/10.1016/j.ejpe.2015.03.011>
- Abramova, A., Chernianskii, S., Marchenko, N., Terskaya, E., 2016. Distribution of polycyclic aromatic hydrocarbons in snow particulates around Longyearbyen and Barentsburg settlements, Spitsbergen. *Polar Rec. (Gr. Brit).* 52, 645–659. <https://doi.org/10.1017/S0032247416000243>
- Agilent Technologies, 2015. Agilent 8800 Triple Quadrupole ICP-MS: Technology Transformed. Performance Redefined [WWW Document]. URL http://www.agilent.com/cs/library/brochures/5991-0079EN_8800_ICPQQQ_Brochure.pdf (accessed 6.3.22).
- Agrell, C., Larsson, P., Okla, L., Agrell, J., 2002. PCB congeners in precipitation, wash out ratios and depositional fluxes within the Baltic Sea region, Europe. *Atmos. Environ.* 36, 371–383. [https://doi.org/10.1016/S1352-2310\(01\)00228-X](https://doi.org/10.1016/S1352-2310(01)00228-X)
- AMAP, 2017. AMAP Assessment 2016: Chemicals of Emerging Arctic Concern. Oslo, Norway.
- AMAP, 2005. AMAP Assessment 2002: Heavy Metals in the Arctic. Oslo, Norway.
- AMAP, 2004. AMAP assessment 2002: Persistent organic pollutants in the Arctic. Oslo, Norway.
- Arp, H.P.H., Morin, N.A.O., Andersson, P.L., Hale, S.E., Wania, F., Breivik, K., Breedveld, G.D., 2020. The presence, emission and partitioning behavior of polychlorinated biphenyls in waste, leachate and aerosols from Norwegian waste-handling facilities. *Sci. Total Environ.* 715. <https://doi.org/10.1016/j.scitotenv.2020.136824>
- Asimakopoulos, A.G., Wang, L., Thomaidis, N.S., Kannan, K., 2014. A multi-class bioanalytical methodology for the determination of bisphenol A diglycidyl ethers, p-hydroxybenzoic acid esters, benzophenone-type ultraviolet filters, triclosan, and triclocarban in human urine by liquid chromatography-tandem mass spectrometry. *J. Chromatogr. A* 1324, 141–148. <https://doi.org/10.1016/j.chroma.2013.11.031>
- Atkins, P.W., De Paula, J., Keeler, J., 2018. Atkins' physical chemistry, 11th ed. Oxford University Press, Oxford.
- Balmer, J.E., Hung, H., Yu, Y., Letcher, R.J., Muir, D.C.G., 2019. Sources and environmental fate of pyrogenic polycyclic aromatic hydrocarbons (PAHs) in the Arctic. *Emerg. Contam.* 5, 128–142. <https://doi.org/10.1016/j.emcon.2019.04.002>
- Barcelo, D., 2000. Sample handling and trace analysis of pollutants - Techniques, applications and quality assurance, 1st ed, *Techniques and Instrumentation in Analytical Chemistry*. Elsevier, Amsterdam.
- Berg, T., Aas, W., Pacyna, J., Uggerud, H.T., Vadset, M., 2008. Atmospheric trace metal concentrations at Norwegian background sites during 25 years and its relation to European emissions. *Atmos. Environ.* 42, 7494–7501. <https://doi.org/10.1016/j.atmosenv.2008.05.020>
- Budde, W.L.; J.W., Eichelberger, T.D., Behymer, W.L., 1995. Method 525.2 - Determination

of organic compounds in drinking water by liquid-solid extraction and capillary column gas chromatography/mass spectrometry. Cincinnati, Ohio.

- Chance, R., Jickells, T.D., Baker, A.R., 2015. Atmospheric trace metal concentrations, solubility and deposition fluxes in remote marine air over the south-east Atlantic. *Mar. Chem.* 177, 45–56. <https://doi.org/10.1016/j.marchem.2015.06.028>
- Chen, A., Wu, X., Simonich, S.L.M., Kang, H., Xie, Z., 2021. Volatilization of polycyclic aromatic hydrocarbons (PAHs) over the North Pacific and adjacent Arctic Ocean: The impact of offshore oil drilling. *Environ. Pollut.* 268. <https://doi.org/10.1016/j.envpol.2020.115963>
- Christensen, E.R., Steinnes, E., Eggen, O.A., 2018. Anthropogenic and geogenic mass input of trace elements to moss and natural surface soil in Norway. *Sci. Total Environ.* 613–614, 371–378. <https://doi.org/10.1016/J.SCITOTENV.2017.09.094>
- Cleemann, M., Riget, F., Paulsen, G.B., De Boer, J., Klungsøyr, J., Aastrup, P., 2000. Organochlorines in Greenland lake sediments and landlocked Arctic char (*Salvelinus alpinus*). *Sci. Total Environ.* 245, 173–185. [https://doi.org/10.1016/S0048-9697\(99\)00442-8](https://doi.org/10.1016/S0048-9697(99)00442-8)
- Colin, J.L., Lim, B., Herms, E., Genet, F., Drab, E., Jaffrezo, J.L., Davidson, C.I., 1997. Air-to-snow mineral transfer - crustal elements in aerosols, fresh snow and snowpits on the Greenland ice sheet. *Atmos. Environ.* 31, 3395–3406. [https://doi.org/10.1016/S1352-2310\(97\)00122-2](https://doi.org/10.1016/S1352-2310(97)00122-2)
- Conca, E., Abollino, O., Giacomino, A., Buoso, S., Traversi, R., Becagli, S., Grotti, M., Malandrino, M., 2019. Source identification and temporal evolution of trace elements in PM10 collected near to Ny-Ålesund (Norwegian Arctic). *Atmos. Environ.* 203, 153–165. <https://doi.org/10.1016/j.atmosenv.2019.02.001>
- De Caritat, P., Hall, G., Gislason, S., Belsey, W., Braun, M., Goloubeva, N.I., Olsen, H.K., Scheie, J.O., Vaive, J.E., 2005. Chemical composition of arctic snow: Concentration levels and regional distribution of major elements. *Sci. Total Environ.* 336, 183–199. <https://doi.org/10.1016/j.scitotenv.2004.05.031>
- Drotikova, T., Ali, A.M., Karine Halse, A., Reinardy, H.C., Kallenborn, R., 2020. Polycyclic aromatic hydrocarbons (PAHs) and oxy- And nitro-PAHs in ambient air of the Arctic town Longyearbyen, Svalbard. *Atmos. Chem. Phys.* 20, 9997–10014. <https://doi.org/10.5194/acp-20-9997-2020>
- Drotikova, T., Dekhtyareva, A., Kallenborn, R., Albinet, A., 2021. Polycyclic aromatic hydrocarbons (PAHs) and their nitrated and oxygenated derivatives in the Arctic boundary layer: Seasonal trends and local anthropogenic influence. *Atmos. Chem. Phys.* 21, 14351–14370. <https://doi.org/10.5194/acp-21-14351-2021>
- Duxbury, A.C., Byrne, R.H., Mackenzie, F.T., 2020. Seawater [WWW Document]. *Encycl. Br.* URL <https://www.britannica.com/science/seawater> (accessed 4.20.22).
- EPA, 2022. Learn about Polychlorinated Biphenyls (PCBs) | US EPA [WWW Document]. URL <https://www.epa.gov/pcbs/learn-about-polychlorinated-biphenyls-pcbs> (accessed 6.28.22).
- EPA, 2021. Toxic and Priority Pollutants Under the Clean Water Act | US EPA [WWW Document]. URL <https://www.epa.gov/eg/toxic-and-priority-pollutants-under-clean->

water-act#priority (accessed 7.22.22).

- Fajgelj, A., Coates, S., Vernengo, M.J., 1999. Harmonised guidelines for the use of recovery information in analytical measurement, Accreditation and Quality Assurance. <https://doi.org/https://doi.org/10.1007/PL00010412>
- Falconer, R.L., Bidleman, T.F., 1994. Vapor pressures and predicted particle/gas distributions of polychlorinated biphenyl congeners as functions of temperature and ortho-chlorine substitution. *Atmos. Environ.* 28, 547–554. [https://doi.org/10.1016/1352-2310\(94\)90130-9](https://doi.org/10.1016/1352-2310(94)90130-9)
- Ferreira, A.P., 2008. Public health and environmental pollution: precautionary paradigms. *Rev. Bras. em Promoção da Saúde* 21, 69–74. <https://doi.org/10.5020/18061230.2008.p69>
- Fjeld, E., Rognerud, S., 2001. Trace Element Contamination of Norwegian Lake Sediments. *Ambio* 30, 11–19.
- Friedman, C.L., Selin, N.E., 2012. Long-range atmospheric transport of polycyclic aromatic hydrocarbons: A global 3-D model analysis including evaluation of arctic sources. *Environ. Sci. Technol.* 46, 9501–9510. <https://doi.org/10.1021/es301904d>
- Gad, S.C., 2014. Barium. *Encycl. Toxicol.* Third Ed. <https://doi.org/https://doi.org/10.1016/B978-0-12-386454-3.00819-8>
- Gallet, J.-C., Björkman, M., Borstad, C., Hodson, A., Jacobi, H.-W., Larose, C., Luks, B., Spolaor, A., Urazgildeeva, A., Zdanowicz, C., 2019. Snow research in Svalbard: current status and knowledge gaps. *SESS Rep. 2018 - State Environ. Sci. Svalbard*.
- Garmash, O., Hermanson, M.H., Isaksson, E., Schwikowski, M., Divine, D., Teixeira, C., Muir, D.C.G., 2013. Deposition history of polychlorinated biphenyls to the lomonosovfonna glacier, Svalbard: A 209 congener analysis. *Environ. Sci. Technol.* 47, 12064–12072. <https://doi.org/10.1021/es402430t>
- Garrido, A., Jiménez-Guerrero, P., Ratola, N., 2014. Levels, trends and health concerns of atmospheric PAHs in Europe. *Atmos. Environ.* 99, 474–484. <https://doi.org/10.1016/j.atmosenv.2014.10.011>
- Giannarelli, S., Onor, M., Abete, C., Termine, M., Fuoco, R., 2019. Effect of altitude and distance from the sea on fractionation processes of Persistent Organic Pollutants (POPs) associated to atmospheric aerosol from Ross Sea to Dome C, Antarctica. *Microchem. J.* 149. <https://doi.org/10.1016/j.microc.2019.05.012>
- Harmens, H., Norris, D.A., Steinnes, E., Kubin, E., Piispanen, J., Alber, R., Aleksiyenak, Y., Blum, O., Coşkun, M., Dam, M., De Temmerman, L., Fernández, J.A., Frolova, M., Frontasyeva, M., González-Miqueo, L., Grodzińska, K., Jeran, Z., Korzekwa, S., Krmar, M., Kvietkus, K., Leblond, S., Liiv, S., Magnússon, S.H., Maňkovská, B., Pesch, R., Rühling, A., Santamaria, J.M., Schröder, W., Spiric, Z., Suchara, I., Thöni, L., Urumov, V., Yurukova, L., Zechmeister, H.G., 2010. Mosses as biomonitors of atmospheric heavy metal deposition: Spatial patterns and temporal trends in Europe. *Environ. Pollut.* 158, 3144–3156. <https://doi.org/10.1016/j.envpol.2010.06.039>
- Hermanson, M.H., Isaksson, E., Divine, D., Teixeira, C., Muir, D.C.G., 2020a. Atmospheric deposition of polychlorinated biphenyls to seasonal surface snow at four glacier sites on Svalbard, 2013–2014. *Chemosphere* 243, 125324.

<https://doi.org/10.1016/j.chemosphere.2019.125324>

- Hermanson, M.H., Isaksson, E., Hann, R., Teixeira, C., Muir, D.C.G., 2020b. Deposition of Polychlorinated Biphenyls to Firn and Ice Cores at Opposite Polar Sites: Site M, Dronning Maud Land, Antarctica, and Holtedahlfonna, Svalbard. *ACS Earth Sp. Chem.* 4, 2096–2104. <https://doi.org/10.1021/acsearthspacechem.0c00227>
- Hibberd, S., 1984. A Model for Pollutant concentration during snow-melt. *J. Glaciol.* 30, 58–65.
- Hübschmann, H.-J., 2015. *Handbook of GC-MS: Fundamentals and Applications*, 3rd ed. WILEY-VCH, Weinheim, Germany.
- Hylland, K., 2006. Polycyclic aromatic hydrocarbon (PAH) ecotoxicology in marine ecosystems. *J. Toxicol. Environ. Heal. - Part A* 69, 109–123. <https://doi.org/10.1080/15287390500259327>
- Interactive map - Norwegianpetroleum.no [WWW Document], n.d. URL <https://www.norskpetroleum.no/en/interactive-map-quick-downloads/interactive-map/?mapv2ObjType=license&mapv2ObjId=34039231> (accessed 6.10.22).
- Jacob, J., 1995. Method development for the determination of polycyclic aromatic hydrocarbons (PAHs) in environmental matrices, in: Quevauviller, P., Maier, E.A., Griepink, B. (Eds.), *Quality Assurance for Environmental Analysis : Method Evaluation within the Measurements and Testing Programme (BCR)*. Elsevier, pp. 563–589.
- Jaward, F.M., Meijer, S.N., Steinnes, E., Thomas, G.O., Jones, K.C., 2004. Further Studies on the Latitudinal and Temporal Trends of Persistent Organic Pollutants in Norwegian and U.K. Background Air. *Environ. Sci. Technol.* 38, 2523–2530. <https://doi.org/10.1021/es035292t>
- Jiang, S., Shi, G., Cole-Dai, J., An, C., Sun, B., 2021. Occurrence, latitudinal gradient and potential sources of perchlorate in the atmosphere across the hemispheres (31°N to 80°S). *Environ. Int.* 156. <https://doi.org/10.1016/j.envint.2021.106611>
- Jolliffe, I.T., Cadima, J., 2016. Principal component analysis: a review and recent developments. *Philos. Trans. R. Soc. A Math. Phys. Eng. Sci.* 374. <https://doi.org/10.1098/RSTA.2015.0202>
- Kakareka, S., Kukharchyk, T., Kurman, P., 2022. Trace and major elements in surface snow and fresh water bodies of the Marguerite Bay Islands, Antarctic Peninsula. *Polar Sci.* 32. <https://doi.org/10.1016/J.POLAR.2022.100792>
- Keenan, J.D., Auer, M.T., 1974. The influence of phosphorus luxury uptake on algal bioassays. *J. Water Pollut. Control Fed.* 46, 532–542.
- Kennedy, M.E., 1998. Elements: Trace, in: *Geochemistry. Encyclopedia of Earth Science*. Springer, Dodrecht, pp. 221–223. https://doi.org/10.1007/1-4020-4496-8_111
- Keyte, I.J., Harrison, R.M., Lammel, G., 2013. Chemical reactivity and long-range transport potential of polycyclic aromatic hydrocarbons-a review. *Chem. Soc. Rev.* 42, 9333–9391. <https://doi.org/10.1039/c3cs60147a>
- Khaustov, A., Redina, M., Goryainov, S., 2022. Migration of PAHs and Phthalates from Package Materials during Water Storage: Glass or Plastic? *Polycycl. Aromat. Compd.* 42, 358–370. <https://doi.org/10.1080/10406638.2020.1734033>

- Knap, A.H., Kaiser, M.-S., 1988. The Long-Range Atmospheric Transport of Natural and Contaminant Substances, Knap, A.H. ed. Springer Dodrecht.
<https://doi.org/https://doi.org/10.1007/978-94-009-0503-0>
- Koller, M., Saleh, H.M., 2018. Introductory Chapter: Introducing Heavy Metals, in: Saleh, H., Algan, R.F. (Eds.), Heavy Metals. IntechOpen, p. 13.
<https://doi.org/10.5772/intechopen.74783>
- Koziol, K., Uszczyk, A., Pawlak, F., Frankowski, M., Polkowska, Ż., 2021. Seasonal and Spatial Differences in Metal and Metalloid Concentrations in the Snow Cover of Hansbreen, Svalbard. *Front. Earth Sci.* 8, 1–8. <https://doi.org/10.3389/feart.2020.538762>
- Lagowski, J.J., Taylor, Roger, J., Mason, Brian, H., 2018. chemical element [WWW Document]. *Encycl. Br.* URL <https://www.britannica.com/science/chemical-element> (accessed 7.4.22).
- Lammel, G., Sehili, A.M., Bond, T.C., Feichter, J., Grassl, H., 2009. Gas/particle partitioning and global distribution of polycyclic aromatic hydrocarbons - A modelling approach. *Chemosphere* 76, 98–106. <https://doi.org/10.1016/j.chemosphere.2009.02.017>
- Leelőssy, Á., Molnár, F., Izsák, F., Havasi, Á., Lagzi, I., Mészáros, R., 2014. Dispersion modeling of air pollutants in the atmosphere: a review. *Cent. Eur. J. Geosci.* 6, 257–278. <https://doi.org/10.2478/s13533-012-0188-6>
- Levshina, S., 2019. Distribution and Characteristic of PAHs in snow of the Urban and Reserve Areas of Southern Far East Russia. *Bull. Environ. Contam. Toxicol.* 102, 160–167. <https://doi.org/10.1007/S00128-018-02533-6/TABLES/4>
- Li, N., Wania, F., Lei, Y.D., Daly, G.L., 2003. A Comprehensive and Critical Compilation, Evaluation, and Selection of Physical-Chemical Property Data for Selected Polychlorinated Biphenyls. *J. Phys. Chem. Ref. Data* 32, 1545–1590.
<https://doi.org/10.1063/1.1562632>
- Lundanes, E., Reubsæet, L., Greibrokk, T., 2014. *Chromatography: Basic Principles, Sample Preparations and Related Methods.* WILEY-VCH.
- Lunder Halvorsen, H., Bohlin-Nizzetto, P., Eckhardt, S., Gusev, A., Krogseth, I.S., Moeckel, C., Shatalov, V., Skogeng, L.P., Breivik, K., 2021. Main sources controlling atmospheric burdens of persistent organic pollutants on a national scale. *Ecotoxicol. Environ. Saf.* 217. <https://doi.org/10.1016/j.ecoenv.2021.112172>
- Manahan, S.E., 2010. *Environmental chemistry*, 9th ed. CRC Press, Boca Raton.
- Mccutcheon, J., Lutz, S., Williamson, C., Cook, J.M., Tedstone, A.J., Vanderstraeten, A., Wilson, S.A., Stockdale, A., Bonneville, S., Anesio, A.M., Yallop, M.L., Mcquaid, J.B., Tranter, M., Benning, L.G., 2021. Mineral phosphorus drives glacier algal blooms on the Greenland Ice Sheet. *Nat. Commun.* 12, 1–11. <https://doi.org/10.1038/s41467-020-20627-w>
- MOSJ, 2022. Cruiseturisme - MOSJ – Miljøovervåking Svalbard og Jan Mayen [WWW Document]. URL https://www.mosj.no/no/pavirkning/ferdsel/cruiseturisme.html?fbclid=IwAR255gANEPPiR_nkXshsEn-5pr-v5uxRNuL1FOJb7GndaSLFbxaVUEVJHE (accessed 6.26.22).
- Mwanza, M.M., Ndunda, E.N., Bosire, G.O., Nyamori, V.O., Martincigh, B.S., 2021. Advances in sample pretreatment and detection of PCBs in the environment. *J. Hazard.*

Mater. Adv. 4. <https://doi.org/10.1016/j.hazadv.2021.100028>

- Na, G., Liu, C., Wang, Z., Ge, L., Ma, X., Yao, Z., 2011. Distribution and characteristic of PAHs in snow of Fildes Peninsula. *J. Environ. Sci.* 23, 1445–1451. [https://doi.org/10.1016/S1001-0742\(10\)60605-5](https://doi.org/10.1016/S1001-0742(10)60605-5)
- Olmez, I., Gordon, G.E., 1985. Rare Earths : Atmospheric Signatures for Oil-Fired Power Plants and Refineries. *Am. Assoc. Adv. Sci.* 229, 966–968.
- Pacyna, E.G., Pacyna, J.M., Fudala, J., Strzelecka-Jastrzab, E., Hlawiczka, S., Panasiuk, D., Nitter, S., Pregger, T., Pfeiffer, H., Friedrich, R., 2007. Current and future emissions of selected heavy metals to the atmosphere from anthropogenic sources in Europe. *Atmos. Environ.* 41, 8557–8566. <https://doi.org/10.1016/J.ATMOSENV.2007.07.040>
- Pecharsky, V.K., Gschneidner, K.A., 2019. rare-earth element [WWW Document]. *Br. Online Encycl.* URL <https://www.britannica.com/print/article/491579> (accessed 6.6.22).
- Platt, S.M., Hov, Ø., Berg, T., Breivik, K., Eckhardt, S., Eleftheriadis, K., Evangelidou, N., Fiebig, M., Fisher, R., Hansen, G., Hansson, H.-C., Heintzenberg, J., Hermansen, O., Heslin-Rees, D., Holmén, K., Hudson, S., Kallenborn, R., Krejci, R., Krognes, T., Larssen, S., Lowry, D., Lund Myhre, C., Lunder, C., Nisbet, E., Nizzetto, P.B., Park, K.-T., Pedersen, C.A., Aspö, Pfaffhuber, K., Röckmann, T., Schmidbauer, N., Solberg, S., Stohl, A., Ström, J., Svendby, T., Tunved, P., Tørnkvist, K., van der Veen, C., Vratolis, S., Yoon, Y.J., Yttri, K.E., Zieger, P., Aas, W., Tørseth, K., 2022. Atmospheric composition in the European Arctic and 30 years of the Zeppelin Observatory, Ny-Ålesund. *Atmos. Chem. Phys.* 22, 3321–3369. <https://doi.org/10.5194/ACP-22-3321-2022>
- Polkowska, Z., Cichala-Kamrowska, K., Ruman, M., Koziol, K., Krawczyk, W.E., Namieśnik, J., 2011. Organic pollution in surface waters from the Fuglebekken basin in Svalbard, Norwegian Arctic. *Sensors* 11, 8910–8929. <https://doi.org/10.3390/s110908910>
- Rakhsha, M., Kees, C.E., Negrut, D., 2021. Lagrangian vs. Eulerian: An Analysis of Two Solution Methods for Free-Surface Flows and Fluid Solid Interaction Problems. *Fluids* 6, 1–27. <https://doi.org/10.3390/fluids6120460>
- Ravindra, K., Sokhi, R., Van Grieken, R., 2008. Atmospheric polycyclic aromatic hydrocarbons: Source attribution, emission factors and regulation. *Atmos. Environ.* 42, 2895–2921. <https://doi.org/10.1016/j.atmosenv.2007.12.010>
- Regjeringen, 2001. Business and industry in Norway - The metals industry - regjeringen.no [WWW Document]. URL <https://www.regjeringen.no/en/dokumenter/Business-and-industry-in-Norway---The-metals-industry/id419341/> (accessed 6.26.22).
- Ringnér, M., 2008. What is principal component analysis? *Nat. Biotechnol.* 26, 303–304. <https://doi.org/10.1038/nbt0308-303>
- Shen, L., Wania, F., Lei, Y.D., Teixeira, C., Muir, D.C.G., Bidleman, T.F., 2005. Atmospheric distribution and long-range transport behavior of organochlorine pesticides in North America. *Environ. Sci. Technol.* 39, 409–420. <https://doi.org/10.1021/es049489c>
- Shrader, S., 2013. *Introductory Mass Spectrometry*, 2nd ed. CRC Press LLC, Boca Raton.
- Šillerová, H., Chrastný, V., Vítková, M., Francová, A., Jehlička, J., Gutsch, M.R.,

- Kocourková, J., Aspholm, P.E., Nilsson, L.O., Berglen, T.F., Jensen, H.K.B., Komárek, M., 2017. Stable isotope tracing of Ni and Cu pollution in North-East Norway: Potentials and drawbacks. *Environ. Pollut.* 228, 149–157.
<https://doi.org/10.1016/j.envpol.2017.05.030>
- Singh, S.M., Gawas-Sakhalkar, P., Naik, S., Ravindra, R., Sharma, J., Upadhyay, A.K., Mulik, R.U., Bohare, P., 2015. Elemental composition and bacterial incidence in firn-cores at Midre Lovénbreen glacier, Svalbard. *Polar Rec. (Gr. Brit.)* 51, 39–48.
<https://doi.org/10.1017/S0032247413000533>
- Sparkman, O.D., Penton, Z.E., Kitson, F.G., 2011. Quantitation with GC/MS, in: *Gas Chromatography and Mass Spectrometry: A Practical Guide*. Academic Press, pp. 207–218. <https://doi.org/10.1016/b978-0-12-373628-4.00006-x>
- Spolaor, A., Varin, C., Pedeli, X., Christille, J.M., Kirchgeorg, T., Giardi, F., Cappelletti, D., Turetta, C., Cairns, W.R.L., Gambaro, A., Bernagozzi, A., Gallet, J.C., Björkman, M.P., Barbaro, E., 2021. Source, timing and dynamics of ionic species mobility in the Svalbard annual snowpack. *Sci. Total Environ.* 751.
<https://doi.org/10.1016/j.scitotenv.2020.141640>
- Stein, A.F., Draxler, R.R., Rolph, G.D., Stunder, B.J.B., Cohen, M.D., Ngan, F., 2015. NOAA's HYSPLIT atmospheric transport and dispersion modeling system. *Bull. Am. Meteorol. Soc.* 96, 2059–2077. <https://doi.org/10.1175/BAMS-D-14-00110.1>
- Steinnes, E., 1995. A critical evaluation of the use of naturally growing moss to monitor the deposition of atmospheric metals. *Sci. Total Environ.* 160–161, 243–249.
[https://doi.org/10.1016/0048-9697\(95\)04360-D](https://doi.org/10.1016/0048-9697(95)04360-D)
- Steinnes, E., Lierhagen, S., 2018. Geographical distribution of trace elements in natural surface soils: Atmospheric influence from natural and anthropogenic sources. *Appl. Geochemistry* 88, 2–9. <https://doi.org/10.1016/j.apgeochem.2017.03.013>
- Stout, S.A., Emsbo-Mattingly, S.D., Douglas, G.S., Uhler, A.D., McCarthy, K.J., 2015. Beyond 16 Priority Pollutant PAHs: A Review of PACs used in Environmental Forensic Chemistry. *Polycycl. Aromat. Compd.* 35, 285–315.
<https://doi.org/10.1080/10406638.2014.891144>
- Szczybelski, A.S., van den Heuvel-Greve, M.J., Kampen, T., Wang, C., van den Brink, N.W., Koelmans, A.A., 2016. Bioaccumulation of polycyclic aromatic hydrocarbons, polychlorinated biphenyls and hexachlorobenzene by three Arctic benthic species from Kongsfjorden (Svalbard, Norway). *Mar. Pollut. Bull.* 112, 65–74.
<https://doi.org/https://doi.org/10.1016/j.marpolbul.2016.08.041>
- Szumińska, D., Potapowicz, J., Szopińska, M., Czapiewski, S., Falk, U., Frankowski, M., Polkowska, Ż., 2021. Sources and composition of chemical pollution in Maritime Antarctica (King George Island), part 2: Organic and inorganic chemicals in snow cover at the Warszawa Icefield. *Sci. Total Environ.* 796.
<https://doi.org/10.1016/j.scitotenv.2021.149054>
- Thomas, R., 2013. *Practical guide to ICP-MS : a tutorial for beginners*, 3rd ed. Taylor & Francis Group, Boca Raton. <https://doi.org/https://doi.org/10.1201/b14923>
- Thorsnæs, G., Askheim, S., 2022. Bremanger [WWW Document]. *Stora Nor. Leks.* URL <https://www.allkunne.no/framside/fylkesleksikon-sogn-og-fjordane/samfunn/industri-naring-og-bedrifter/bremanger-smelteverk---hjornesteinen-i->

kommunesenteret/1900/81204/ (accessed 6.2.22).

- Tobiszewski, M., Namieśnik, J., 2012. PAH diagnostic ratios for the identification of pollution emission sources. *Environ. Pollut.* 162, 110–119.
<https://doi.org/10.1016/j.envpol.2011.10.025>
- Ubl, S., Scheringer, M., Stohl, A., Burkhardt, J.F., Hungerbühler, K., 2012. Primary source regions of polychlorinated biphenyls (PCBs) measured in the Arctic. *Atmos. Environ.* 62, 391–399. <https://doi.org/10.1016/j.atmosenv.2012.07.061>
- Vecchiato, M., Barbaro, E., Spolaor, A., Burgay, F., Barbante, C., Piazza, R., Gambaro, A., 2018. Fragrances and PAHs in snow and seawater of Ny-Ålesund (Svalbard): Local and long-range contamination. *Environ. Pollut.* 242, 1740–1747.
<https://doi.org/10.1016/j.envpol.2018.07.095>
- Wang, R., Tao, S., Wang, B., Yang, Y., Lang, C., Zhang, Y., Hu, J., Ma, J., Hung, H., 2010. Sources and pathways of polycyclic aromatic hydrocarbons transported to alert, the Canadian High arctic. *Environ. Sci. Technol.* 44, 1017–1022.
<https://doi.org/10.1021/es902203w>
- Wania, F., Mackay, D., 1996a. Tracking the Distribution of Persistent Organic Pollutants. *Environ. Sci. Technol.* 30, 390–396. [https://doi.org/10.1016/s0926-3373\(97\)80026-4](https://doi.org/10.1016/s0926-3373(97)80026-4)
- Wania, F., Mackay, D., 1996b. Tracking the distribution of persistent organic pollutants. *Environ. Sci. Technol.* 30. [https://doi.org/10.1016/s0926-3373\(97\)80026-4](https://doi.org/10.1016/s0926-3373(97)80026-4)
- Wania, F., Mackay, D., 1993. Global fractionation and cold condensation of low volatility organochlorine compounds in polar regions. *Ambio* 22, 10–18.
<https://doi.org/10.2307/4314030>
- Welch, C.J., 2000. The determination of trace amounts of organic compounds, in: Fifield, F.W., Haines, P.J. (Eds.), *Environmental Analytical Chemistry*. Wiley-Blackwell, pp. 429–452.
- Wilschefski, S.C., Baxter, M.R., 2019. Inductively Coupled Plasma Mass Spectrometry: Introduction to Analytical Aspects. *Clin. Biochem. Rev.* 40, 115–133.
<https://doi.org/10.33176/AACB-19-00024>
- Wold, S., Esbensen, K., Geladi, P., 1987. Principal Component Analysis. *Chemom. Intell. Lab. Syst.* 2, 37–52. [https://doi.org/https://doi.org/10.1016/0169-7439\(87\)80084-9](https://doi.org/https://doi.org/10.1016/0169-7439(87)80084-9)
- Wong, F., Hung, H., Dryfhout-Clark, H., Aas, W., Bohlin-Nizzetto, P., Breivik, K., Mastromonaco, M.N., Lundén, E.B., Ólafsdóttir, K., Sigurðsson, Á., Vorkamp, K., Bossi, R., Skov, H., Hakola, H., Barresi, E., Sverko, E., Fellin, P., Li, H., Vlasenko, A., Zapevalov, M., Samsonov, D., Wilson, S., 2021. Time trends of persistent organic pollutants (POPs) and Chemicals of Emerging Arctic Concern (CEAC) in Arctic air from 25 years of monitoring. *Sci. Total Environ.* 775.
<https://doi.org/10.1016/j.scitotenv.2021.145109>
- World Health Organization, 2000. General description Polychlorinated biphenyls (PCBs). *Air Qual. Guid.* 2, 1–22.
- Yeung, V., Miller, D.D., Rutzke, M.A., 2017. Atomic Absorption Spectroscopy, Atomic Emission Spectroscopy, and Inductively Coupled Plasma-Mass Spectrometry, in: Nielsen, S.S. (Ed.), *Food Analysis*. Springer, pp. 129–150.

- Zhang, J., Liu, C.Q., 2004. Major and rare earth elements in rainwaters from Japan and East China Sea: Natural and anthropogenic sources. *Chem. Geol.* 209, 315–326.
<https://doi.org/10.1016/j.chemgeo.2004.06.014>
- Zhang, X., Chen, Z., Liu, Y., 2017. Chapter 1 - Introduction, in: Zhang, X., Chen, Z., Liu, Y. (Eds.), *The Material Point Method*. Academic Press, pp. 1–9.
<https://doi.org/10.1016/B978-0-12-407716-4.00001-6>

Appendices

A. Sampling Sites

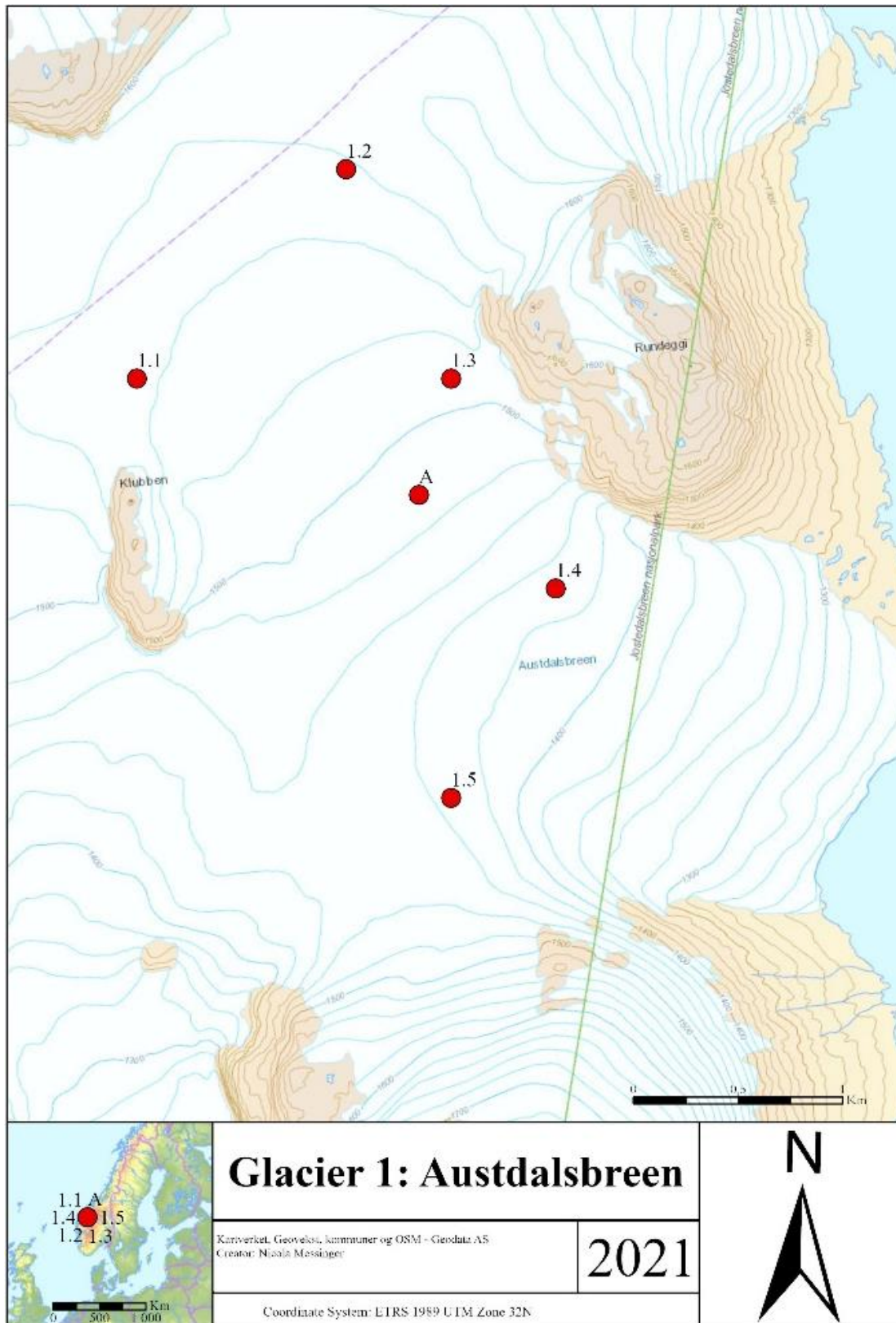


Figure A.1 Sample location for element analysis (1.1-1.5), and PAH and PCB analysis (A) on Austdalsbreen (1).

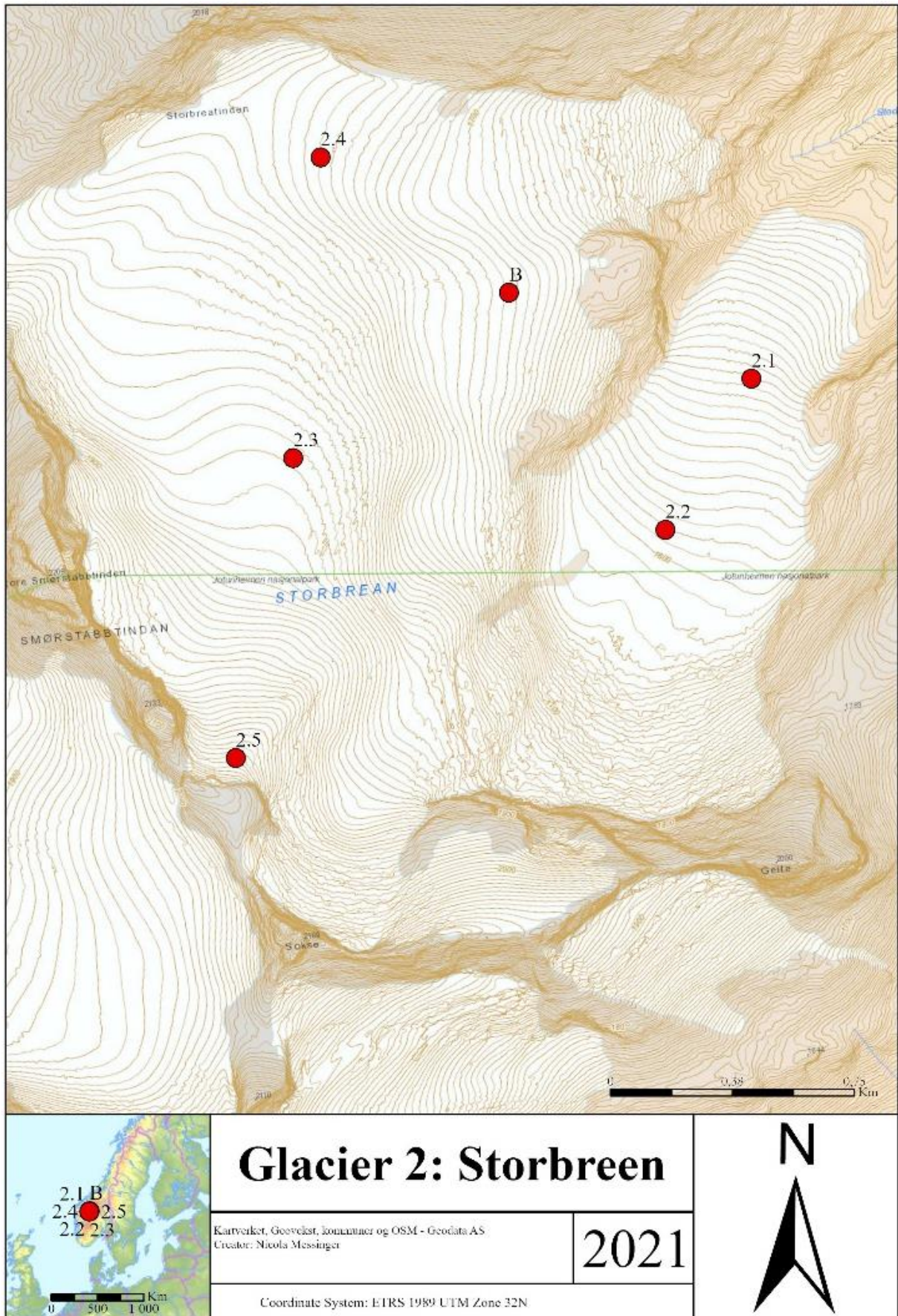


Figure A.2 Sample location for element analysis (2.1-2.5), and PAH and PCB analysis (B) on Storbrean (2).

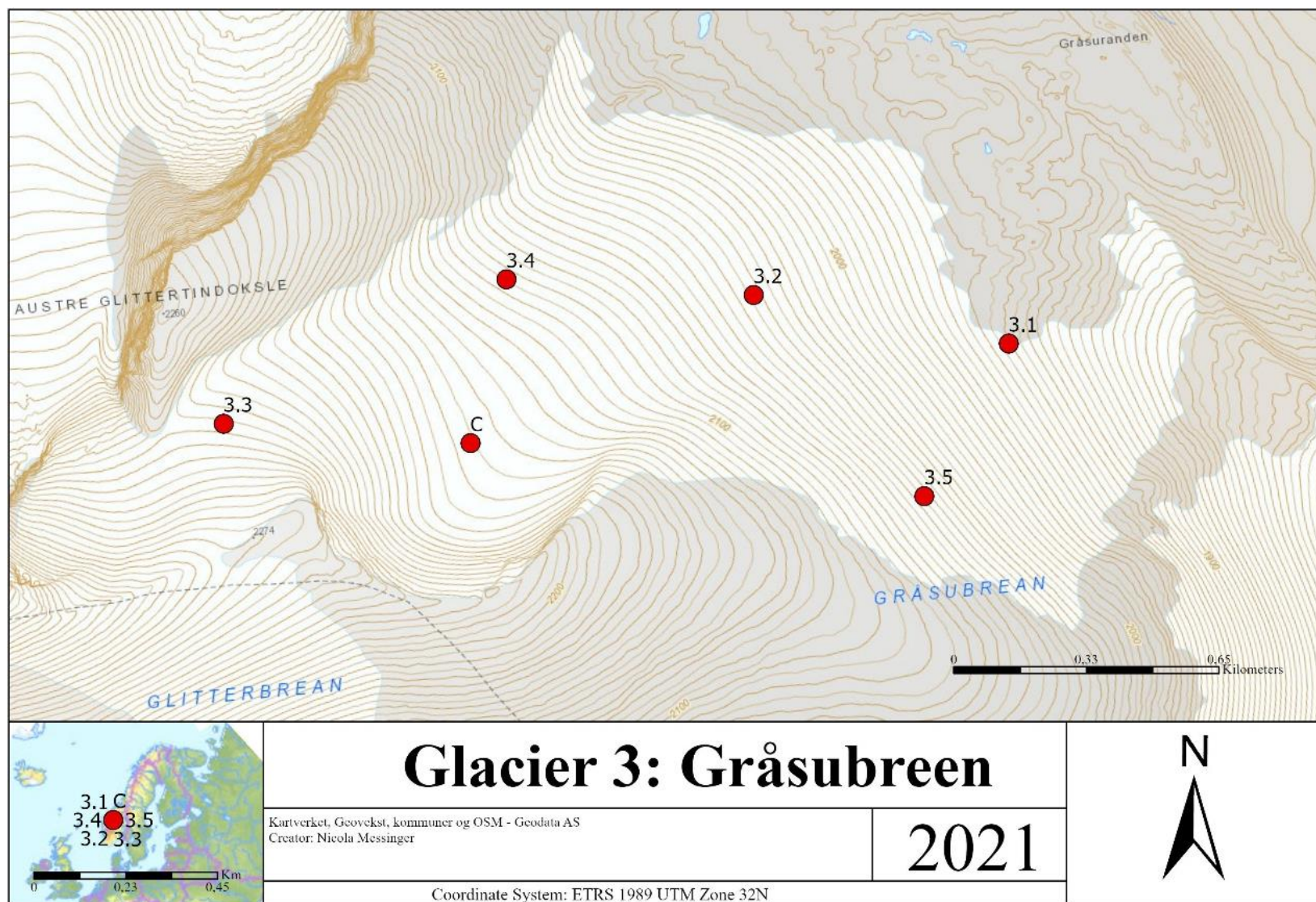


Figure A.3 Sample location for element analysis (3.1-3.5) and PAH and PCB analysis (C) on Gråsubreen (3).

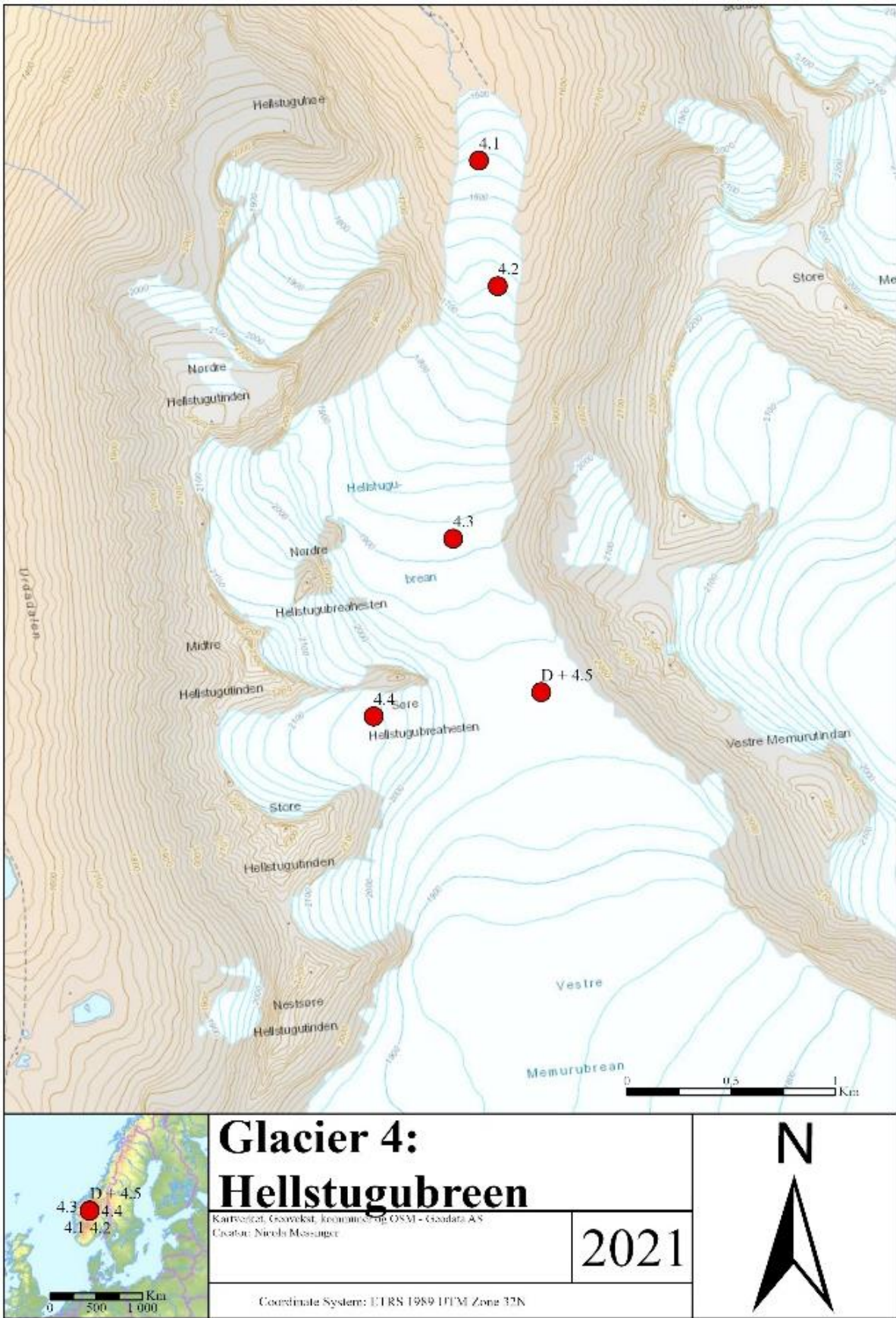


Figure A.4 Sample location for element analysis (4.1-4.5) and PAH and PCB analysis (D) on Hellstugubreen (4).

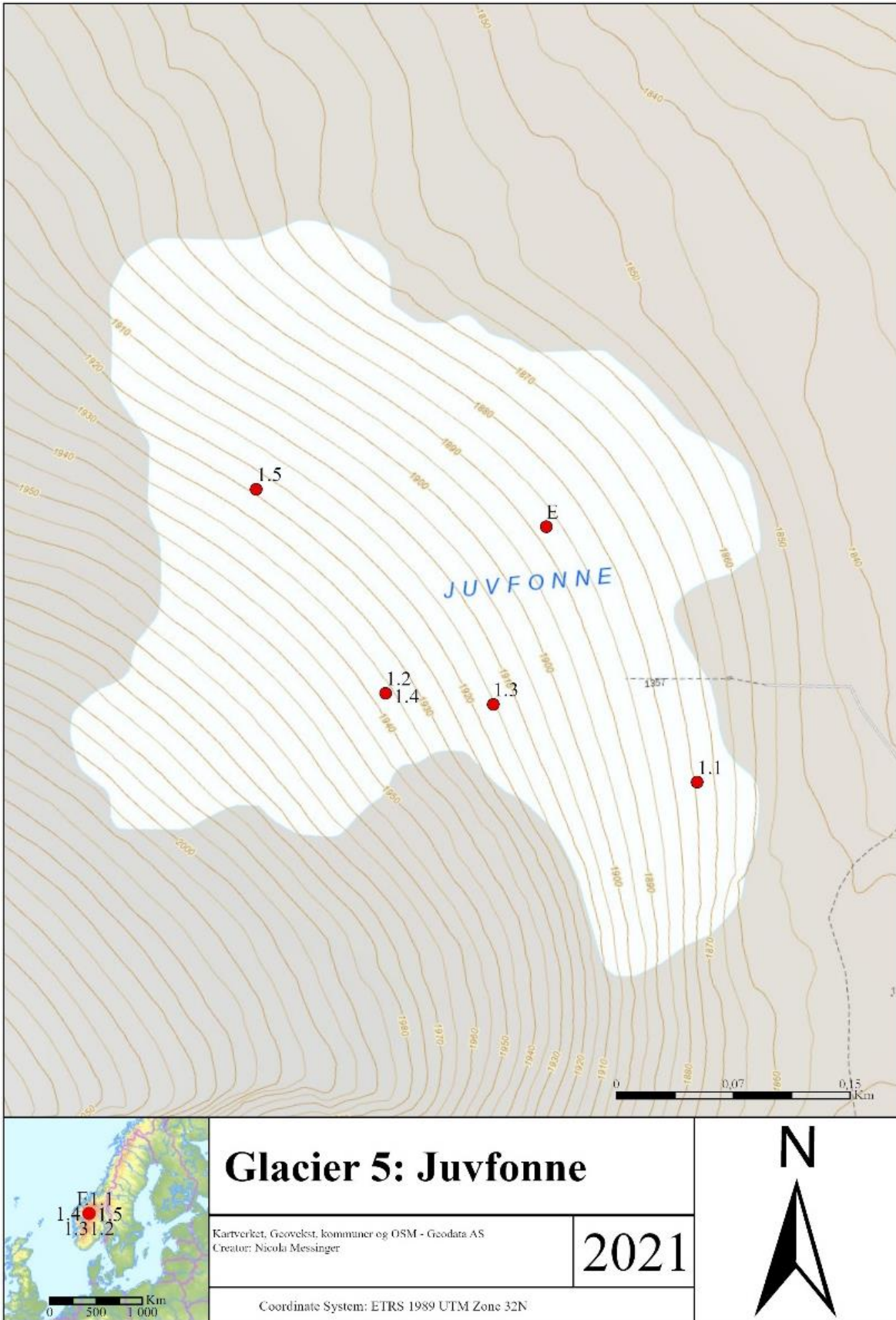


Figure A.5 Sample location for element analysis (5.1-5.5) and PAH and PCB analysis (E) on Juvfonna (5).

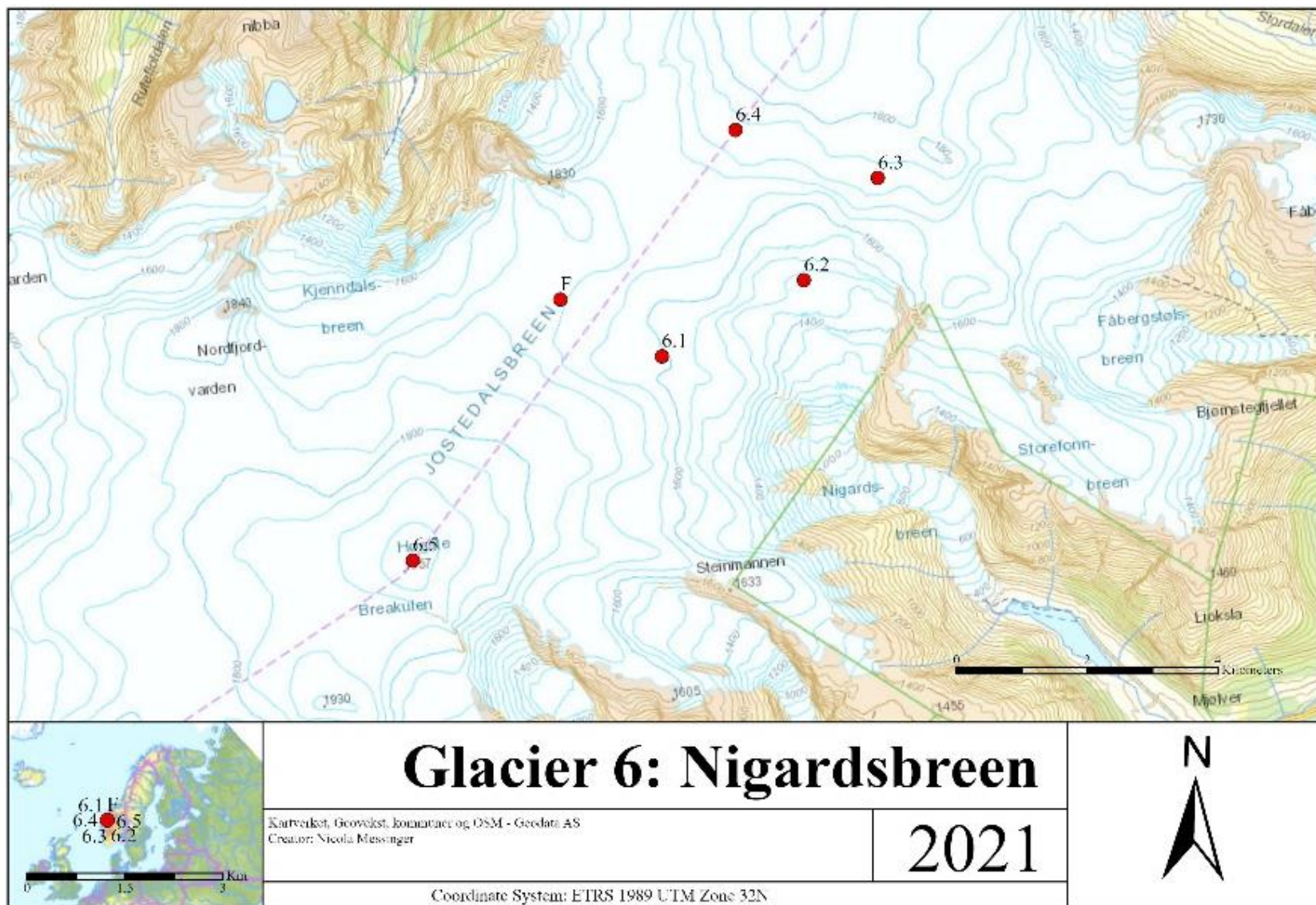


Figure A.6 Sample location for element analysis (6.1-6.5), and PAH and PCB analysis (F) on Nigardsbreen (6).

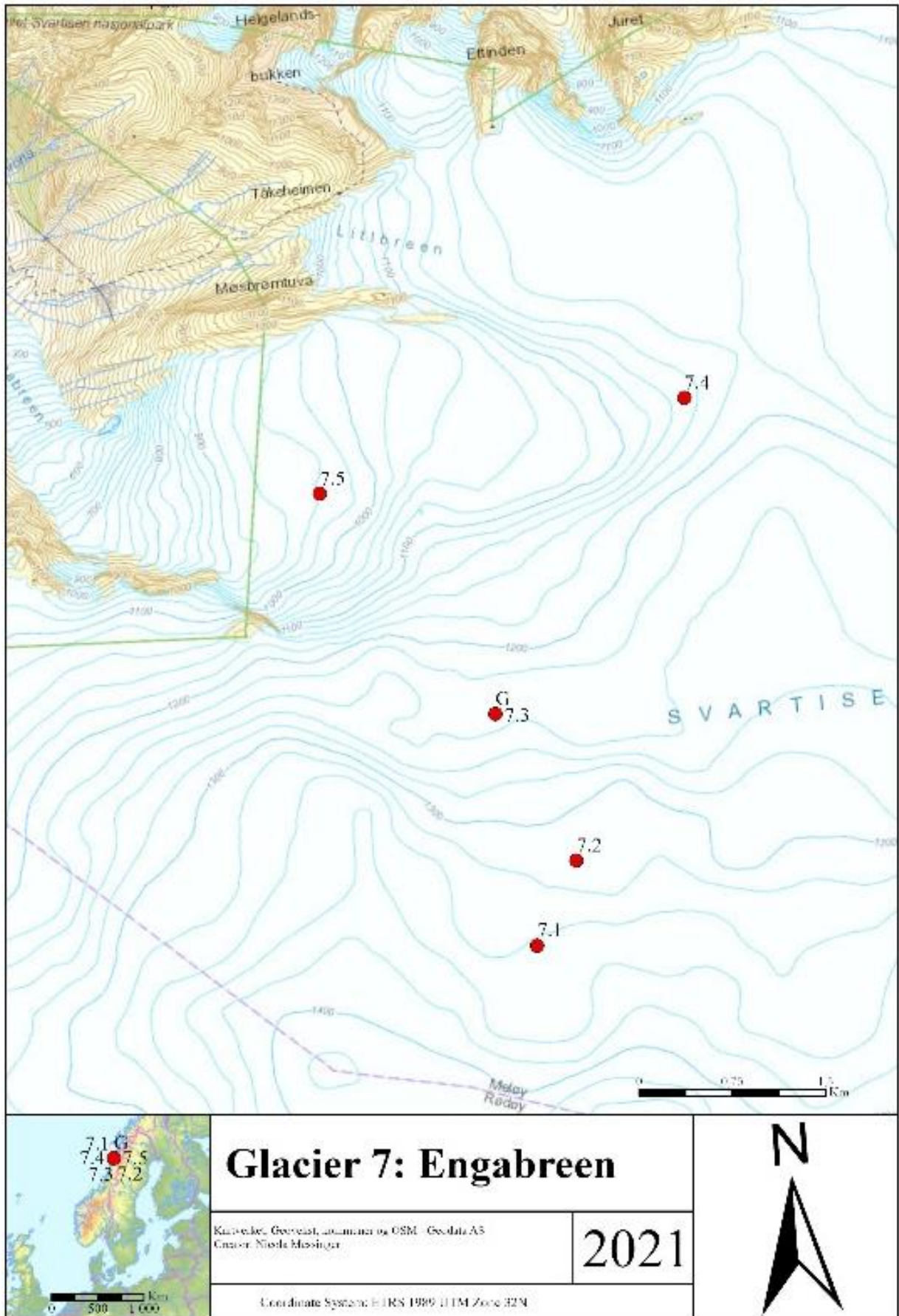


Figure A.7 Sample location for element analysis (7.1-7.5), and PAH and PCB analysis (G) on Engabreen (7).

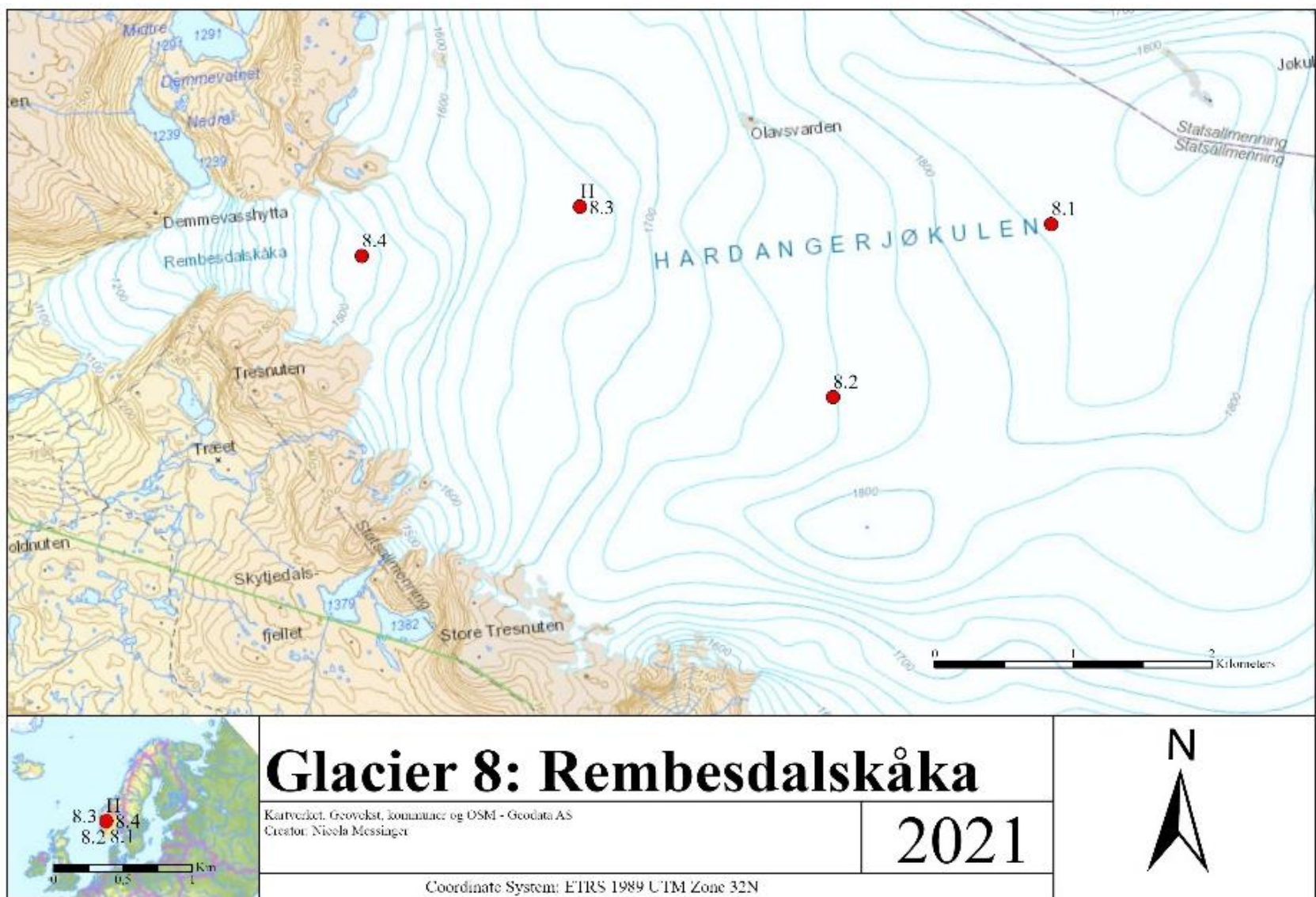


Figure A.8 Sample location for element analysis (8.1-8.4), and PAH and PCB analysis (H) on Rembesdalskåka (8).

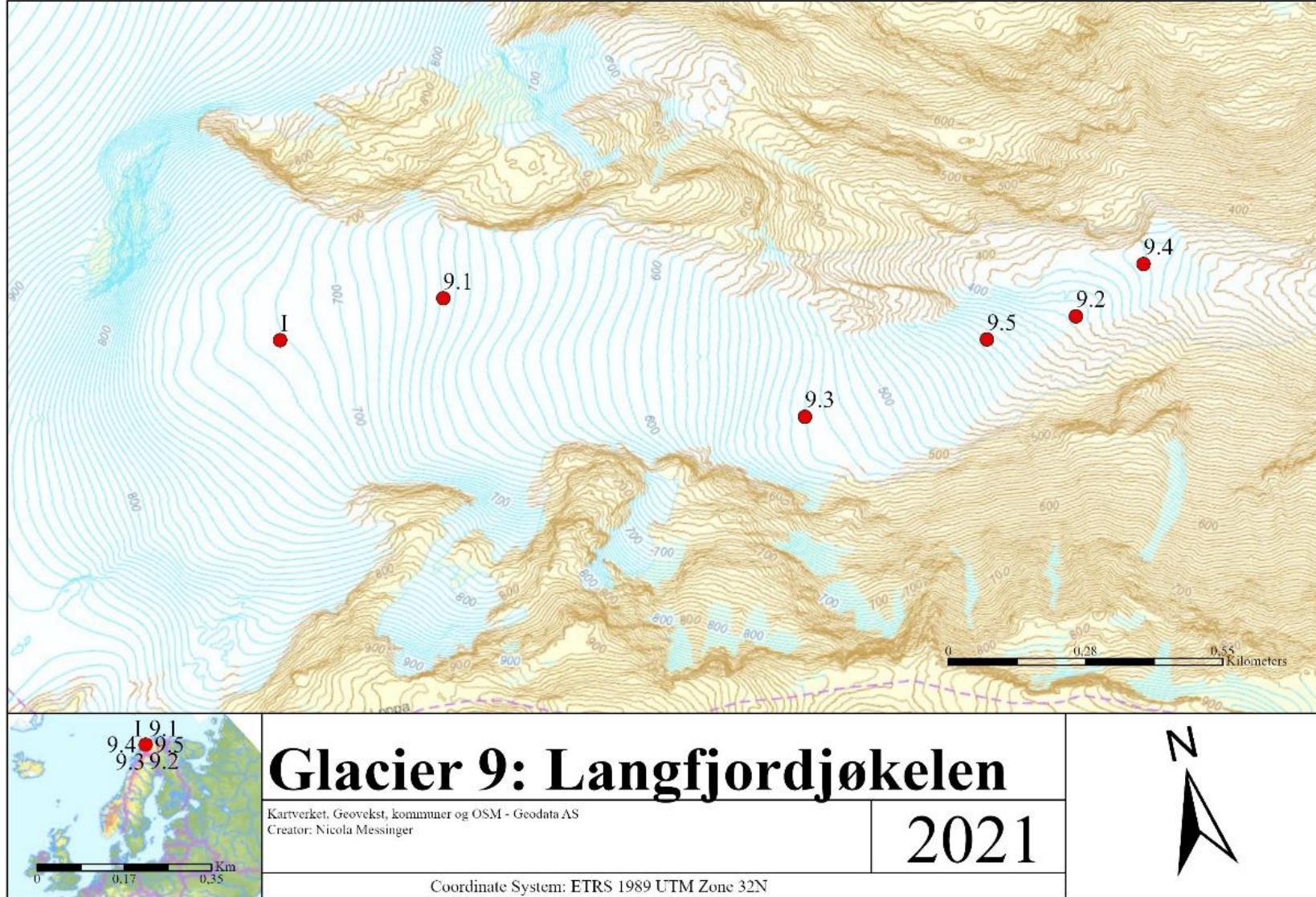


Figure A.9 Sample location for element analysis (9.1-9.5) and PAH and PCB analysis (I) on Langfjordjøkelen (9).

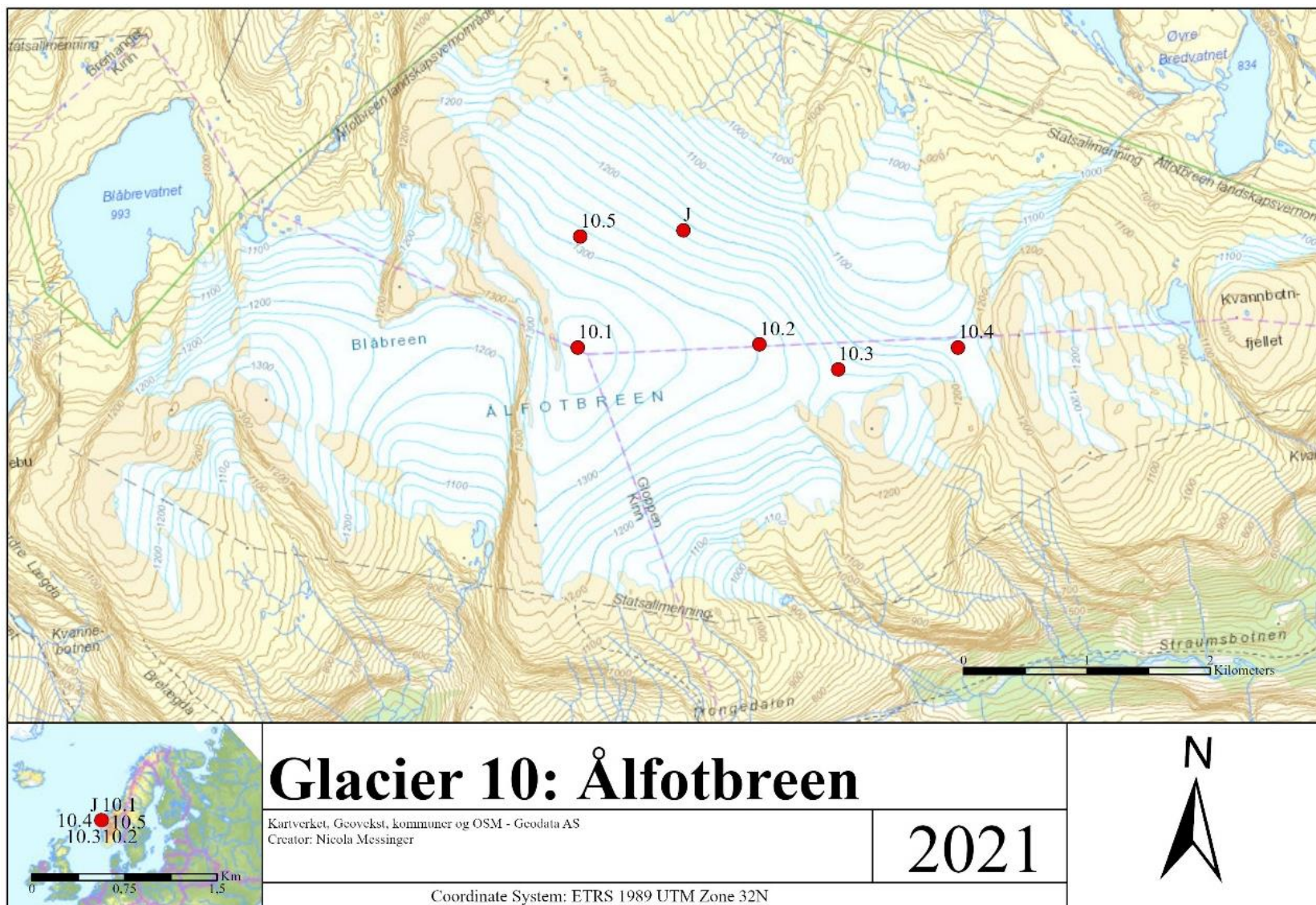


Figure A.10 Sample location for element analysis (10.1-10.5) and PAH and PCB analysis (J) on Ålfotbreen (10).

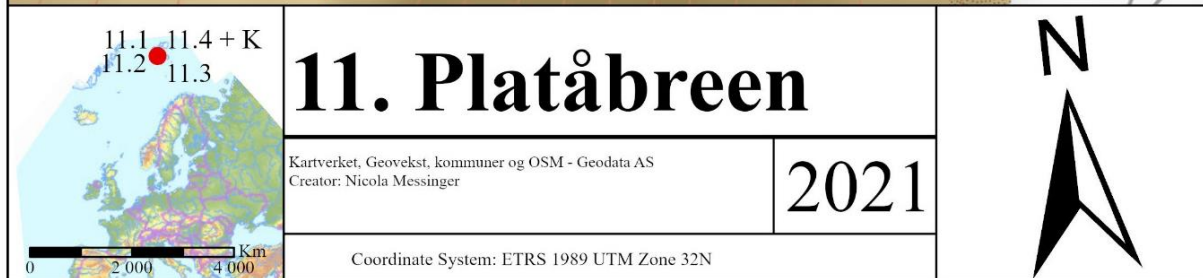
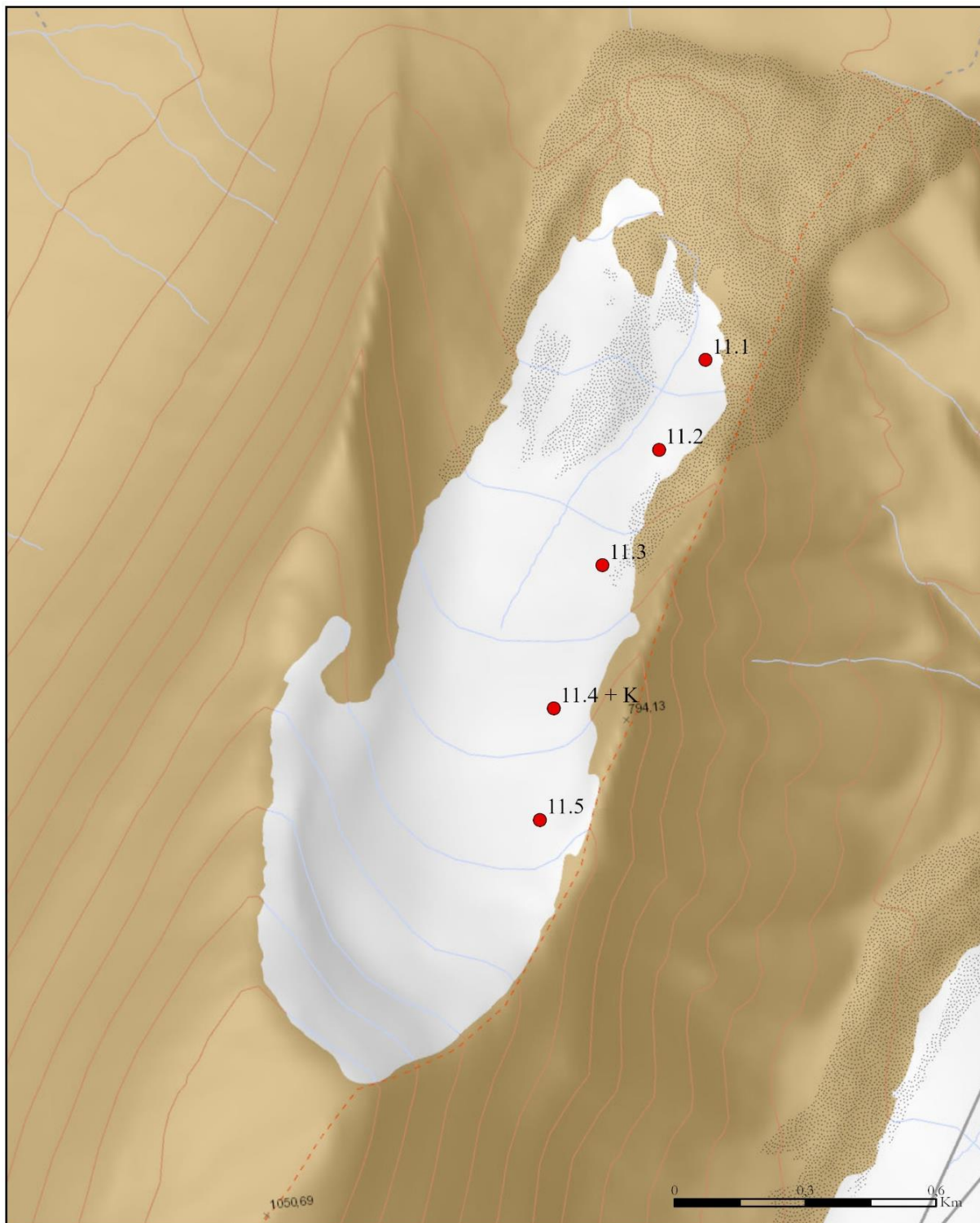


Figure A.11 Sample location for element analysis (11.1-11.5) and PAH and PCB analysis (K) on Platåbreen (11).

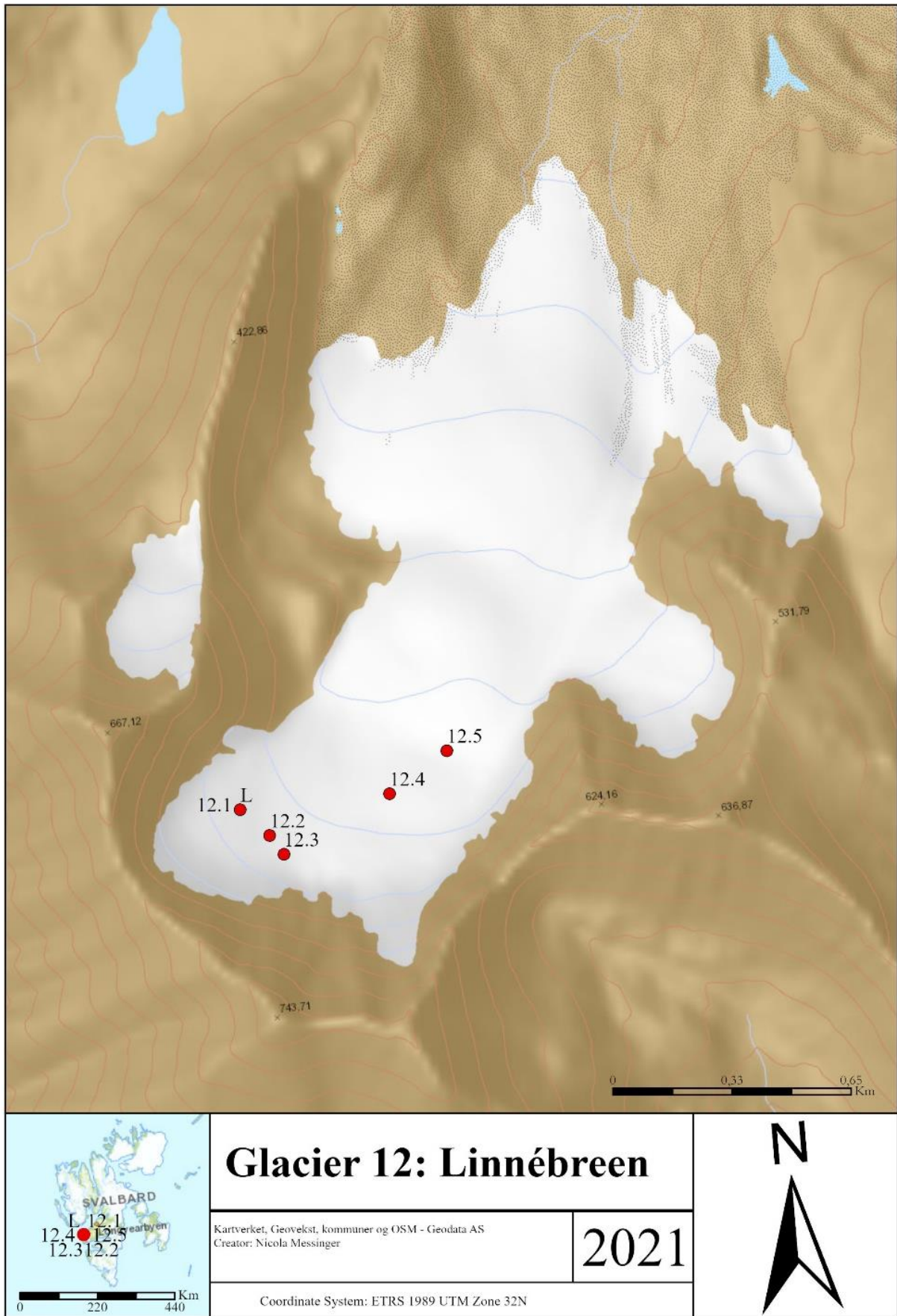


Figure A.12 Sample location for element analysis (12.1-12.5) and PAH and PCB analysis (L) on Linnébreen (12).

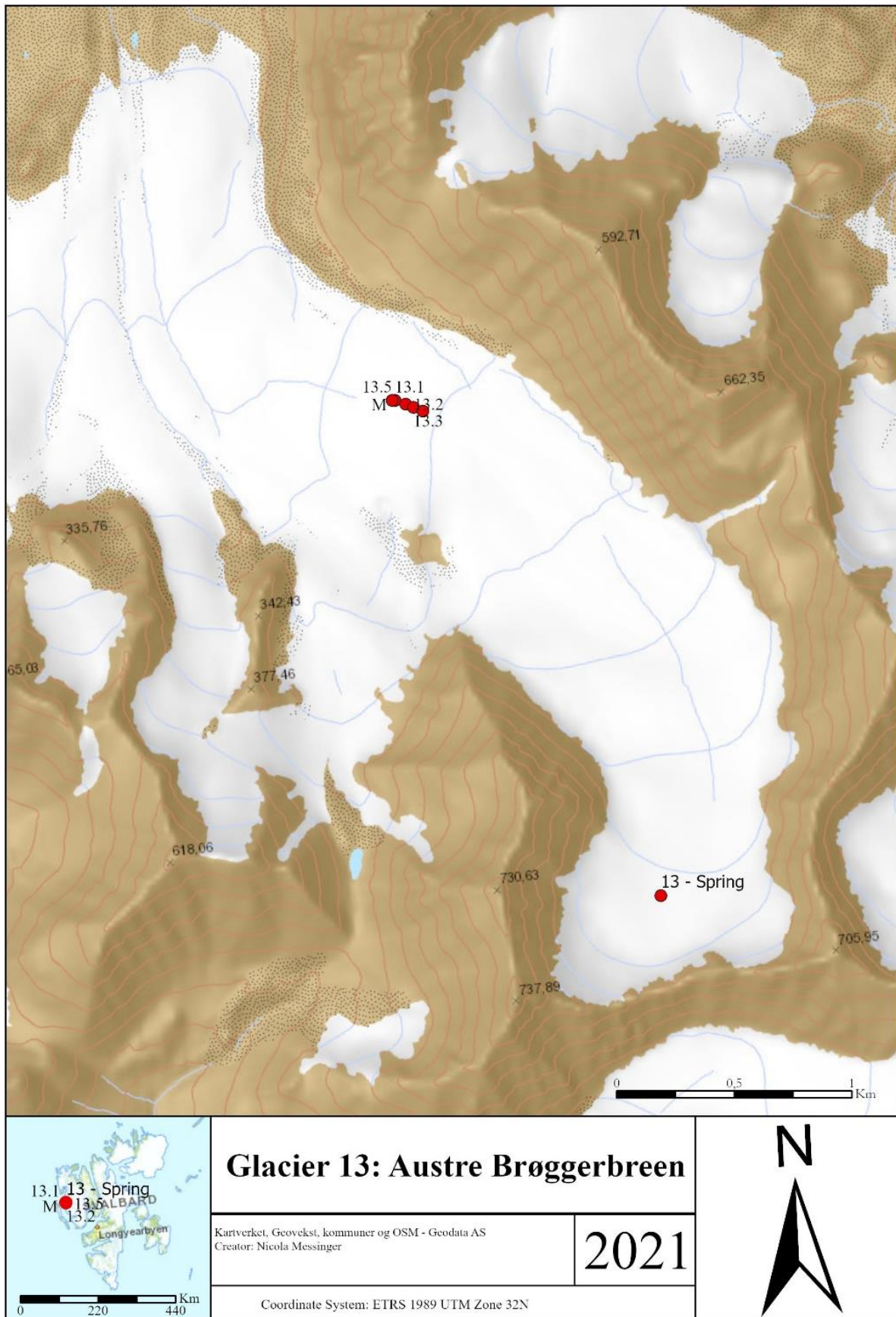


Figure A.13 Sample location for element analysis (13.1-13.5), and PAH and PCB analysis (M) on Austre Brøggerbreen (13).

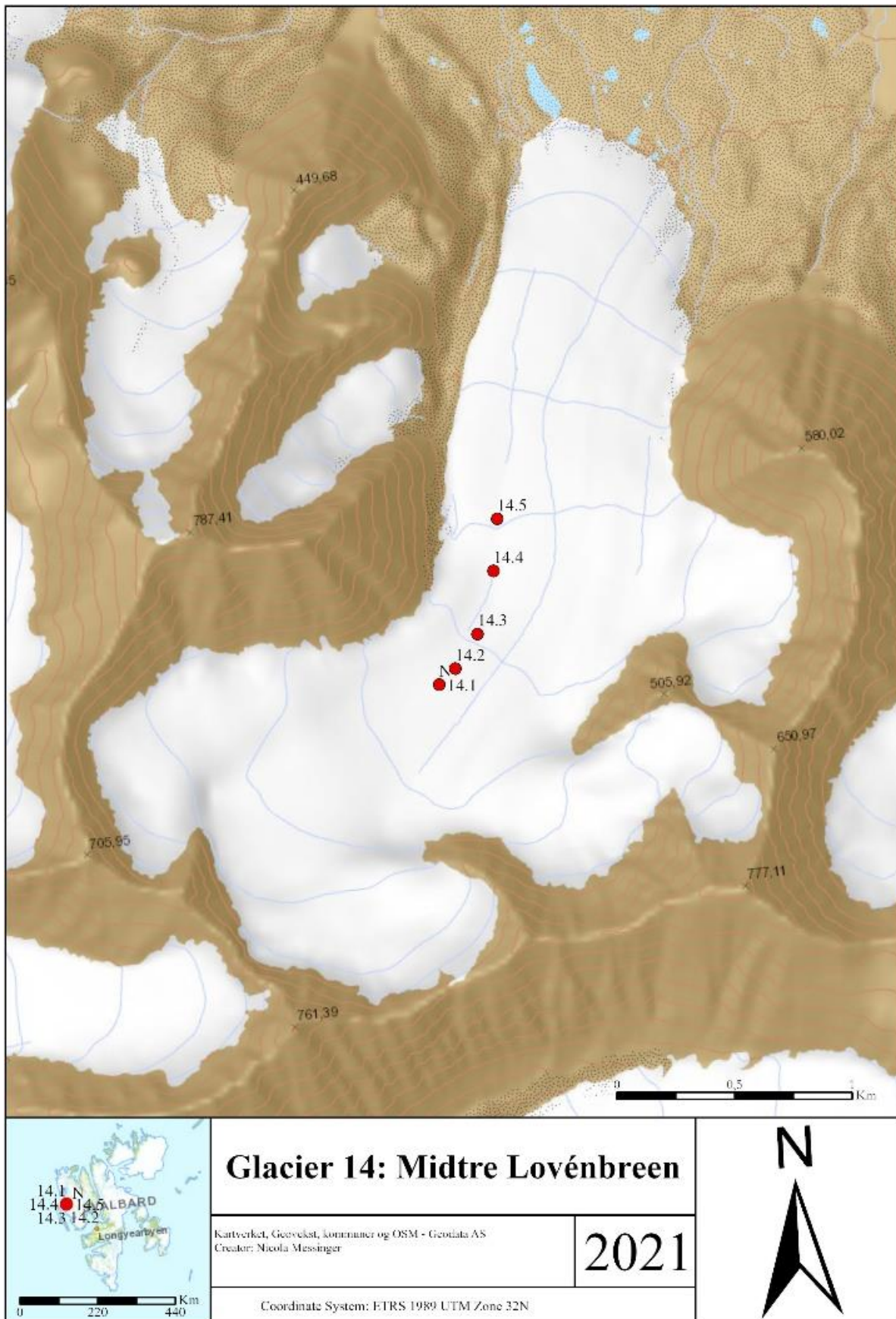


Figure A.14 Sample location for element analysis (14.1-14.5), and PAH and PCB analysis (N) on Midtre Lovénbreen (14).

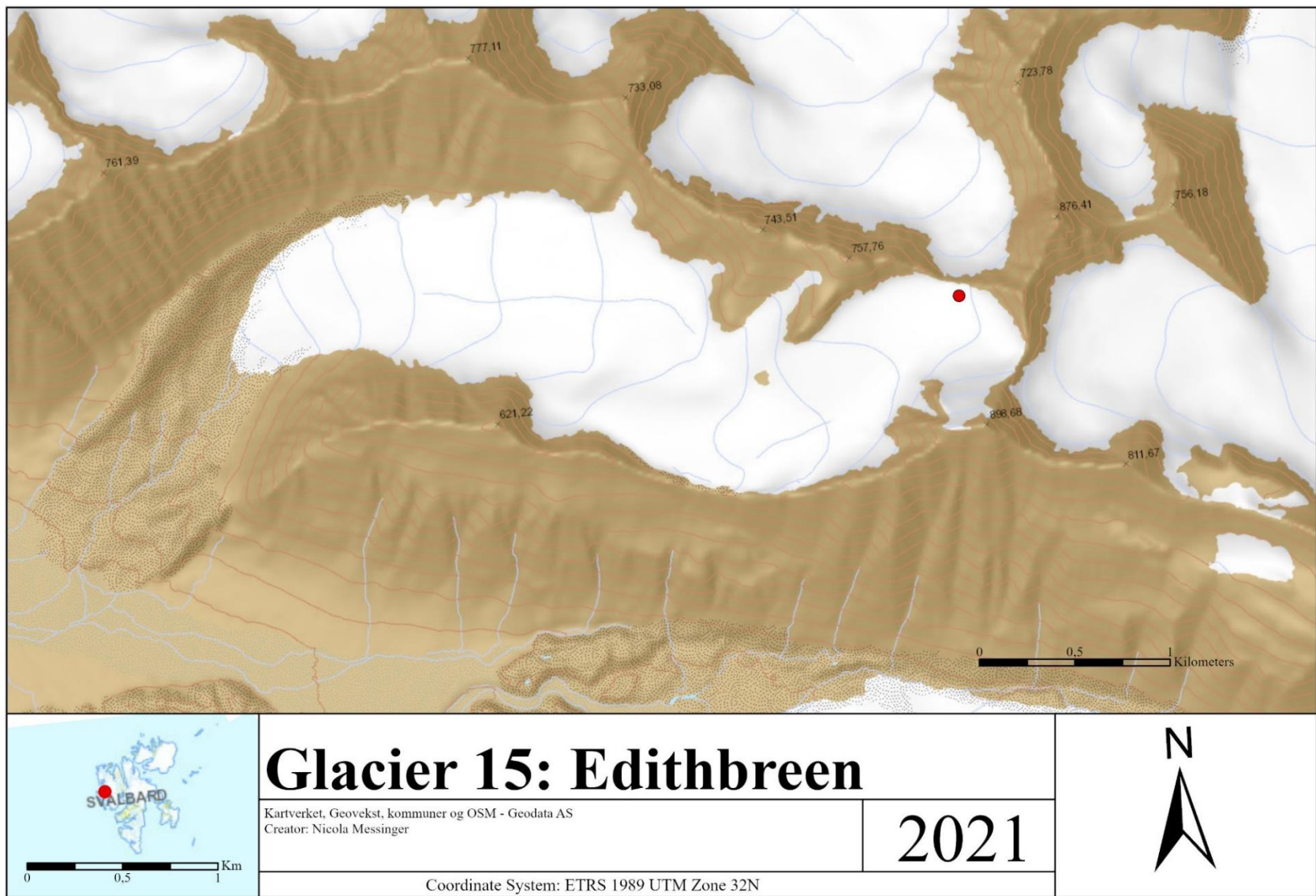


Figure A.15 Sample location for element, PAH and PCB analysis on Edithbreen (15).

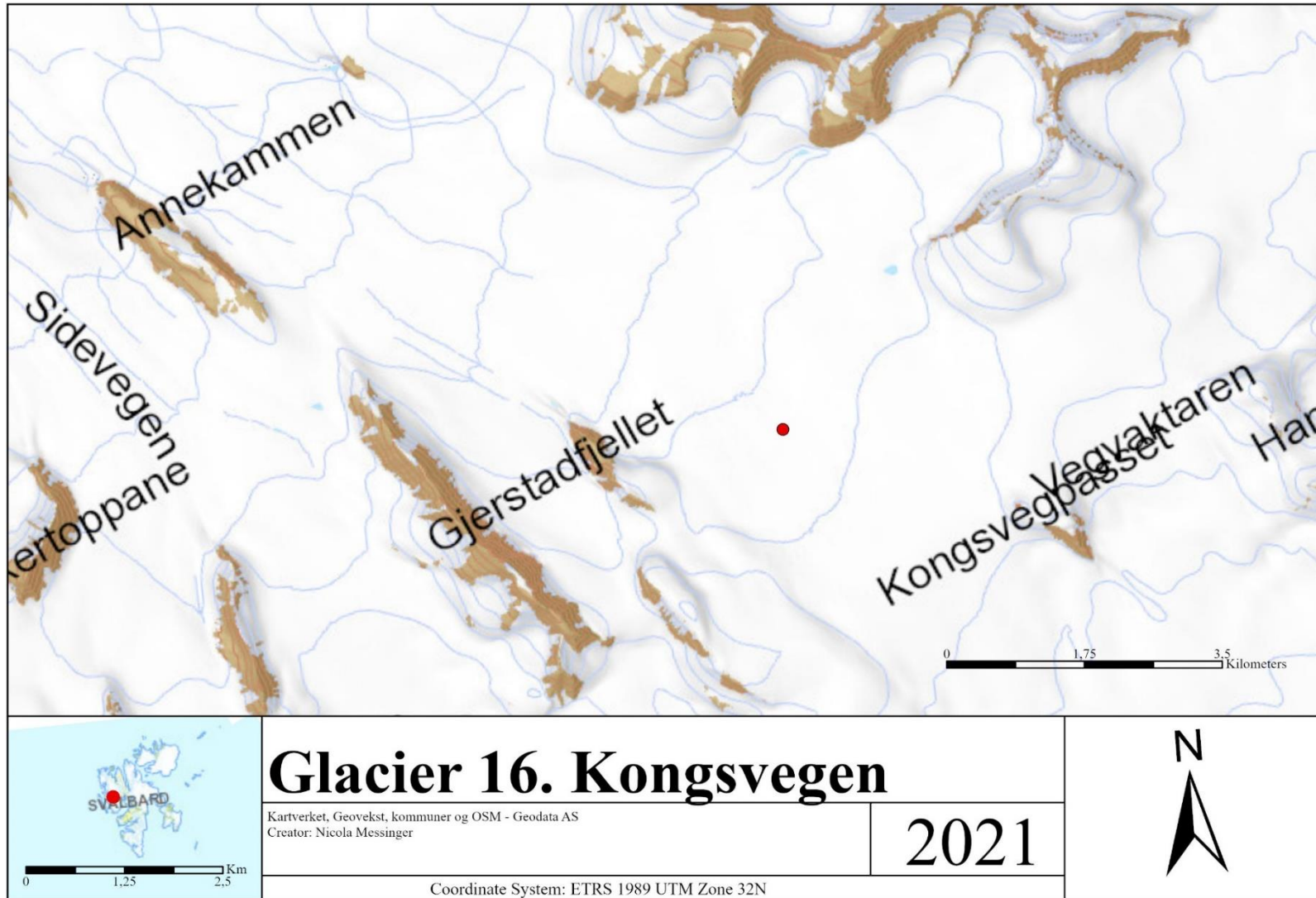


Figure A.16 Sample location for element, PAH and PCB analysis on Kongsvegen (16).

B. Materials and Chemicals

Table B.1 Materials and chemicals used in the study, their article number and supplier.

Material	Article number	Supplier
Aluminum flasks (1200mL)	215-0262	VWR
Slider zip bags	VWRI129-1201_P	VWR
Centrifuge tubes	525-0610	VWR
Metal scoop	231-0109	VWR
Syringe filters (0,45µm)	525-1121	VWR
Syringe (20mL)	5200-000V0	VWR
Empty polypropylene SPE Tube	54223-U	Sigma-Aldrich
Polypropylene Frits 12 mL	57182-U	Sigma- Aldrich
Chemicals		
Ultra-pure nitric acid (14.4M)	239-240	VWR
Ethyl acetate (ACS grade)	141-78-6	VWR
Methanol (HPLC grade)	67-56-1	VWR
Acetone (HPLC grade)	67-64-1	VWR
Dichloromethane – GC- capillary grade	75-09-2	VWR
Bondesil – C18 40µm, 100gm	12213012	Agilent Technologies

C. Sample Weight

Table C.1 Weight of the sample used for analysis of each glacier.

Sample	Glacier name	Sample weight (g)
A	Austdalsbreen	1018
B	Storbreen	1039
C	Gråsubreen	754.1
D	Hellstugubreen	1096
E	Juvfonne	1092
F	Nigardsbreen	991.8
G	Engabreen	1019
H	Rembesdalskåka	1096
I	Langfjordjøkelen	952.0
J	Ålfotbreen	672.7
K	Platåbreen (Summer)	1117
L	Linnébreen (Summer)	1035
M	Austre Brøggerbreen (Summer)	999.5
N	Midtre Lovénbreen (Summer)	917.7
O	Austre Brøggerbreen	1067
P	Edithbreen	786.6
Q	Kongsvegen	964.2

D. Trajectory Models

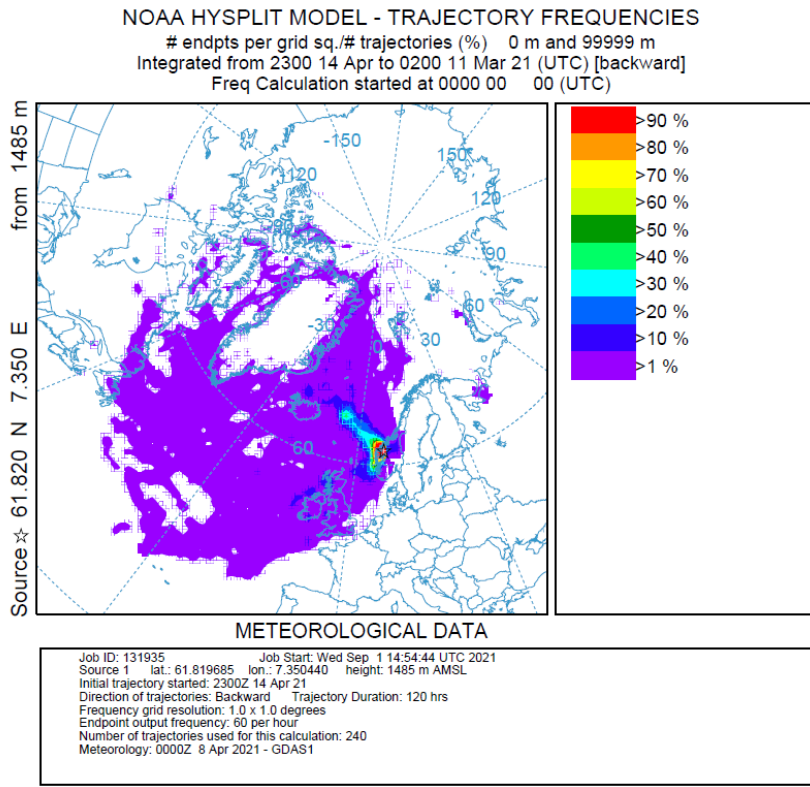


Figure D.1 NOAA HYSPLIT atmospheric back trajectory models of Austdalsbreen (1) for 30 days before sampling.

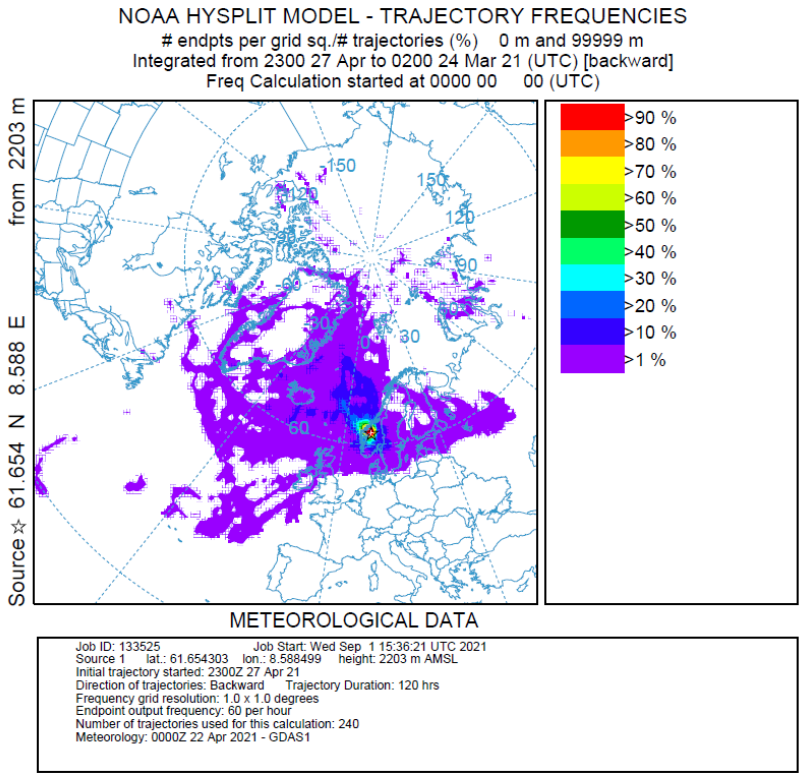


Figure D.2 NOAA HYSPLIT atmospheric back trajectory models of Gråsubreen (3) for 30 days before sampling.

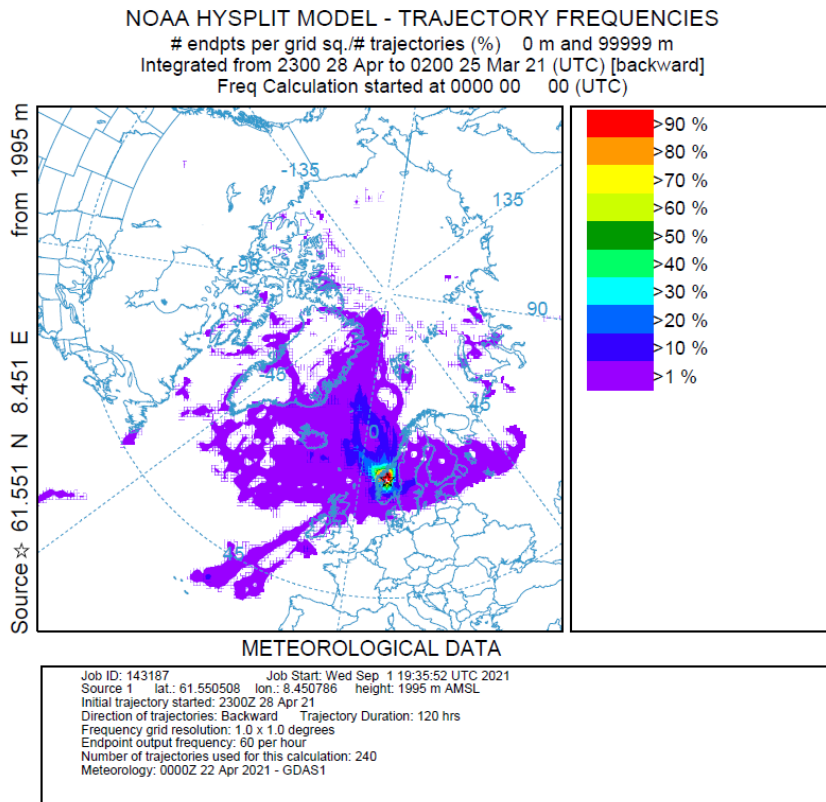


Figure D.3 NOAA HYSPLIT atmospheric back trajectory models of Hellstugubreen (4.) for 30 days before sampling.

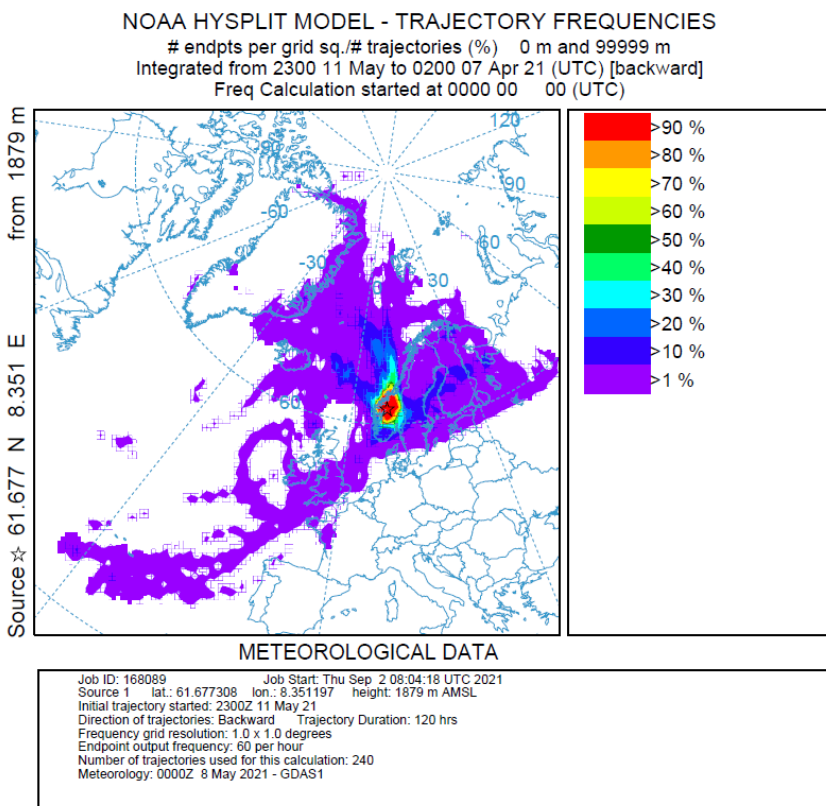


Figure D.4 NOAA HYSPLIT atmospheric back trajectory models of Juvfonna (5.) for 30 days before sampling.

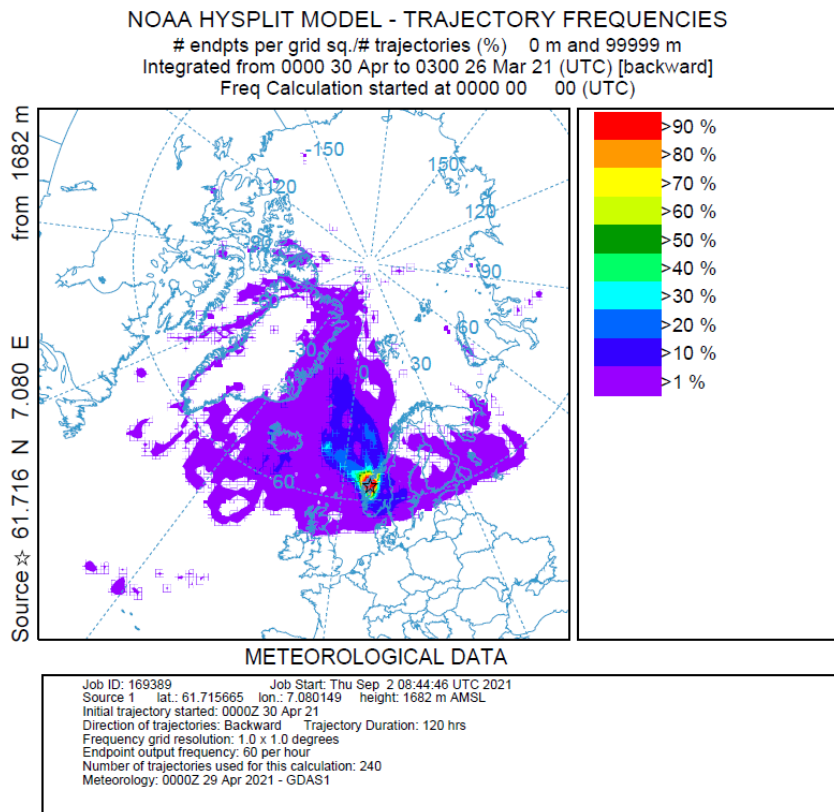


Figure D.5 NOAA HYSPLIT atmospheric back trajectory models of Nigardsbreen (6) for 30 days before sampling.

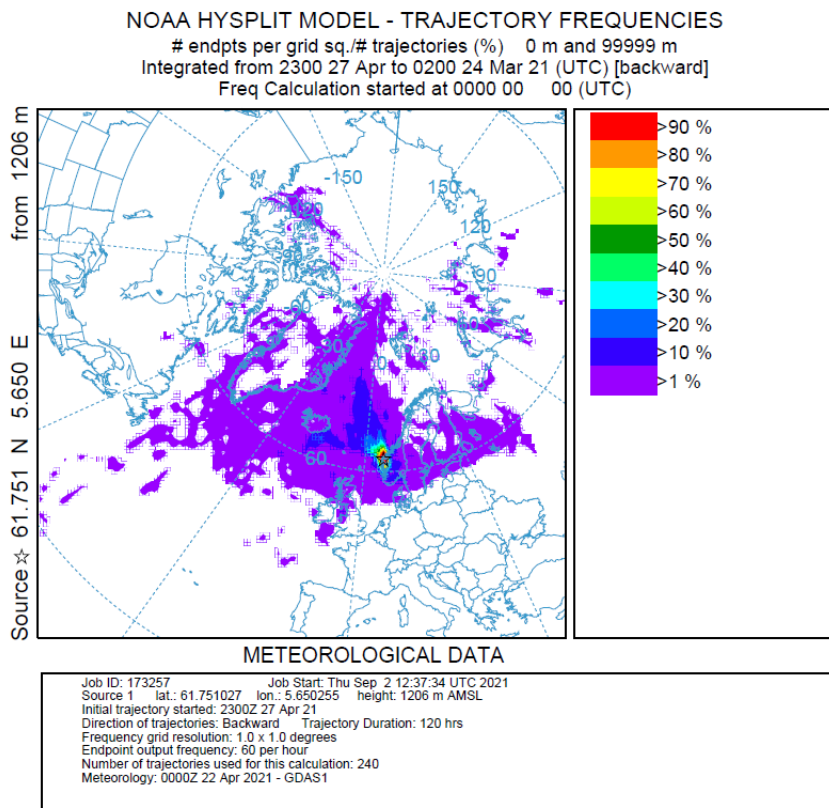


Figure D.6 NOAA HYSPLIT atmospheric back trajectory models of Ålfotbreen (10) for 30 days before sampling.

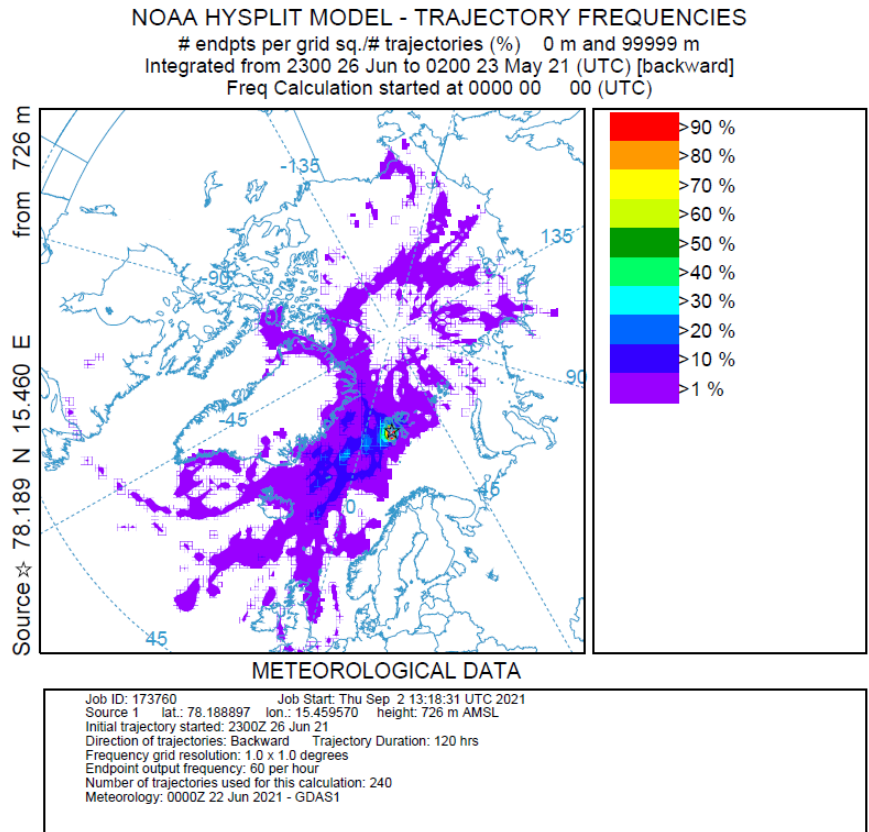


Figure D.7 NOAA HYSPLIT atmospheric back trajectory models of Platåbreen (11) for 30 days before sampling.

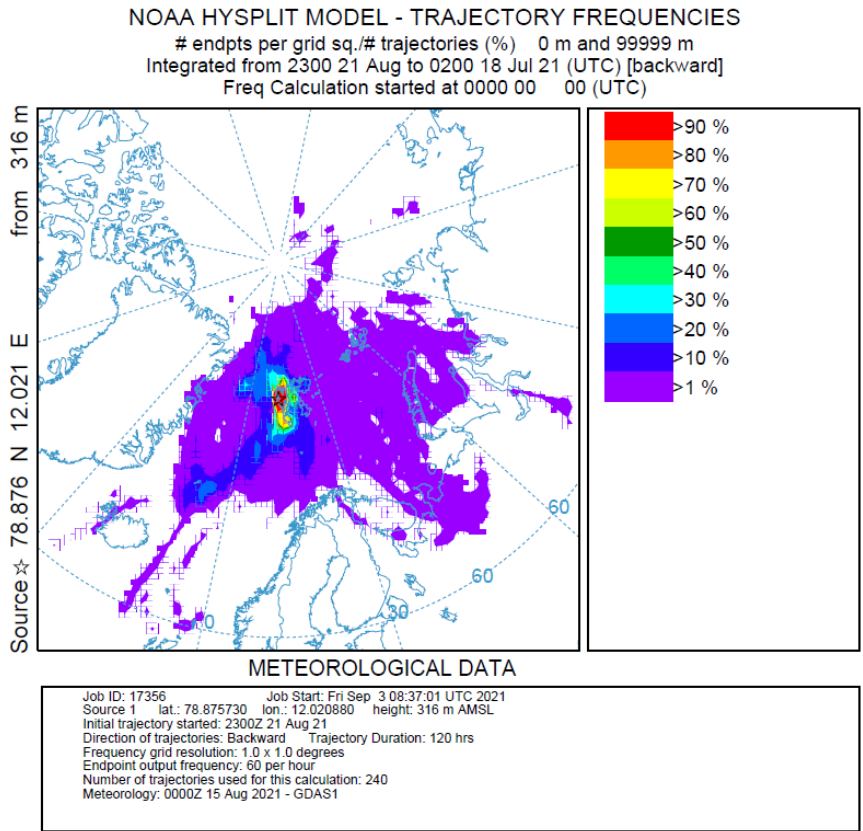


Figure D.8 NOAA HYSPLIT atmospheric back trajectory models of Midtre Lovénbreen (14) for 30 days before sampling.

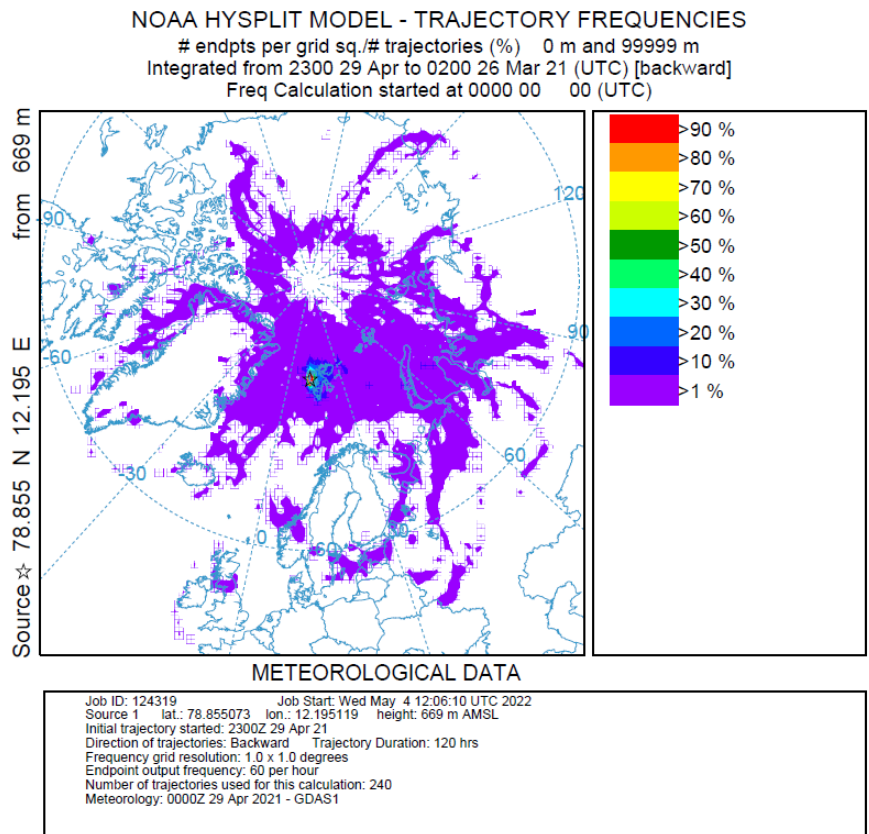


Figure D.9 NOAA HYSPLIT atmospheric back trajectory models of Edithbreen (15) for 30 days before sampling.

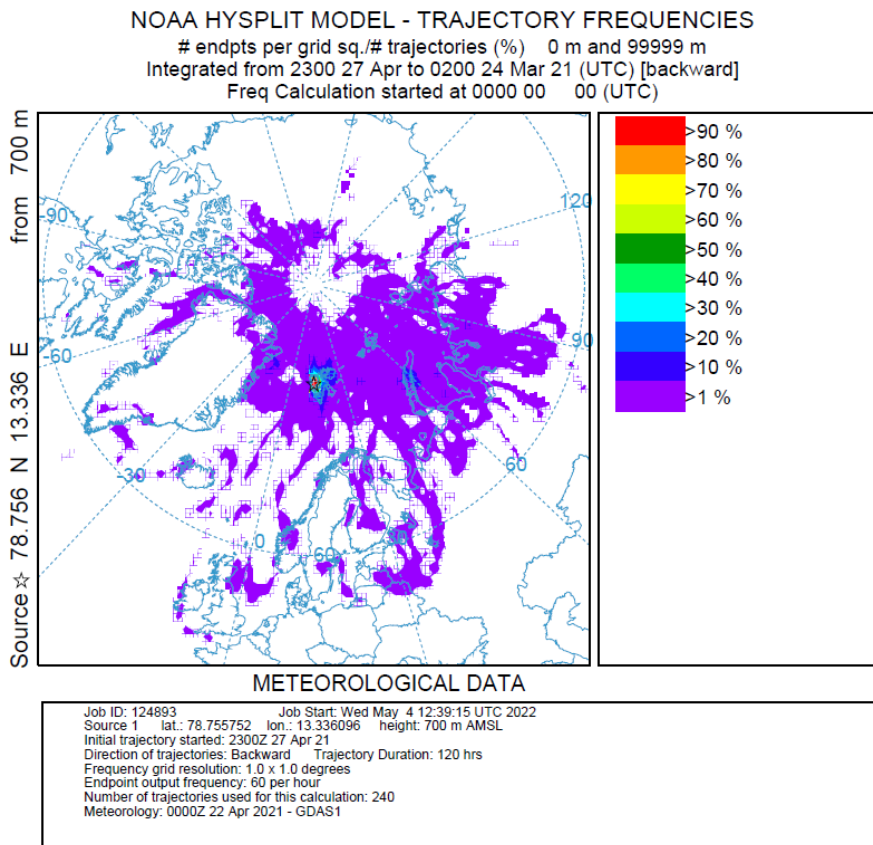


Figure A.10 NOAA HYSPLIT atmospheric back trajectory models of Kongsvegen (16) for 30 days before sampling.

E. Results elements

Table E.1 Detection limit of the 62 measured elements.

Tune Mode	Scan Type	Q1	Q2	Name	R	DL	BEC	Units
No Gas	MS/MS	7	7	Li	1,0000	2,19E-03	2,79E-02	µg L ⁻¹
No Gas	MS/MS	9	9	Be	1,0000	5,16E-04	1,99E-04	µg L ⁻¹
H2	MS/MS	9	9	Be	0,9998	1,37E-03	2,64E-04	µg L ⁻¹
O2	MS/MS	11	11	B	0,9998	9,72E-02	5,63E-01	µg L ⁻¹
O2	MS/MS	23	23	Na	1,0000	7,39E-02	2,36E+00	µg L ⁻¹
O2	MS/MS	24	24	Mg	1,0000	6,25E-03	2,70E-02	µg L ⁻¹
H2	MS/MS	27	27	Al	1,0000	3,21E-03	1,11E-02	µg L ⁻¹
H2	MS/MS	28	28	Si	1,0000	1,42E-01	1,58E+00	µg L ⁻¹
O2	MS/MS	28	44	Si	0,9999	7,36E-01	1,58E+00	µg L ⁻¹
O2	MS/MS	31	47	P	0,9998	2,51E-02	7,75E-02	µg L ⁻¹
O2	MS/MS	32	48	S	1,0000	9,93E-02	1,58E+00	µg L ⁻¹
O2	MS/MS	35	51	Cl	0,9999	7,13E+01	1,07E+03	µg L ⁻¹
O2	MS/MS	39	39	K	1,0000	3,19E-02	1,86E+00	µg L ⁻¹
H2	MS/MS	40	40	Ca	1,0000	1,44E-03	9,52E-02	µg L ⁻¹
O2	MS/MS	45	61	Sc	1,0000	1,51E-04	1,32E-04	µg L ⁻¹
O2	MS/MS	47	63	Ti	1,0000	1,61E-03	9,52E-04	µg L ⁻¹
O2	MS/MS	51	67	V	1,0000	1,38E-04	9,90E-04	µg L ⁻¹
O2	MS/MS	52	52	Cr	1,0000	1,06E-02	1,01E-01	µg L ⁻¹
O2	MS/MS	55	55	Mn	1,0000	1,62E-03	6,08E-03	µg L ⁻¹
H2	MS/MS	56	56	Fe	1,0000	3,68E-03	8,34E-02	µg L ⁻¹
O2	MS/MS	59	59	Co	1,0000	1,06E-03	7,04E-03	µg L ⁻¹
O2	MS/MS	60	60	Ni	1,0000	8,27E-03	1,81E-02	µg L ⁻¹
O2	MS/MS	63	63	Cu	0,9999	7,35E-03	2,77E-02	µg L ⁻¹
H2	MS/MS	66	66	Zn	0,9997	2,75E-03	2,51E-02	µg L ⁻¹
H2	MS/MS	71	71	Ga	1,0000	5,01E-04	1,17E-03	µg L ⁻¹
O2	MS/MS	75	91	As	0,9999	9,69E-04	7,65E-04	µg L ⁻¹
H2	MS/MS	78	78	Se	1,0000	5,17E-03	1,13E-02	µg L ⁻¹
O2	MS/MS	81	81	Br	0,9999	1,86E-01	2,75E-01	µg L ⁻¹
O2	MS/MS	85	85	Rb	0,9999	1,15E-03	6,82E-03	µg L ⁻¹
H2	MS/MS	88	88	Sr	1,0000	1,20E-03	3,44E-03	µg L ⁻¹
O2	MS/MS	89	105	Y	1,0000	7,44E-05	2,81E-05	µg L ⁻¹
O2	MS/MS	90	106	Zr	0,9999	2,88E-04	1,39E-04	µg L ⁻¹
O2	MS/MS	93	125	Nb	1,0000	5,89E-05	1,70E-05	µg L ⁻¹
O2	MS/MS	95	127	Mo	1,0000	1,64E-04	4,92E-04	µg L ⁻¹
O2	MS/MS	111	111	Cd	0,9999	1,51E-04	2,91E-05	µg L ⁻¹
O2	MS/MS	115	115	In	1,0000	1,67E-05	2,20E-05	µg L ⁻¹
O2	MS/MS	118	118	Sn	1,0000	1,10E-03	1,58E-03	µg L ⁻¹
O2	MS/MS	121	137	Sb	1,0000	1,59E-04	6,13E-05	µg L ⁻¹
O2	MS/MS	133	133	Cs	0,9999	1,97E-04	1,56E-03	µg L ⁻¹
O2	MS/MS	137	137	Ba	1,0000	9,82E-04	4,72E-04	µg L ⁻¹
O2	MS/MS	139	155	La	1,0000	5,50E-05	1,47E-05	µg L ⁻¹

O2	MS/MS	140	156	Ce	1,0000	5,38E-07	1,96E-05	µg L ⁻¹
O2	MS/MS	141	157	Pr	1,0000	2,37E-05	7,89E-06	µg L ⁻¹
O2	MS/MS	146	162	Nd	1,0000	7,80E-05	3,00E-05	µg L ⁻¹
O2	MS/MS	147	163	Sm	1,0000	0,00E+00	0,00E+00	µg L ⁻¹
O2	MS/MS	153	153	Eu	0,9999	5,81E-07	2,45E-05	µg L ⁻¹
O2	MS/MS	157	173	Gd	0,9999	9,77E-05	1,88E-05	µg L ⁻¹
O2	MS/MS	159	175	Tb	1,0000	4,48E-05	1,73E-05	µg L ⁻¹
O2	MS/MS	163	179	Dy	1,0000	5,92E-05	1,14E-05	µg L ⁻¹
O2	MS/MS	165	181	Ho	1,0000	1,09E-04	2,10E-05	µg L ⁻¹
O2	MS/MS	166	182	Er	1,0000	8,21E-05	2,72E-05	µg L ⁻¹
O2	MS/MS	169	185	Tm	1,0000	4,66E-05	1,35E-05	µg L ⁻¹
O2	MS/MS	172	172	Yb	1,0000	2,82E-04	9,40E-05	µg L ⁻¹
O2	MS/MS	175	191	Lu	1,0000	5,25E-05	1,01E-05	µg L ⁻¹
O2	MS/MS	178	194	Hf	1,0000	1,14E-04	2,20E-05	µg L ⁻¹
O2	MS/MS	181	213	Ta	0,9999	1,62E-07	1,34E-05	µg L ⁻¹
O2	MS/MS	182	214	W	0,9999	2,30E-04	2,25E-04	µg L ⁻¹
O2	MS/MS	195	195	Pt	0,9998	9,33E-04	1,28E-03	µg L ⁻¹
O2	MS/MS	197	197	Au	0,9999	1,24E-02	2,76E-02	µg L ⁻¹
O2	MS/MS	202	202	Hg	1,0000	9,60E-03	1,91E-02	µg L ⁻¹
H2	MS/MS	205	205	Tl	1,0000	4,41E-04	1,05E-03	µg L ⁻¹
O2	MS/MS	206	206	[Pb]	1,0000	2,36E-03	5,29E-03	µg L ⁻¹
O2	MS/MS	207	207	[Pb]	1,0000	2,57E-03	9,32E-03	µg L ⁻¹
O2	MS/MS	208	208	Pb	1,0000	1,09E-03	6,27E-03	µg L ⁻¹
H2	MS/MS	209	209	Bi	1,0000	9,35E-05	3,12E-05	µg L ⁻¹
O2	MS/MS	232	248	Th	0,9999	5,16E-04	9,93E-05	µg L ⁻¹
H2	MS/MS	238	238	U	1,0000	2,74E-04	1,05E-04	µg L ⁻¹

Table E.2 Mean lanthanoid concentration ($\mu\text{g L}^{-1}$) of each glacier and the standard deviation (STD) of the samples.

Glacier	La [O2]		Ce [O2]		Pr [O2]		Nd [O2]		Sm [O2]	
	Mean	STD	Mean	STD	Mean	STD	Mean	STD	Mean	STD
1. Austdalsbreen	0.001149	0.00105	0.001583	0.001352	0.000247	0.000269	0.001119	0.001023	<0.00024	0.000227
2. Storbreen	0.000586	0.000416	0.001101	0.000777	9.59E-05	7.76E-05	0.00047	0.000457	<0.00024	0
3. Gråsubreen	0.00014	9.8E-05	0.000498	0.000218	2.79E-05	2.02E-05	0.000304	0.000171	<0.00024	0
4. Hellstugubreen	0.000657	0.000643	0.001334	0.000937	0.000126	0.000129	0.000682	0.000537	<0.00024	3.05E-05
5. Juvfonne	0.000694	0.000739	0.002829	0.002524	0.000113	0.000146	0.000587	0.0005	<0.00024	4.15E-05
6. Nigardsbreen	0.00085	0.000823	0.001679	0.001334	0.000244	0.00022	0.000977	0.000926	<0.00024	0
7. Engabreen	0.000271	0.000348	0.000644	0.00056	0.000151	0.000272	0.000285	0.000236	0.00025	0.000259
8. Rembesdalskåka	0.000279	0.000233	0.000681	0.000359	3.7E-05	2.19E-05	0.000286	0.000209	<0.00024	0
9. Langfjordsjøkelen	0.000198	0.000132	0.000404	0.000348	<0.00002	1.67E-06	0.000207	0.000147	<0.00024	0
10. Ålfofbreen	0.000209	0.000176	0.000499	0.000261	3.3E-05	3.27E-05	0.000267	0.000199	<0.00024	0
11. Platåbreen(S)	0.000179	0.000366	0.001016	0.001199	9.06E-05	0.000163	0.000788	0.000844	0.000284	0.000258
12. Linnébreen(S)	0.000606	0.000693	0.001717	0.002175	0.000283	0.000302	0.001387	0.001769	0.000622	0.000708
13.2 Austre Brøggerbreen(S)	0.002483	0.001503	0.00494	0.003222	0.000883	0.000612	0.003529	0.002359	0.001027	0.000703
14.Midtre Lovénbreen(S)	0.000486	0.000321	0.001197	0.000866	0.000185	0.000143	0.000883	0.000629	0.000272	0.000246
16. Kongsvegen	0.000867		0.002251		0.000394		0.00145		0.000978	
13.1 Austré Brøggerbreen	0.001117		0.003239		0.000506		0.002901		0.000806	
15. Edithbreen	0.000489		0.001287		0.000207		0.00113		0.000229	

Table E.2 cont. Mean lanthanoid concentration ($\mu\text{g L}^{-1}$) of each glacier and the standard deviation (STD) of the samples taken on the glaciers.

Lanthanides cont. Glacier	Eu [O2]		Gd [O2]		Tb [O2]		Dy [O2]		Ho [O2]	
	Mean	STD	Mean	STD	Mean	STD	Mean	STD	Mean	STD
1. Austdalsbreen	0.000135	0.000111	0.000233	0.000201	5.11E-05	8.22E-05	0.000187	0.000186	7.05E-05	9.11E-05
2. Storbreen	<0.00010	3.66E-05	0.000151	0.000148	<0.00002	0	<0.00007	4.66E-05	<0.00005	0
3. Gråsubreen	0.000162	0.000166	<0.00012	0	<0.00002	0	<0.00007	0	<0.00005	0
4. Hellstugubreen	<0.00010	0	<0.00012	5.64E-05	<0.00002	0	0.000137	0.000154	<0.00005	7.32E-06
5. Juvfonne	0.000203	7.17E-05	0.000156	0.000191	<0.00002	0	9.3E-05	0.000116	<0.00005	0
6. Nigardsbreen	<0.00010	0	<0.00012	5.3E-05	<0.00002	0	<0.00007	0	<0.00005	0
7. Engabreen	0.000115	0.00013	<0.00012	0.000125	9.97E-05	0.000139	0.000113	0.000123	9.12E-05	0.00013
8. Rembesdalskåka	<0.00010	0	<0.00012	2.44E-05	<0.00002	0	<0.00007	0	<0.00005	0
9. Langfjordsjøkelen	<0.00010	0	<0.00012	0	<0.00002	0	<0.00007	0	<0.00005	0
10. Ålfotbreen	<0.00010	0	<0.00012	1.6E-05	<0.00002	0	<0.00007	0	<0.00005	0
11. Platåbreen (S)	<0.00010	0	0.00024	0.000247	4.85E-05	5.63E-05	0.000614	0.000553	8.01E-05	5.71E-05
12. Linnébreen (S)	0.00022	0.000166	0.000596	0.000877	0.000162	0.000203	0.00145	0.00202	0.000385	0.000427
13.2 Austre Brøggerbreen (S)	0.000243	0.000181	0.000911	0.000713	0.000145	0.000106	0.000664	0.000497	0.00012	8.12E-05
14. Midtre Lovénbreen (S)	5.23E-05	7.33E-05	0.000222	0.000185	<0.00004	1.8E-05	0.000172	0.000137	<0.00011	0
16. Kongsvegen	0.000214		0.000666		4.85E-05		0.000324		<0.00011	
13.1 Austré Brøggerbreen	0.000112		0.000608		7.56E-05		0.000541		<0.00011	
15. Edithbreen	0.000128		0.000176		<0.00004		0.000144		<0.00011	

Table E.2 cont. Mean lanthanoid concentration ($\mu\text{g L}^{-1}$) of each glacier and the standard deviation (STD) of the samples taken on the glaciers.

Lanthanides cont.	Er [O2]		Tm [O2]		Yb [O2]		Lu [O2]		Lanthanoids
Glacier	Mean	STD	Mean	STD	Mean	STD	Mean	STD	Total conc.
1. Austdalsbreen	<0.00014	5.17E-05	5.8E-05	9.61E-05	<0.00036	0.000115	3.34E-05	4.91E-05	0.005236
2. Storbreen	<0.00014	0	<0.00002	0	<0.00036	0	<0.00002	0	0.002914
3. Gråsubreen	<0.00014	0	<0.00002	0	<0.00036	0	<0.00002	0	0.001652
4. Hellstugubreen	<0.00014	7.18E-05	8.09E-06	3.81E-06	<0.00036	0.000292	2.6E-05	3.2E-05	0.003485
5. Juvfonne	<0.00014	1.49E-05	<0.00002	0	<0.00036	0	<0.00002	0	0.0051
6. Nigardsbreen	<0.00014	0	<0.00002	0	<0.00036	0	<0.00002	0	0.00432
7. Engabreen	<0.00014	6.08E-05	7.19E-05	0.000121	<0.00036	0	5.95E-05	9.89E-05	0.002461
8. Rembesdalskåka	<0.00014	0	<0.00002	0	<0.00036	7.97E-05	<0.00002	0	0.001853
9. Langfjordsjøkelen	<0.00014	0	<0.00002	0	<0.00036	0	<0.00002	0	0.00139
10. Ålfbreen	<0.00014	0	<0.00002	0	<0.00036	0	<0.00002	0	0.001578
11. Platåbreen(S)	0.000343	0.00023	<0.00002	3.56E-06	0.000485	0.000263	<0.00002	1.54E-05	0.004239
12. Linnébreen(S)	0.001099	0.001374	0.000244	0.00022	0.001094	0.001357	0.00021	0.000178	0.010076
13.2 Austre Brøggerbreen(S)	0.000254	0.000245	<0.00005	0	<0.00028	0.000135	<0.00005	1.35E-05	0.015391
14. Midtre Lovénbreen(S)	<0.00008	3.15E-05	<0.00005	0	<0.00028	0	<0.00005	0	0.003775
16. Kongsvegen	0.000191		<0.00005		<0.00028		<0.00005		0.007628
13.1 Austré Brøggerbreen	0.00022		<0.00005		0.000488		<0.00005		0.01072
15. Edithbreen	0.000143		<0.00005		<0.00028		<0.00005		0.004197

Table E.3 Mean major element concentration ($\mu\text{g L}^{-1}$) of each glacier and the standard deviation (STD) of the samples.

Glacier	Na [O2]		Mg [O2]		Al [H2]		Si 28 [H2]		P [O2]	
	Mean	STD	Mean	STD	Mean	STD	Mean	STD	Mean	STD
1. Austdalsbreen	693.8069	646.5172	48.85673	24.85752	1.764451	2.73009	4.075282	3.159805	13.06638	13.42763
2. Storbreen	175.8919	70.89967	18.04527	7.500131	0.621032	0.385246	2.926757	1.544522	6.055492	6.294286
3. Gråsubreen	153.8452	94.15503	13.81978	8.161039	1.737983	1.524798	2.965529	0.978257	3.350418	2.79427
4. Hellstugubreen	390.7744	490.7062	22.89993	12.78412	1.794302	1.504717	2.407993	1.076657	11.63526	14.92843
5. Juvfonne	294.6361	168.0729	17.23309	5.805245	0.731498	0.176665	3.205403	1.439392	3.977353	4.196872
6. Nigardsbreen	338.4252	52.61729	40.91714	6.844137	2.585719	3.452954	2.176218	1.080867	2.925422	3.237055
7. Engabreen	132.1663	82.16678	3.039922	1.790991	0.219431	0.162314	1.624616	0.347993	1.091802	0.635402
8. Rembesdalskåka	61.71786	34.18231	3.217851	1.767855	0.412036	0.23926	4.50575	1.638166	0.781528	0.455375
9. Langfjordsjøkelen	3961.63	1846.186	490.9407	226.5142	0.686034	0.425926	3.565199	1.331901	2.883536	2.263659
10. Ålftobreen	2339.646	631.1417	270.5856	81.14045	1.034689	0.879432	3.082053	1.647877	6.026238	3.798441
11. Platåbreen(S)	272.7419	138.8957	43.48222	39.56472	0.813183	0.488009	2.390615	1.69877	3.045313	1.699088
12. Linnébreen(S)	457.8886	222.3318	20.03537	11.18242	0.395073	0.303769	3.077464	0.576291	5.155742	3.160125
13.2 Austre Brøggerbreen(S)	535.7073	202.3877	7.234912	1.613439	0.568994	0.462141	1.146359	0.477002	3.976417	0.95908
14.Midtre Lovénbreen(S)	239.7866	148.6133	10.31467	6.282003	0.405189	0.487304	1.62021	0.496947	3.571551	1.19839
16. Kongsvegen	928.3055		134.4649		0.619422		2.432531		1.43187	
13.1 Austré Brøggerbreen	1955.278		269.7888		0.548234		2.216849		0.261831	
15. Edithbreen	1791.002		230.7022		1.065548		2.334558		0.415884	

Table E.3 cont. Mean major element concentration ($\mu\text{g L}^{-1}$) of each glacier and the standard deviation (STD) of the samples taken on the glaciers.

	S [O2]		Cl [O2]		K [O2]		Ca [O2]		Ti [O2]	
Glacier	Mean	STD	Mean	STD	Mean	STD	Mean	STD	Mean	STD
1. Austdalsbreen	177.4369	120.136	1173.685	968.2895	409.0516	758.4774	123.4164	133.5948	0.028709	0.034701
2. Storbreen	91.14226	38.62371	301.0008	77.17731	59.12925	65.08813	60.88415	31.988	<0,00057	0.000824
3. Gråsubreen	46.40717	16.61092	341.2463	138.1186	80.08248	59.31326	46.90466	29.67397	0.00222	0.005818
4. Hellstugubreen	74.00634	40.51697	632.9601	682.2695	535.3897	902.8579	71.35759	45.74145	0.010862	0.016377
5. Juvfonne	58.90681	15.24559	502.8188	222.8588	212.1665	130.5959	67.54126	33.04766	0.002227	0.00466
6. Nigardsbreen	92.18292	22.48494	572.5587	83.91506	25.41026	8.151024	31.27434	3.241351	0.005578	0.0061
7. Engabreen	8.500044	6.283411	217.1225	135.7394	15.38326	13.88121	8.96305	3.469814	0.000638	0.002798
8. Rembesdalskåka	23.59903	15.21501	90.01539	57.39755	38.86493	24.33409	18.77814	9.337024	0.009779	0.003942
9. Langfjordsjøkelen	448.2665	161.2382	6840.428	3158.57	234.9531	197.5643	156.2733	71.51615	0.004199	0.003369
10. Ålfotbreen	316.5629	76.86631	3964.269	1094.017	218.4785	229.8522	115.9627	33.54855	0.016072	0.014315
11. Platåbreen(S)	22.14745	18.38491	448.852	213.3623	162.9566	201.8759	106.9756	77.17152	0.007903	0.007244
12. Linnébreen(S)	7.257015	3.121134	639.6936	289.7011	35.3979	27.47533	87.59377	26.57164	0.015295	0.009824
13.2 Austre Brøggerbreen(S)	5.108164	2.40417	766.4853	283.4855	41.43769	36.81137	80.59697	14.86273	0.006281	0.001398
14.Midtre Lovénbreen(S)	4.537142	2.888455	358.1243	211.2919	57.63079	81.51067	60.45206	23.18197	0.010362	0.00524
16. Kongsvegen	123.3661		1629.167		39.60772		161.598		0.011146	
13.1Austré Brøggerbreen	236.5373		3414.163		75.6279		276.1811		0.028151	
15. Edithbreen	213.8448		3098.52		68.59767		139.625		0.035286	

Table E.3 cont. Mean major element concentration ($\mu\text{g L}^{-1}$) of each glacier and the standard deviation (STD) of the samples taken on the glaciers.

Glacier	Fe [O2]		Major elements
	Mean	STD	Total conc
1. Austdalsbreen	0.935436	1.595378	2646.124
2. Storbreen	0.171303	0.149951	715.8686
3. Gråsubreen	1.065375	1.04751	691.4272
4. Hellstugubreen	0.887021	0.818031	1744.124
5. Juvfonne	0.329646	0.140197	1161.549
6. Nigardsbreen	0.224061	0.392562	1108.685
7. Engabreen	0.048387	0.031798	388.16
8. Rembesdalskåka	0.479757	0.474957	242.3821
9. Langfjordsjøkelen	0.2865	0.385413	12139.92
10. Ålfotbreen	0.191227	0.179872	7235.855
11. Platåbreen(S)	0.67323	0.424993	1064.086
12. Linnébreen(S)	0.347592	0.214764	1256.857
13.2 Austre Brøggerbreen(S)	1.053666	1.151868	1443.322
14.Midtre Lovénbreen(S)	0.406846	0.485441	736.8597
16. Kongsvegen	0.329854		3021.334
13.1 Austré Brøggerbreen	0.31169		6230.943
15. Edithbreen	0.503994		5546.647

Table E.4 Mean trace element concentration ($\mu\text{g L}^{-1}$) of each glacier and the standard deviation (STD) of the samples.

Glacier	Li		Be [no gas]		Be [H2]		B [O2]		Sc [O2]	
	Mean	STD	Mean	STD	Mean	STD	Mean	STD	Mean	STD
1. Austdalsbreen	0.03592	0.056623	<0.00040	0	<0.00158	0.00	1.46544	1.872413	0.000334	0.000169
2. Storbreen	0.003523	0.005256	<0.00040	0.000128	<0.00158	0.00	<0.15877	0.053362	<0.00028	0
3. Gråsubreen	0.001789	0.001104	<0.00040	8.67E-05	<0.00158	0.00	<0.15877	0.059937	<0.00028	0
4. Hellstugubreen	0.007543	0.014714	<0.00040	0	<0.00158	0.00	0.171088	0.139522	<0.00028	0.000144
5. Juvfonne	0.006295	0.004205	<0.00040	0	<0.00158	0.00	0.353335	0.344395	<0.00028	0
6. Nigardsbreen	0.001886	0.00077	<0.00040	0	<0.00158	0.00	0.51155	0.086071	<0.00028	0
7. Engabreen	<0.00133	0	<0.00040	0	<0.00158	0.00	<0.15877	0	<0.00028	5.97E-05
8. Rembesdalskåka	0.004286	0.004257	<0.00040	0	<0.00158	0.00	<0.15877	0	<0.00028	0
9. Langfjordsjøkelen	0.062687	0.032728	<0.00040	0	<0.00158	0.00	2.654807	0.931598	<0.00028	0
10. Ålfotbreen	0.038917	0.013003	<0.00040	0	<0.00158	0.00	1.576727	0.464078	<0.00028	0
11. Platåbreen(S)	0.009269	0.008188	0.000618	0.000234	<0.00158	0.00	<0.15877	0	<0.00028	0
12. Linnébreen(S)	0.001371	0.000553	0.000541	0.000375	<0.00137	0.000318	<0.09721	0	<0.00015	6.08E-05
13.2 Austre Brøggerbreen(S)	0.002496	0.002801	<0.00052	0	<0.00137	0	0.452995	0.066111	<0.00015	0
14.Midtre Lovénbreen(S)	0.006364	0.010538	<0.00052	0	<0.00137	0	<0.09721	0	<0.00015	0
16. Kongsvegen	0.014214		<0.00052		<0.00137		0.595156		0.000153	
13.1 Austré Brøggerbreen	0.027732		0.000525		<0.00137		1.136851		0.000463	
15. Edithbreen	0.028319		<0.00052		<0.00137		0.982735		0.00015	

Table E.4 cont. Mean trace element concentration ($\mu\text{g L}^{-1}$) of each glacier and the standard deviation (STD) of the samples taken on the glaciers.

	Co [O2]		Ga [H2]		Se [H2]		Br [O2]		Rb [O2]	
Glacier	Mean	STD	Mean	STD	Mean	STD	Mean	STD	Mean	STD
1. Austdalsbreen	0.032105	0.055824	0.002401	0.003263	0.042002	0.018674	3.38484	0.998814	0.335641	0.643678
2. Storbreen	0.002727	0.003942	<0.00154	0	0.018052	0.008279	1.905971	0.422254	0.034617	0.038687
3. Gråsubreen	0.0153	0.019225	<0.00154	0	0.009418	0.003679	1.674245	0.35672	0.053704	0.040321
4. Hellstugubreen	0.015987	0.02202	<0.00154	0.000792	0.01882	0.006865	2.041282	0.521296	0.341134	0.576216
5. Juvfonne	0.024544	0.02929	<0.00154	0.000404	0.009675	0.005722	1.740432	0.555401	0.151548	0.092982
6. Nigardsbreen	0.001761	0.003042	<0.00154	0	0.030739	0.008359	1.719131	0.338832	0.009675	0.006391
7. Engabreen	0.000979	0.001478	<0.00154	0	<0.01020	0	0.643427	0.300937	0.006644	0.00819
8. Rembesdalskåka	0.001161	0.001194	<0.00154	0	0.007419	0.004017	0.364583	0.185432	0.052357	0.043895
9. Langfjordsjøkelen	0.000818	0.000891	<0.00154	0	0.093719	0.015483	21.39183	10.25051	0.055575	0.023857
10. Ålfotbreen	0.007396	0.013827	<0.00154	0	0.077057	0.013193	9.977375	2.123408	0.115241	0.160711
11. Platåbreen(S)	0.027248	0.014788	<0.00154	0.000355	0.007875	0.003442	1.266026	0.423075	0.051433	0.026702
12. Linnébreen(S)	0.006523	0.005736	0.001687	0.000604	0.010959	0.006492	2.518564	1.003571	0.030995	0.015725
13.2 Austre Brøggerbreen(S)	0.003282	0.002488	<0.00050	0.000246	0.033583	0.03468	2.892335	0.932806	0.031371	0.022874
14. Midtre Lovénbreen(S)	0.005294	0.002418	<0.00050	0.00013	0.011437	0.007007	1.339777	0.63708	0.046793	0.05637
16. Kongsvegen	0.006355		<0.00050		0.023205		7.886202		0.018354	
13.1 Austré Brøggerbreen	0.006422		<0.00050		0.050172		11.70809		0.027363	
15. Edithbreen	0.006432		0.00094		0.049643		10.31193		0.022452	

Table E.4 cont. Mean trace element concentration ($\mu\text{g L}^{-1}$) of each glacier and the standard deviation (STD) of the samples taken on the glaciers.

	Sr [H2]		Y [O2]		Zr [O2]		Nb [O2]		Cs [O2]	
Glacier	Mean	STD	Mean	STD	Mean	STD	Mean	STD	Mean	STD
1. Austdalsbreen	0.511291	0.38134	0.00091	0.000849	0.005366	0.010293	0.000207	0.00019	0.00207	0.003239
2. Storbreen	0.50983	0.268547	0.000459	0.000478	0.000989	0.000871	0.000121	6.66E-05	<0.00072	8.35E-05
3. Gråsubreen	0.522496	0.425618	0.00026	0.000167	0.001739	0.001599	0.000135	0.00017	<0.00072	0
4. Hellstugubreen	0.36317	0.117626	0.000943	0.00125	0.004191	0.005382	0.000148	0.000115	<0.00072	0.000419
5. Juvfonne	0.380951	0.114349	0.000407	0.000541	0.001975	0.001225	4.15E-05	3.25E-05	<0.00072	0.00016
6. Nigardsbreen	0.32779	0.04742	7.2E-05	9E-05	0.000103	0.000107	0.00019	0.000169	<0.00072	0
7. Engabreen	0.042657	0.019117	0.000143	0.000153	0.000172	0.000152	2.64E-05	2.06E-05	<0.00072	0.000402
8. Rembesdalskåka	0.073501	0.033799	6.75E-05	5.03E-05	0.000303	0.000319	7.07E-05	4.71E-05	<0.00072	0.000375
9. Langfjordsjøkelen	2.91233	1.32811	0.000669	0.000834	<0.00010	0	7.19E-05	4.51E-05	<0.00072	1.56E-05
10. Ålfotbreen	1.729159	0.499913	0.000182	0.000153	0.00065	0.001194	6.97E-05	4.83E-05	<0.00072	0.00023
11. Platåbreen(S)	0.275038	0.146973	0.002823	0.002687	0.001366	0.001437	3.09E-05	1.55E-05	<0.00072	0.000286
12. Linnébreen(S)	0.193124	0.034947	0.005303	0.008616	0.000773	0.000429	<0.00006	9.09E-06	0.000907	0.00025
13.2 Austre Brøggerbreen(S)	0.065906	0.010563	0.002951	0.001847	0.000391	0.000301	<0.00006	0	0.000765	0.000251
14.Midtre Lovénbreen(S)	0.055428	0.018332	0.000789	0.000622	0.000492	0.000592	<0.00006	0	0.000694	0.000147
16. Kongsvegen	0.953486		0.00191		0.001564		<0.00006		0.000304	
13.1Austré Brøggerbreen	1.685192		0.002186		0.001519		<0.00006		0.000707	
15. Edithbreen	1.406573		0.00059		0.007717		<0.00006		0.000357	

Table E.4 cont. Mean trace element concentration ($\mu\text{g L}^{-1}$) of each glacier and the standard deviation (STD) of the samples taken on the glaciers.

	Ba [O2]		Hf [O2]		Ta [O2]		W [O2]		Pt [O2]	
Glacier	Mean	STD	Mean	STD	Mean	STD	Mean	STD	Mean	STD
1. Austdalsbreen	0.724656	0.668545	<0.00023	0.000114	<0.00005	0	0.009665	0.015709	<0.00101	0.000346
2. Storbreen	0.882192	0.446021	<0.00023	0	<0.00005	0	0.000704	0.000651	<0.00101	0
3. Gråsubreen	1.403871	1.223381	<0.00023	4.89E-05	<0.00005	0	0.003107	0.003929	<0.00101	0.000316
4. Hellstugubreen	0.67478	0.345204	<0.00023	6.36E-05	<0.00005	0	0.00222	0.002159	<0.00101	0
5. Juvfonne	2.79021	0.904479	<0.00023	8.43E-05	<0.00005	0	0.001172	0.000495	<0.00101	0
6. Nigardsbreen	0.327823	0.077773	<0.00023	0	<0.00005	0	0.001265	0.000396	<0.00101	0
7. Engabreen	0.106143	0.051658	<0.00023	0.000115	<0.00005	0	0.001029	0.000518	<0.00101	0
8. Rembesdalskåka	0.406259	0.239982	<0.00023	0	<0.00005	0	0.000652	0.000479	<0.00101	0
9. Langfjordsjøkelen	0.472758	0.229675	<0.00023	0	<0.00005	0	0.001282	0.000657	<0.00101	0
10. Ålfotbreen	0.473705	0.132602	<0.00023	0	<0.00005	0	0.001284	0.001408	<0.00101	0
11. Platåbreen(S)	0.357461	0.246251	<0.00023	0	<0.00005	0	0.000577	0.000324	<0.00101	0
12. Linnébreen(S)	0.227764	0.105529	<0.00011	5.89E-05	5.61E-06	6.84E-06	0.00053	0.000143	<0.00093	0.000224
13.2 Austre Brøggerbreen(S)	0.065961	0.033405	0.000124	5.69E-05	<0.00000	0	0.000463	0.000201	<0.00093	0
14.Midtre Lovénbreen(S)	0.094436	0.036474	<0.00011	0	1.88E-06	2.31E-06	0.000494	0.000297	<0.00093	0
16. Kongsvegen	0.280127		0.000165		<0.00000		0.000281		<0.00093	
13.1Austré Brøggerbreen	0.240392		0.000142		<0.00000		0.000259		<0.00093	
15. Edithbreen	0.163959		<0.00011		<0.00000		0.00028		<0.00093	

Table E.4 cont. Mean trace element concentration ($\mu\text{g L}^{-1}$) of each glacier and the standard deviation (STD) of the samples taken on the glaciers.

Glacier	Au [O2]		Bi [H2]		Th [O2]		U [O2]		Trace elements
	Mean	STD	Mean	STD	Mean	STD	Mean	STD	Total conc.
1. Austdalsbreen	<0.00123	0.000467	0.001763	0.001985	0.000387	0.000474	0.00303	0.00545	6.517487
2. Storbreen	<0.00123	9.77E-05	0.00034	0.000106	<0.00030	0.000103	0.000176	0.000216	3.423915
3. Gråsubreen	<0.00123	0	0.001088	0.001247	<0.00030	0	0.000387	0.000352	3.760386
4. Hellstugubreen	<0.00123	9.14E-05	0.004316	0.0067	<0.00030	0	0.001163	0.00134	3.630846
5. Juvfonne	<0.00123	0	0.001717	0.00092	<0.00030	0.000125	0.000237	0.000236	5.455745
6. Nigardsbreen	<0.00123	0.000192	0.000356	0.00027	<0.00030	0	<0.00011	0	2.904538
7. Engabreen	<0.00123	0	0.000528	0.000304	<0.00030	0	<0.00011	8.9E-05	0.884731
8. Rembesdalskåka	<0.00123	0	0.003006	0.002073	<0.00030	0	0.000108	9.12E-05	0.988618
9. Langfjordsjøkelen	<0.00123	0.000327	0.000769	0.000776	<0.00030	0	<0.00011	2.79E-05	27.55659
10. Ålfotbreen	<0.00123	0.000216	0.000496	0.000467	<0.00030	0	0.000135	7.94E-05	13.92422
11. Platåbreen(S)	<0.00123	9.99E-05	0.000182	0.000194	<0.00030	0	0.00057	0.000398	2.074708
12. Linnébreen(S)	<0.01236	0	0.000159	0.000175	<0.00052	0	0.000386	0.000145	3.044304
13.2 Austre Brøggerbreen(S)	<0.01236	0	0.000184	0.000213	<0.00052	0.000223	0.001934	0.002143	3.528677
14.Midtre Lovénbreen(S)	<0.01236	0	0.000124	8.03E-05	<0.00052	0	<0.00027	0	2.011391
16. Kongsvegen	<0.01236		0.000174		<0.00052		<0.00027		9.766026
13.1Austré Brøggerbreen	<0.01236		0.000297		<0.00052		0.000653		14.84598
15. Edithbreen	<0.01236		0.000478		<0.00052		<0.00027		12.9403

Table E.5 Mean heavy metal concentration ($\mu\text{g L}^{-1}$) of each glacier and the standard deviation (STD) of the samples.

Glacier	V [O2]		Cr [O2]		Mn [O2]		Ni [O2]		Cu [O2]	
	Mean	STD	Mean	STD	Mean	STD	Mean	STD	Mean	STD
1. Austdalsbreen	0.01554	0.026118	0.019141	0.009947	<0,00049	0	0.243163	0.36522	35.30712	35.96914
2. Storbreen	0.013147	0.010557	0.350122	0.657873	<0,00049	0	0.074695	0.062811	8.467195	5.107588
3. Gråsubreen	0.008814	0.009004	0.636026	0.825728	<0,00049	0	0.06446	0.053948	10.76798	4.506925
4. Hellstugubreen	0.010558	0.014972	0.097816	0.073374	<0,00049	0	0.133399	0.187204	10.15448	5.216473
5. Juvfonne	0.015155	0.005974	0.065831	0.103402	<0,00049	0	0.13835	0.081125	18.44455	7.337406
6. Nigardsbreen	0.005179	0.007467	0.21682	0.107333	3.409417	6.81834	0.023312	0.012063	14.61153	15.24314
7. Engabreen	0.001805	0.006772	0.002541	0.00454	<0,00049	0	0.016663	0.021403	4.13572	2.657445
8. Rembesdalskåka	0.004381	0.003955	0.113359	0.167261	<0,00049	0	0.039615	0.032041	11.99553	8.214397
9. Langfjordsjøkelen	0.007213	0.005974	0.136075	0.110105	<0,00049	0	0.026803	0.019542	9.807962	4.05355
10. Ålfotbreen	0.011282	0.00226	0.020427	0.011786	<0,00049	0	0.09347	0.122357	23.92821	21.32714
11. Platåbreen(S)	0.005285	0.008397	0.105157	0.192997	<0,00049	0	0.022697	0.01329	0.112953	0.301046
12. Linnébreen(S)	0.025902	0.003827	0.029178	0.032029	0.482388	0.383062	0.011913	0.005914	0.097415	0.079396
13.2 AustreBrøggerbreen(S)	0.025159	0.012424	<0.01062	0	0.29594	0.166703	0.011879	0.009731	0.222917	0.368297
14.MidtreLovénbreen(S)	0.020664	0.007618	<0.01062	0.003848	0.389216	0.189055	0.033552	0.043741	0.23491	0.411607
16. Kongsvegen	0.012723		<0.01062		0.847937		0.0185		0.120095	
13.1AustréBrøggerbreen	0.012239		<0.01062		1.512475		0.014694		0.092999	
15. Edithbreen	0.012109		0.012565		0.543085		0.035119		0.127882	

Table E.5 cont. Mean heavy metal concentration ($\mu\text{g L}^{-1}$) of each glacier and the standard deviation (STD) of the samples taken on the glaciers.

Glacier	Zn [H2]		As [O2]		Mo [O2]		Cd [O2]		In [O2]	
	Mean	STD	Mean	STD	Mean	STD	Mean	STD	Mean	STD
1. Austdalsbreen	22.57198	38.49103	0.048507	0.076283	0.012562	0.017209	0.012036	0.017766	5.22E-05	6.49E-05
2. Storbreen	4.701583	3.036864	0.015933	0.008662	0.004111	0.003923	0.004338	0.00336	<0.00004	1.23E-06
3. Gråsubreen	5.675138	3.619993	0.007779	0.00292	0.004486	0.004096	0.00267	0.001349	<0.00004	4.42E-06
4. Hellstugubreen	8.644703	10.67638	0.027477	0.023374	0.008261	0.006605	0.005289	0.003997	8.85E-05	0.000127
5. Juvfonne	8.378202	3.105394	0.010122	0.001565	0.003057	0.002313	0.003088	0.000944	<0.00004	8.31E-06
6. Nigardsbreen	2.415362	1.554618	0.009587	0.004627	0.00329	0.003033	0.003436	0.001591	<0.00004	0
7. Engabreen	0.745229	0.55863	0.002553	0.001507	0.003408	0.002413	0.00046	0.000397	<0.00004	2.48E-05
8. Rembesdalskåka	6.582956	7.719889	0.008493	0.002451	0.00305	0.000664	0.002105	0.001536	<0.00004	0
9. Langfjordsjøkelen	3.23078	1.420971	0.012296	0.002004	0.005316	0.002726	0.002935	0.001031	<0.00004	0
10. Ålfotbreen	10.39986	15.44271	0.036151	0.039513	0.006578	0.004834	0.010396	0.011819	<0.00004	9.09E-07
11. Platåbreen(S)	1.192648	0.389366	0.016858	0.011583	0.001782	0.001452	0.000675	0.000327	<0.00004	7.41E-06
12. Linnébreen(S)	1.64772	0.591121	0.019964	0.004367	0.00241	0.000749	0.000706	0.000286	<0.00002	1.04E-05
13.2 Austre Brøggerbreen (S)	1.835404	0.886716	0.012956	0.006873	0.001777	0.000973	0.000721	0.000501	<0.00002	0
14.MidtreLovénbreen(S)	1.670184	1.10097	0.010248	0.003189	0.001798	0.000867	0.001037	0.000849	<0.00002	0
16. Kongsvegen	0.842408		0.008649		0.003347		0.002485		<0.00002	
13.1AustréBrøggerbreen	0.668203		0.010912		0.002971		0.002189		<0.00002	
15. Edithbreen	3.986495		0.010323		0.003237		0.002355		<0.00002	

Table E.5 cont. Mean heavy metal concentration ($\mu\text{g L}^{-1}$) of each glacier and the standard deviation (STD) of the samples taken on the glaciers.

	Sn [O2]		Sb [O2]		Hg [O2]		Tl [O2]		Pb 206 [O2]	
Glacier	Mean	STD	Mean	STD	Mean	STD	Mean	STD	Mean	STD
1. Austdalsbreen	0.01439	0.026644	0.047232	0.078965	<0.00471	0	0.001088	0.001169	0.62761	0.934104
2. Storbreen	0.00344	0.002834	0.006875	0.006916	<0.00471	0	<0.00045	0.000194	0.065361	0.041016
3. Gråsubreen	0.004359	0.005195	0.007572	0.006479	<0.00471	0	<0.00045	0	0.041674	0.031564
4. Hellstugubreen	0.023689	0.041626	0.022572	0.027189	<0.00471	0	<0.00045	0.000289	0.175011	0.253615
5. Juvfonne	0.008236	0.004529	0.044724	0.032721	<0.00471	0	<0.00045	0	0.052999	0.043622
6. Nigardsbreen	<0.00028	0.000249	0.006258	0.003629	<0.00471	0	<0.00045	0	0.090466	0.136911
7. Engabreen	<0.00028	5.03E-05	0.001391	0.001496	<0.00471	0	<0.00045	0	0.01313	0.007661
8. Rembesdalskåka	0.003318	0.001418	0.008513	0.000908	<0.00471	0	<0.00045	0	0.018148	0.00407
9. Langfjordsjøkelen	0.000291	0.00023	0.00514	0.00127	<0.00471	0	<0.00045	0.000107	0.054316	0.020048
10. Ålfotbreen	0.002151	0.004022	0.032272	0.053178	<0.00471	0	0.000534	0.000285	0.148838	0.140032
11. Platåbreen(S)	0.001311	0.002238	0.024612	0.036286	<0.00471	0	<0.00045	0.000368	0.009281	0.009324
12. Linnébreen(S)	<0.00110	0	0.00377	0.002003	<0.00960	0	<0.00044	0	0.015175	0.020861
13.2 Austre Brøggerbreen (S)	0.001393	0.00112	0.075864	0.148696	<0.00960	0	<0.00044	0	0.015262	0.00893
14.MidtreLovénbreen(S)	0.001456	0.001232	0.022499	0.04346	<0.00960	0	<0.00044	0	0.007297	0.006227
16. Kongsvegen	<0.00110		0.000846		<0.00960		<0.00044		0.011078	
13.1AustréBrøggerbreen	0.001838		0.000916		<0.00960		<0.00044		0.026311	
15. Edithbreen	0.017136		0.003385		<0.00960		<0.00044		0.048152	

Table E.5 cont. Mean heavy metal concentration ($\mu\text{g L}^{-1}$) of each glacier and the standard deviation (STD) of the samples taken on the glaciers.

Glacier	Pb 207 [O2]		Pb 208 [O2]		Heavy metals
	Mean	STD	Mean	STD	Total conc.
1. Austdalsbreen	0.628684	0.931683	0.626003	0.932044	58.96609
2. Storbreen	0.064203	0.039652	0.062223	0.040506	13.72654
3. Gråsubreen	0.040129	0.030791	0.039579	0.031258	17.23168
4. Hellstugubreen	0.170823	0.250705	0.170037	0.250498	19.32081
5. Juvfonne	0.052482	0.045483	0.050517	0.0443	27.17632
6. Nigardsbreen	0.087618	0.133556	0.08712	0.13527	20.82529
7. Engabreen	0.013243	0.007853	0.010967	0.008251	4.9311
8. Rembesdalskåka	0.017538	0.003588	0.016098	0.003951	18.78913
9. Langfjordsjøkelen	0.052985	0.020057	0.052091	0.019711	13.38436
10. Ålfotbreen	0.144213	0.137542	0.143151	0.136091	34.76523
11. Platåbreen(S)	0.008537	0.008354	0.007749	0.008842	1.503237
12. Linnébreen(S)	0.015221	0.020255	0.015016	0.020417	2.353126
13.2 Austre Brøggerbreen (S)	0.014375	0.006143	0.014577	0.007286	2.542309
14. Midtre Lovénbreen(S)	0.007553	0.005584	0.007449	0.005852	2.414893
16. Kongsvegen	0.012689		0.012053		1.903775
13.1 Austré Brøggerbreen	0.026632		0.025451		2.406579
15. Edithbreen	0.048047		0.049536		4.856411

F. Results PAHs

Table F.1 Concentration of PAHs with 2 and 3-rings (ng L⁻¹). (S): Sampled in Summer. LOD: Limit of detection. LOQ: Limit of Quantification.

Glaciers	NAP	ACY	FLU	PHE	ANT	FLT	PYR	BaA	CHR
1. Austdalsbreen	68.04	1.01	3.18	6.01	<LOD	1.44	1.18	<LOQ	<LOQ
2. Storbreen	2.50	1.06	0.91	5.50	<LOQ	1.56	1.27	<LOD	<LOQ
3. Gråsubreen	17.47	0.62	1.47	13.35	<LOQ	14.40	6.60	<LOD	0.91
4. Hellstugubreen	14.04	0.64	1.05	5.24	<LOQ	1.50	1.32	<LOQ	<LOQ
5. Juvfonne	44.64	0.60	1.14	5.61	<LOQ	1.65	1.33	<LOD	<LOQ
6. Nigardsbreen	6.81	0.90	0.61	5.62	<LOQ	1.83	1.35	<LOD	<LOQ
7. Engabreen	9.46	1.35	1.03	7.82	<LOQ	2.15	1.84	<LOD	<LOQ
8. Rembesdalskåka	1.35	2.98	1.37	9.45	0.33	2.58	2.08	<LOQ	<LOQ
9. Langfjordsjøkelen	3.68	0.29	0.57	4.20	<LOQ	1.10	0.93	<LOQ	<LOQ
10. Ålfotbreen	15.30	5.67	4.62	17.89	0.73	5.72	4.86	<LOQ	0.84
13.1 Austre Brøggerbreen	40.33	0.36	0.92	3.01	<LOQ	0.61	0.75	<LOD	<LOQ
13.2 Austre Brøggerbreen (S)	6.18	0.48	0.30	4.96	<LOQ	1.26	0.87	<LOQ	0.70
14. Midtre Lovénbreen (S)	11.43	2.34	1.62	10.55	0.64	3.03	2.45	<LOQ	<LOQ
12. Linnébreen (S)	30.71	0.33	0.78	14.10	0.79	2.63	1.85	<LOQ	3.02
11. Platåbreen (S)	10.48	0.32	0.65	4.61	0.64	0.87	0.74	<LOD	<LOQ
16. Kongsvegen	27.00	0.80	1.60	3.73	<LOQ	0.61	1.19	<LOD	<LOQ
15. Edithbreen	14.96	0.55	0.68	3.91	<LOQ	0.99	0.89	<LOD	<LOQ

Table F.2 Concentration of PAHs with 4 and 5-rings (ng L⁻¹). (S): Sampled in Summer. LOD: Limit of detection. LOQ: Limit of Quantification.

Glaciers	BbF	BkF	BaP	IND	DBA	BgP
1. Austdalsbreen	<LOD	<LOQ	2.25	<LOD	<LOD	<LOQ
2. Storbreen	<LOD	<LOQ	2.17	<LOD	<LOD	<LOD
3. Gråsubreen	<LOQ	<LOD	<LOD	<LOD	<LOD	<LOD
4. Hellstugubreen	<LOD	<LOQ	2.95	<LOD	<LOD	<LOD
5. Juvfonne	<LOD	<LOQ	2.33	<LOD	<LOD	<LOD
6. Nigardsbreen	<LOD	<LOQ	2.03	<LOD	<LOD	<LOD
7. Engabreen	<LOD	<LOQ	2.39	<LOD	<LOD	<LOD
8. Rembesdalskåka	<LOD	<LOQ	1.94	<LOD	<LOD	<LOD
9. Langfjordsjøkelen	<LOD	<LOQ	<LOQ	<LOD	<LOD	<LOD
10. Ålfotbreen	<LOQ	1.77	6.59	<LOQ	<LOD	<LOQ
11. Platåbreen (S)	<LOD	<LOQ	<LOD	<LOD	<LOD	<LOD
12. Linnébreen (S)	1.65	<LOQ	<LOD	<LOD	<LOD	<LOQ
13.1 Austre Brøggerbreen	<LOD	<LOQ	<LOD	<LOD	<LOD	<LOD
13.2 Austre Brøggerbreen (S)	<LOD	<LOD	<LOD	<LOD	<LOD	<LOQ
14. Midtre Lovénbreen (S)	<LOD	1.03	3.15	<LOD	<LOD	<LOD
15. Edithbreen	<LOD	<LOQ	<LOQ	<LOD	<LOD	<LOD
16. Kongsvegen	<LOD	<LOQ	<LOD	<LOD	<LOD	<LOD

